UNCLASS
SECURITY CLASSIFICATION OF PAGE (When Data Entered)

REPORT DOCUMENTATION PAGE		READ INSTRUCTIONS BEFORE COMPLETING FORM
1. REPORT NUMBER AFIT/CI/NR 85-29T	2. GOVT ACCESSION NO	3. RECIPIENT'S CATALOG NUMBER
4. TITLE (and Subtitle) Sonars With High Noise And Clutter Rejection For Use With Adaptive Robots		5. TYPE OF REPORT & PERIOD COVERED THESIS/DISSERTATION
		6. PERFORMING ORG. REPORT NUMBER
7. AUTHOR(s) Michael Francis Guyote		8. CONTRACT OR GRANT NUMBER(s)
9. PERFORMING ORGANIZATION NAME AND ADDRESS AFIT STUDENT AT: Oxford University, UK		10. PROGRAM ELEMENT, PROJECT, TASK AREA & WORK UNIT NUMBERS
11. CONTROLLING OFFICE NAME AND ADDRESS AFIT/NR WPAFB OH 45433		12. REPORT DATE 1984 13. NUMBER OF PAGES
14. MONITORING AGENCY NAME & ADDRESS(if different from Controlling Office) AD-A151 875		15. SECURITY CLASS. (of this report) UNCLASS 15a. DECLASSIFICATION/DOWNGRADING SCHEDULE

16. DISTRIBUTION STATEMENT (of this Report)
APPROVED FOR PUBLIC RELEASE; DISTRIBUTION UNLIMITED

17. DISTRIBUTION STATEMENT (of the abstract entered in Block 20, if different from Report)

18. SUPPLEMENTARY NOTES
APPROVED FOR PUBLIC RELEASE: IAW AFR 190-1

LYNN E. WOLAVER 27 Feb 85
Dean for Research and Professional Development
AFIT, Wright-Patterson AFB OH

19. KEY WORDS (Continue on reverse side if necessary and identify by block number)

20. ABSTRACT (Continue on reverse side if necessary and identify by block number)
ATTACHED

DD FORM 1 JAN 73 1473 EDITION OF 1 NOV 65 IS OBSOLETE UNCLASS
SECURITY CLASSIFICATION OF THIS PAGE (When Data Entered)

SONARS WITH HIGH NOISE AND CLUTTER REJECTION FOR USE WITH ADAPTIVE ROBOTS

BY

Michael Francis Guyote

Merton College

A thesis submitted for the degree of Doctor of Philosophy in The University of Oxford

Department of Engineering Science

Parks Road

Oxford

Trinity Term, 1984

ABSTRACT

SONARS WITH HIGH NOISE AND CLUTTER REJECTION FOR USE WITH ADAPTIVE ROBOTS, by Michael Francis Guyote, Merton College. A thesis submitted for the degree of Doctor of Philosophy in the University of Oxford, Trinity Term, 1984.

The goal of this thesis is to develop an ultrasonic ranging system capable of providing range and azimuth information on targets buried in noise and clutter. The information is to be usable by adaptive robots. The two methods selected for research are frequency-modulated, continuous wave (FMCW) ranging, and pseudo-random binary sequence (PRBS) ranging.

An experimental FMCW tracking system is designed, tested, and found able to provide useful tracking information under adverse noise conditions. However, theoretical limits on the amount of noise reduction attainable stop further development.

The research is then directed towards PRBS correlation systems, which offer theoretically unlimited noise reduction. However, the basic correlation function is not ideal for control purposes. Two methods are developed which produce modified correlation functions more suitable for control. These methods, phase and time-shift modulation, are also used to move the transmitted spectrum to an area more usable by the transducers. The first experimental PRBS ranging system proves incapable of providing the desired cross-correlation function due to transducer bandwidth limitations and the link between bandwidth and frequency of operation.

The second experimental PRBS ranging system uses double sideband modulation and asynchronous demodulation. It cross-correlates the received signal with two time-shift modulated reference signals, and is capable of producing the desired correlator output and passing high-noise tests.

The PRBS system is further modified to include target range and azimuth tracking capabilities. ~~Two receivers are used, and the correlator outputs drive specifically designed range/azimuth servo systems.~~ The system proves capable of tracking selected targets under conditions of high noise and clutter. An additional method of target tracking is discussed and factors affecting system accuracy are discussed.

ACKNOWLEDGEMENTS

I am indebted to David Witt for his supervision and constant demand for excellence throughout the last three years. Also, I wish to thank Pete Davey, Bob Vidler, Colin Morgan, Johnathan Bromley, Michael Howarth, and Jon Hodges for their help and encouragement during my association with the Engineering Department Robotics Group.

The research work was carried out with the Oxford University Robotics Group in a project funded by the S.E.R.C. I received the support of the United States Air Force through its graduate school, the Air Force Institute of Technology.

I would like to give a special thanks to Mrs. Esther Rose for her cheerful handling of my seemingly never ending requests for printed material, and to Brigitte Michell for her professional artwork on all illustrations and equations.

I wish also to acknowledge the debt I owe to my father and mother who, by their example, set a path for me to follow.

ABSTRACT

SONARS WITH HIGH NOISE AND CLUTTER REJECTION FOR USE WITH ADAPTIVE ROBOTS, by Michael Francis Guyote, Merton College. A thesis submitted for the degree of Doctor of Philosophy in the University of Oxford, Trinity Term, 1984.

The goal of this thesis is to develop an ultrasonic ranging system capable of providing range and azimuth information on targets buried in noise and clutter. The information is to be usable by adaptive robots. The two methods selected for research are frequency-modulated, continuous wave (FMCW) ranging, and pseudo-random binary sequence (PRBS) ranging.

An experimental FMCW tracking system is designed, tested, and found able to provide useful tracking information under adverse noise conditions. However, theoretical limits on the amount of noise reduction attainable stop further development.

The research is then directed towards PRBS correlation systems, which offer theoretically unlimited noise reduction. However, the basic correlation function is not ideal for control purposes. Two methods are developed which produce modified correlation functions more suitable for control. These methods, phase and time-shift modulation, are also used to move the transmitted spectrum to an area more usable by the transducers. The first experimental PRBS ranging system proves incapable of providing the desired cross-correlation function due to transducer bandwidth limitations and the link between bandwidth and frequency of operation.

The second experimental PRBS ranging system uses double sideband modulation and asynchronous demodulation. It cross-correlates the received signal with two time-shift modulated reference signals, and is capable of producing the desired correlator output and passing high-noise tests.

The PRBS system is further modified to include target range and azimuth tracking capabilities. Two receivers are used, and the correlator outputs drive specifically designed range/azimuth servo systems. The system proves capable of tracking selected targets under conditions of high noise and clutter. An additional method of target tracking is discussed and factors affecting system accuracy are discussed.

CONTENTS

CHAPTER SIX: CARRIER CORRELATION SYSTEMS

CHAPTER SEVEN: AN EXPERIMENTAL CARRIER CROSS-CORRELATING RANGING SYSTEM

CHAPTER EIGHT: TRACKING TYPE II SYSTEMS

APPENDIX A: FMCW TRACKING SYSTEM SCHEMATICS

APPENDIX B: PRBS CORRELATION SYSTEM SCHEMATICS

APPENDIX C: CROSS-CORRELATION FUNCTIONS, TYPE I SYSTEM

APPENDIX D: CROSS-CORRELATION FUNCTIONS, TYPE II SYSTEM

APPENDIX E: TRANSDUCER FREQUENCY RESPONSE TESTS

LIST OF SYMBOLS

A_R	received signal amplitude
A_T	transmitted signal amplitude
B_c	input bandwidth, correlation system (rad/s)
B_f	filter bandwidth (rad/s)
B_{fm}	input bandwidth, FMCW system (rad/s)
B_p	input bandwidth, pulse system (rad/s)
B_t	transducer bandwidth (rad/s)
c	velocity of sound in air (metre/s)
d	transducer spacing
d_c	plate spacing, electrostatic transducer
$F(j\omega)$	complex frequency function
f_c	PRBS clocking frequency (Hz)
f_d	Doppler difference frequency (Hz)
$f_{BP}(t)$	bandpass filter time function
$f_{LPF}(t)$	low-pass filter time function
$f_{ps}(t)$	phase-shift network time function
f_s	Doppler frequency (Hz)
G_r	ramp generator gain, FMCW system
k	ramping constant, FMCW system
M(t)	multiplier output time function
M	max length of pseudo-random binary sequence (PRBS)
m	number of shift registers in PRBS generator
N_f	number of discrete frequencies, discrete Fourier transform

N_s	number of samples, discrete Fourier transform
N_t	number of transmit cycles in one ramp, FMCW system
$N(t)$	noise time function
Q	filter quality factor
R	gas constant
$R_{fg}(\tau)$	cross-correlation function of f(t) and g(t)
$R_{gg}(\tau)$	auto-correlation function of g(t) with itself
R_{max}	maximum target range
r	target range
S_{fg}	cross spectral density of F(jw) and G(jw)
SNRE	signal-to-noise ratio enhancement
T_d	time of valid difference frequency, FMCW system
T_i	integration time
T_p	pulse repetition time, pulse-echo system
T_r	ramping time, FMCW system
T_s	sample period, discrete signal processing
t_e	echo time, FMCW system
t_p	pulse width, pulse-echo system
V_x	velocity parallel to transducer plane, PRBS system
V_y	velocity perpendicular to transducer plane, PRBS system
v	voltage
v_b	bias voltage, electrostatic transducers
v_r	ramp control voltage
v_s	signal voltage, electrostatic transducers
α	duty cycle
γ	ratio of specific heats
ΔR_c	range resolution, PRBS correlation system
ΔR_{FM}	range resolution, FMCW system
ΔR_p	range resolution, pulse-echo system

τ_d	reference signal delay time, PRBS system
τ_f	low-pass filter time constant
τ_r	transmitted signal delay time, PRBS system
τ_Δ	difference between ref delay and trans signal delay
$\Phi(\omega)$	random phase function
ω_d	difference frequency, FMCW system (rad/s)
ω_1	upper cutoff frequency, FMCW system (rad/s)
ω_0	lower cutoff frequency, FMCW system (rad/s)
ω_r	resonant frequency, bandpass filter (rad/s)
ω_t	instantaneous transmitted frequency, FMCW system

CHAPTER ONE.

ULTRASONIC SENSORS FOR ROBOTICS

The field of industrial robotics has grown rapidly during the past ten years, and along with it the requirement for robots which are able to perform increasingly complex tasks. Robots have advanced to the stage where, to paraphrase Nitzan, the 'intelligence' of a robot should be classified as a variable, just as mechanical abilities [52]. The 'intelligence' of any robot depends upon the data which it can gather concerning its surroundings and the subsequent analysis of that data. However, advances in this area of robot programming are hindered due to:

> ...a lack of reliable and affordable sensors, especially those already integrated into the control and programming systems of a robot... [43]

Although various designs have been proposed and implemented for sight, hearing, and touch, sight has been the primary source of information concerning the surrounds and workpieces associated with industrial robots [53]. Sight systems are capable of extremely fine resolution and are able to provide real-time closed loop control of such demanding tasks as robotic welding to accuracies of 0.5 mm [49]. However, robotic vision systems are relatively expensive. The cost of the system mentioned above is well over 27,000 pounds. While such costs

are indeed realistic for large production runs, they are far too high for limited production small batch items. Thus, a need exists for lower-cost sensor systems which could provide similar information to that of light. One possible approach is to use acoustic sensors to provide accurate target ranging and azimuth information.

The field of acoustic sensing is relatively advanced in areas such as medical ultrasonic imaging [14,23,65] , ultrasonic ranging and imaging in water [32,45], non-destructive evaluation (NDE) [11,15,16,18,36,38,50,51], and flow sensing [4,5,13,62,66]. However, until recently, air based ultrasonic systems for use with robotics have been used primarily for ranging and obstacle avoidance [40,41,48]. More advanced acoustically based environment recognition systems have been developed which are capable of constructing a rough 'image' of a robot's surroundings through processing of pulse echo signals [30,60]. Such systems are capable of providing ranging information with a 1% accuracy over distances exceeding 25 feet [47,60], and 0.01% for ranges in the area of 20 cm [17]. However, these systems use basic pulse echo as the ranging method which requires a high signal-to-noise ratio (SNR) for proper operation. Specifically, the reflected signal strength must be much greater than the background noise if the pulse is to be reliably detected.

The purpose of the research detailed in this thesis is to evaluate noise resistant acoustical methods of precise location of selected targets located in the work area of an industrial robot (taken here to mean operating ranges of roughly 10 cm to 1 meter). The methods must be robust enough to tolerate extremely noisy environments such as those encountered in metal, inert gas (MIG) welding, and must be able to pick out and track a target located in a cluttered environment. The goal of

the acoustical ranging system is to reduce position uncertainty of selected targets by acquiring and tracking these targets within restricted range and azimuth parameters. Differences between expected and actual range and azimuth will be available for use by the robot controller for further processing.

1.1 PULSE ECHO TECHNIQUES AND THEIR LIMITATIONS

Basic pulse/echo sonar ranging technique involves transmitting a burst of acoustic energy and noting the amount of time required for the energy to travel to the target and return. The following discussion of basic pulse system parameters is primarily to establish definitions which will be used for the remainder of this thesis. The basic operating parameters of a pulse system are: Pulse width, range resolution, pulse repetition time, and duty cycle. Figure 1.1 illustrates some of these basic operating parameters.

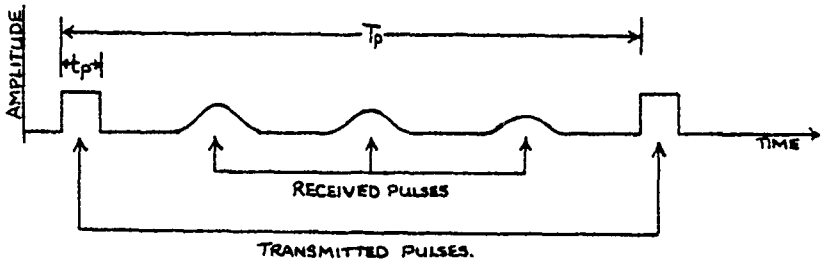

Figure 1.1 Pulse Echo System Parameters

Pulse width is the time width of the transmitted pulse. The minimum pulse width is a function of the system bandwidth and is usually taken to be [63]:

$$t_p = \frac{1}{B_p} \qquad (1.1)$$

where B_p is the pulse system bandwidth in Hz. Range resolution, the minimum spacing in which two targets can be differentiated, is a function of the pulse width.

$$\Delta R_p = \frac{t_p C}{2} \tag{1.2}$$

Pulse repetition time cannot, in this simple system, be shorter than the time required for a pulse to travel to and from a target located as maximum range.

$$T_p \geq \frac{2R_{max}}{C} \tag{1.3}$$

where maximum range R_{max} is the maximum range at which targets are expected. Duty cycle is the ratio of pulse width to pulse repetition time and is defined as:

$$\alpha = \frac{t_p}{T_p} \tag{1.4}$$

The duty cycle also indicates the ratio of peak transmitted power to average transmitted power (if the pulse is square).

The ability of a pulse system to detect incoming pulses is a function of transmitted pulse strength, attenuation properties of the transmission medium, target reflectivity, and noise (both internal and external to the ranging system). Assume a target located within the range of an ultrasonic pulse ranging system is 'visible', that is, the system reliably detects pulse echoes from the target under given conditions. If external noise renders the formerly visible target invisible, there are two possible solutions to the problem: Increase the strength of the transmitted signal, or reduce the effects of the noise.

The first option is limited by the peak signal handling capability of the transducers, and also potentially limited by the maximum safe level of ultrasound. Even though deleterious effects of airborne ultrasound have not been conclusively demonstrated [1], an unlimited increase in peak acoustic emission does not seem advisable. Personal experience obtained during this research indicates that the relatively low output of the ultrasonic transducers available was sufficient to cause tinnitis for short periods of time if the transducers were operated closer than one metre from the ear. Therefore, the second option, that of reducing noise effects, bears closer scrutiny.

1.2 METHODS FOR INCREASING S/N RATIOS IN PULSE SYSTEMS

Assuming that the transmitted signal strength is held constant, there are two main methods for improving SNR in a pulse system. The first is to use signal averaging techniques, which involves attaining information from many pulses and averaging the results [51]. The second is the use of specially designed filter systems, termed 'matched filters' [51,63]. Since signal averaging on a basic pulse system would greatly increase the amount of time required to obtain a usable signal, these systems usually apply methods designed to increase the amount of target information attainable during one pulse repetition time. Such techniques as staggered pulses, frequency coded pulses, and chirped pulses are commonly used. The basic operating principle behind these techniques is that the transmitted signal is supplied with a time code which allows the receiving system to determine the time of transmission. Such time codes allow higher duty cycles, and raise the rate of target information proportionately [63].

Matched filter systems pass the received signal through filter networks whose complex frequency response is specifically tailored to maximize peak signal power to average noise power. Each of these methods is capable of providing improved SNR, and they are usable separately, or together. Obviously, a system which utilizes a combination of both techniques is one which has the greatest probability of providing useful ranging information under the high-noise conditions described above. The two systems considered for development in this thesis both provide this combination.

1.3 FREQUENCY MODULATED, CONTINUOUS WAVE RANGING

One method of providing time 'markers' to the transmitted signal is to cause its instantaneous frequency to vary in a known manner with respect to time. The receiver has access to the transmitted output and, as such, is able to decode the echo signals properly. This enables the transmitter to operate for a higher proportion of time during the pulse repetition period, thus yielding a higher average power of both transmitted and received signals. An FMCW system is capable of greater than 99% duty cycle. Although a basic FMCW system is not a matched filter system [64], the addition of bandpass filters to the basic system will make it perform much as a matched filter system and will allow significant noise reduction. The improvement in SNR is a function of the ratio of system output bandwidth to system input bandwidth, as will be shown in Chapter Two. Further, the system can be easily modified so that it can track one target while excluding others. The FMCW system was the first type to be constructed and tested in the course of this research. It indeed offers great potential for noise reduction, and the modifications discussed in Chapters Two and Three yield a highly noise immune tracking system. However, the method by which the system applies

time codes to the transmitted signal has a weakness in that it does not provide a valid ranging signal for the entire ramping time. This characteristic limits the ultimate noise reduction capabilities. This, and difficulties with maintaining precision forced a search for systems which were less limited in their noise reduction capabilities.

1.4 CORRELATION SYSTEMS

Correlation systems operate by transmitting a reference signal and comparing received signals with a delayed version of the reference signal. Skolnik [64] shows that such systems are matched filter systems, and as such will provide maximum peak signal power to average noise power ratio at the system output. If a reference signal can be found which has an extremely long period, then a correlation system can transmit this signal continuously and receive echo information continuously, thus allowing a 100% duty cycle without worrying about incorrect echo returns from targets at long ranges. Pseudo-random bina sequences (PRBS) are such reference signals, and are the ones which were used in the experimental correlation systems discussed in this thesis. Correlation systems are theoretically unlimited in their ability to enhance SNR, given unlimited time. Newhouse [51] shows that the final SNR attainable in a correlation system is a function of the bandwidth of the correlation filter.

1.5 THESIS LAYOUT

The remaining chapters of this thesis detail theory and research on the two types of ranging systems discussed previously. Chapters Two and Three deal with the theory and experimental version of a modified FMCW system capable of tracking moving targets. Chapters Four and Five cover

the theory and first experimental version of a correlation system. Chapters Six and Seven go into details concerning theory and design of an advanced correlation system which was designed to overcome difficulties encountered with the first experimental correlation system. Chapter Eight covers additions and modifications to the advanced system which allow it to track targets moving in both range and azimuth (angle from transducer to target). This tracking system uses dual receivers to extract range and azimuth information, and drives servo-motors to keep the transducers at the correct range and orientation with respect to the target. Chapter Nine lists factors which influence the advanced correlation system accuracy, (termed secondary effects). In addition, it details another correlation system modification which will allow target tracking using stationary transducers.

1.6 SUMMARY

The object of this thesis is to describe and discuss an ultrasonic ranging and tracking system which would operate in the range of 10 cm to 1 meter and be capable of providing reliable tracking information under conditions of high noise and clutter.

The approach is to explore two ranging systems which offer potential improvements in noise immunity over conventional pulse-echo systems. The first experimental approach uses frequency modulated, continuous wave transmission which achieves enhanced noise immunity by filtering coupled with increased duty cycle. The second experimental approach, and the one which proves most successful, uses cross-correlation systems which use pseudo-random binary sequences as the reference signal. The correlation systems allow 100% duty cycle and are capable of using extremely narrow bandwidth filters.

CHAPTER TWO

FREQUENCY MODULATED CONTINUOUS WAVE RANGING SYSTEMS

Frequency modulated, continuous-wave transmission (FMCW) is one method of attaining a high transmission duty cycle. In an FMCW system the high duty cycle, and hence high average power, is achieved through almost continuous transmission of a frequency marked signal. The transmitted signal is frequency marked by changing its instantaneous frequency in a predetermined manner. The received signal is compared with the transmitted frequency, usually by a multiplication process, and the difference frequencies can be extracted through filtering. In a properly designed system, this difference frequency exists for a much larger percentage of time than does a single pulse from a pulse-echo system. Thus, the theoretical detection performance of an FMCW system should be much higher than that of a simple pulse-echo system. These theoretical advantages were recognized during the mid-forties [63], and test radars using FMCW methods were constructed [3]. From that time until the early 1980's, FMCW's main use seemed to be radar altimeters [7,68]. However, the availability of fast digital frequency analysis has made FMCW systems much more versatile. A state-of-the-art FMCW radar tracking system is presently incorporated in the Tornado F2 NATO interceptor which utilizes a Marconi AI.24 FMCW system [20].

FMCW based sonar systems were explored in the late fifties by Kay [31,32]. He concluded that, given identical bandwidths and peak transmitter power, an FMCW system offers potential advantages over pulse systems due to the fact that the average transmitted power would be much higher, thus yielding improved detection performance. Kay went on to design and patent an FMCW ranging system for use by the blind [33,34], and development of FMCW ranging systems is still an active field [20,24]. Aside from the work done by Kay and his associates, no further research seems to have been done in air-based FMCW systems. An interesting note is that there is evidence to indicate that bats use a form of FMCW for portions of their in-flight obstacle avoidance [58].

No attempts seem to have been made to use FMCW ranging in robotic applications. It would seem that the requirement for single target tracking in a noisy, cluttered environment would be an ideal application for this type of system.

2.1 FMCW BASIC OPERATION

A block diagram of a basic FMCW system is shown in figure 2.1. The ramp generator provides a linear ramping voltage which drives the voltage controlled transmitting oscillator. The transmitting oscillator operates in the frequency range ω_0 to ω_1 which is usually limited by the operating range of the transducers. The frequency arriving from a target is multiplied with the transmitted frequency, and the difference frequency is extracted through multiplication and low-pass filtering.

Figure 2.2 illustrates the transmitted, received, and difference signals for one target. In this diagram, the transmitted signal is shown starting at one frequency and terminating at a higher frequency. There is no particular reason for ramping upward in this manner, and the

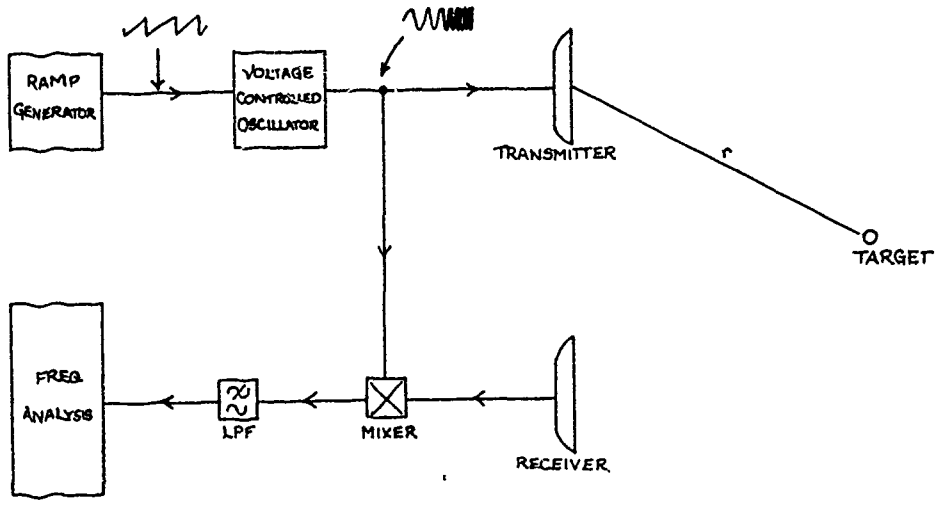

FIGURE 2.1 F.M.C.W. SYSTEM BLOCK DIAGRAM

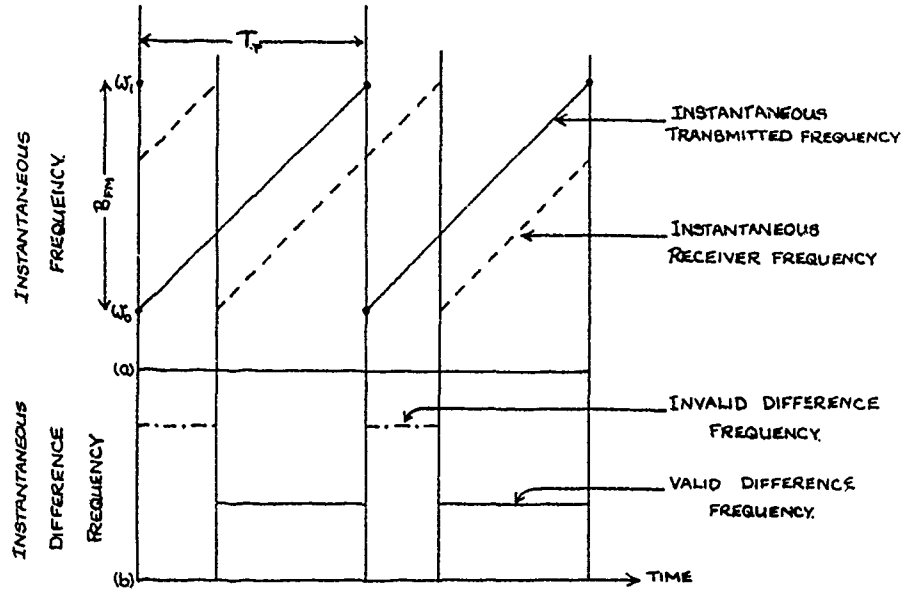

FIGURE 2.2 F.M.C.W. SYSTEM TRANSMITTED, RECEIVED AND DIFFERENCE SIGNALS

diagram could just as easily have shown an downward ramp. However, there are potential advantages to an upward ramp in that the Doppler shift due to target motion produces a difference signal indicating the future position of the target, rather than the past position, which we get with a downward ramp. In figure 2.2, the target information is shown to last for a sizable portion of the ramping period. Note, however, that there are periods in which the difference frequency is not a correct indicator of target range. This is the phenomenon which limits the duty cycle of the actual ranging information. Methods for dealing with invalid frequenies are discussed in greater depth in a following section.

2.2 THEORY OF OPERATION

Assume the transmitted frequency is a sinusoid starting at frequency ω_0 rad/s and ending at ω_1 rad/s with a ramping rate of k rad/sec . At time t, the instantaneous transmitted signal can be expressed as:

$$A_T \cos \int_0^t (\omega_0 + kt)dt = A_T \cos\left(\omega_0 t + \tfrac{1}{2}kt^2\right) \qquad (2.1)$$

A signal returning from a single target located at range r will require a travel time of:

$$t_e = \frac{2r}{C} \qquad (2.2)$$

The signal present at the receiver at time t is:

$$F_R(t) = A_R \cos\left\{\omega_0 + \frac{k}{2}(t-t_e)\right\}(t-t_e) \qquad (2.3)$$

and the transmitted signal is:

$$F_T = A_T \cos\left\{\omega_o + \frac{kt}{2}\right\} t \tag{2.4}$$

The multiplier output is:

$$M(t) = \frac{A_T A_R}{2}\left\{\underbrace{\cos\left(2\omega_o t - \omega_o t_e + kt^2 - ktt_e + \frac{k}{2}t_e^2\right)}_{\text{SUM TERM, (A)}} + \underbrace{\cos\left(\omega_o t_e + ktt_e - \frac{k}{2}t_e^2\right)}_{\text{DIFFERENCE TERM, (B)}}\right\} \tag{2.5}$$

Equation 2.5 contains two terms, each with its own phase. The instantaneous frequency of each of the phase terms is the first derivative with respect to time and is:

$$\frac{dA}{dt} = 2\omega_o + 2kt - kt_e \tag{2.6}$$

for the first bracketed term and

$$\frac{dB}{dt} = -kt_e \tag{2.7}$$

for the second bracketed term.

The frequency represented by eq 2.6 changes with time and is not a useful indicator of range, the frequency represented by eq 2.7 does not change with time and is only a function of range. An appropriately designed low-pass filter section will remove the frequencies represented by eq 2.6 and present the target related information in eq 2.7 for further analysis.

The spectrum produced in the transmitted signal by this frequency modulation is quite difficult to evaluate theoretically. However, the relationship between the ramping frequency and transmitting frequencies are such that the frequency modulation is considered to be wide band [61]. The width of the spectrum produced by such frequency modulation is very nearly the same as the system bandwidth [57,61]. Thus, the overall transmitted signal bandwidth will be considered to be the same as (B_t), the transducer bandwidth.

2.3 RAMPING RATE, MAXIMUM RANGE, AND MAXIMUM DIFFERENCE FREQUENCY

For robotics ranging applications, it is assumed that the signal-to-noise restrictions will be the result of a noisy operating environment. Targets of interest will lie relatively close to the transducers (probably within one meter) and, unless extremely high ultrasonic frequencies are used, the system will not be range limited due to atmospheric attenuation of signal returns from objects at this range.

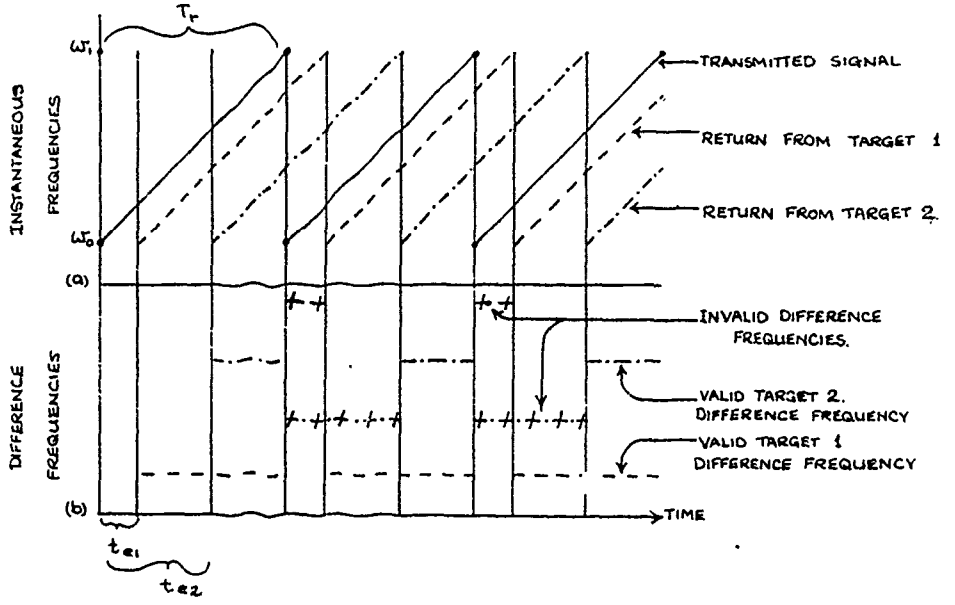

FIGURE 2.3 FMCW Ranging System

a) Transmit/receive signals (multiple targets)

b) Difference frequencies

In order to establish a relationship between maximum usable range (R_{max}) and ramping rate (k), consider figure 2.3. The system ramps from ω_0 to ω_1 in T_R seconds. Two targets, located at ranges r_1 and r_2, produce returns which are delayed by times t_{e1} and t_{e2}. During the first ramp, target 1 produces a valid difference frequency lasting for a period ($T_R - t_{e1}$). Target 2 produces a valid difference frequency lasting ($T_R - t_{e2}$). When the ramp restarts at ω_0, the difference frequencies change. These new frequencies are incorrect in that they are not representative of the true range, and they must be discarded. Since subsequent signal processing stages cannot differentiate between the valid and invalid frequencies, another method of eliminating them must be considered.

If the ramping rate is adjusted so that echoes from a target located at maximum range begin not later than half the ramping period ($T_R/2$), then valid difference frequencies will be equal to or less than half the system bandwidth, and invalid difference frequencies will be greater. The two sets of frequencies can be separated by appropriate design of the low-pass filter which follows the multiplier. Valid difference frequencies will last for almost the entire ramping time for targets at close range, and a minimum of one-half the ramping time for targets at maximum range.

The system can also be modified so that the transmitted signal is ramped through the system frequency range in the maximum reflection time, transmission terminated, and the ramping continued for an equal amount of time, with the ramp output still provided to the multiplier. This would produce difference frequencies which would last for a period equal to one half the ramping period no matter what the target range. This type of FMCW system is the type used by Kay in his experimental work [32]. However, this effectively produces a 50% duty cycle for all target

returns, no matter what the range.

One method of overcoming this problem is to provide more than one reference signal for the multiplier input, and link the reference signals in a predetermined manner. This could, in theory, provide a continuous return from targets in the allowed range. Gough et al. [24] have successfully demonstrated an FMCW system using this technique. Their experimental system has no 'blind time' at all; that is, target information is available all of the time. However, the difference frequencies will contain abrupt phase discontinuities which will occur whenever the reference oscillator changes. These abrupt phase discontinuities could adversely affect the tuned filter output. Therefore, subsequent analyzis of FMCW systems in this chapter will assume a ramping period of twice the amount of time required for a transmitted signal to travel to a target located at maximum range. However, it is realized that theoretical performance could be improved somewhat by using more complex demodulation techniques.

Summarizing the conclusions reached in this section:

1. For a continuously transmitting FM system, the ramping rate will be such that the ramping time is at least double the time required for an echo to arrive from an object located at maximum range. This eliminates incorrect difference frequencies.
2. Time of valid difference frequencies will vary from a maximum of almost the entire ramping time for targets at zero range to a minimum of one-half the ramping time for targets located at maximum range.

3. The largest frequency attainable from a target at maximum range is half of the frequency range of transmission; ie, half of the transducer bandwidth.

These relationships are shown in equations 2.8 through 2.11.

$$T_r = \frac{4R_{max}}{C} = \frac{B_{fm}}{k} \tag{2.8}$$

$$k = \frac{C B_{fm}}{4R_{max}} \tag{2.9}$$

$$\frac{T_r}{2} \leqslant T_d < T_r \tag{2.10}$$

$$\omega_{dmax} = \frac{B_{fm}}{2} \tag{2.11}$$

2.4 RANGE RESOLUTION WITH BANDPASS FILTERS

Kay [31] found that range resolution in an FMCW system was independent of system bandwidth, and this constituted a possible advantage of an FMCW system over a pulse system. However, there is a minimum range resolution which can be attained, and related to this, a maximum reduction in external noise that can be attained. The following theoretical development is different than that taken by Kay; however, the reasoning used offers a useful alternative approach.

Multiple targets will produce multiple frequency returns, and if a linear system is assumed, each frequency will be a function of target distance. Bandpass filters are the usual method of differentiating frequencies and the range resolution of the system will be governed by the bandwidth of these filters. Theoretically, N filters of equal

bandwidth covering the frequency range from dc to $\omega_{d\,max}$ should allow a resolution of R_{max}/N. What is the minimum bandwidth attainable given the constraints of a limited response time?

As a first estimate, let the range of frequencies expected from the the low-pass output lie between 0 and $\omega_{d\,max}$Hz. Range differentiation is accomplished by dividing this frequency range into N parts, each bandpass filter having a bandwidth of $\omega_{d\,max}/N$. For a 1-zero, 2-pole bandpass filter, the relationship between resonant frequency and operating bandwidth is termed Q, or quality factor, and is expressed as:

$$Q = \frac{\omega_r}{B_f} \qquad \begin{array}{l} \omega_r = \text{FILTER RESONANT FREQUENCY} \\ B_f = \text{FILTER BANDWIDTH} \end{array} \qquad (2.12)$$

The limit to the number of filters, and hence range resolution, that could be used to differentiate a given frequency range would at seem to be limited only by the Q attainable. This would indeed be the case if the difference signals could be made to last indefinitely. However, the system bandwidth, coupled with ramp rate and maximum target range place limits on the amount of time that a valid echo signal is received.

As shown in the previous section, a system which transmits the waveform as shown in figure 2.2 will produce difference frequencies from each target which last for a minimum time of half the ramping period. Thus, the filter must respond to this signal within this time if a target within the filter's range annulus is to be detected. The filter response time must then be determined.

2.5 RANGE FILTER RESPONSE TIME

Assume a second order bandpass filter for each range section. The filter response time to a sinusoid can be found by use of Laplace transforms. Consider a second order bandpass filter with resonant frequency ω_r which has as its input a sinusoid at frequency ω_r starting at time t=0.

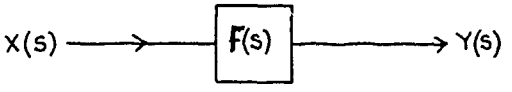

FIGURE 2.4 Bandpass filter time response analysis

The system transfer function is:

$$Y_{(s)} = X_{(s)}\, F_{(s)} \qquad (2.13)$$

The system input is a sinusiod starting at time=0. In s notation this is:

$$X_{(s)} = \frac{\omega_r}{s^2+\omega_r^2} \qquad (2.14)$$

and the filter transfer function is:

$$F_{(s)} = \frac{(\omega_r/Q)\, s}{s^2+(\omega_r/Q)\, s+\omega_r^2} \qquad (2.15)$$

The filter output is then:

$$Y_{(s)} = \frac{\omega_r}{s^2+\omega_r^2} - \left\{ \frac{(1-\tfrac{1}{4}Q^2)^{1/2}\omega_r}{(1-\tfrac{1}{4}Q^2)^{1/2}\left[(s+\omega_r/2Q)^2+(1-\tfrac{1}{4}Q^2)\omega_r^2\right]} \right\} \qquad (2.16)$$

Following some manipulation, the inverse Laplace transform yields the time response:

$$Y_{(t)} = \sin \omega_r t - \left\{ \frac{e^{-\omega_r t/2Q}}{(1-1/4Q^2)^{1/2}} \sin \left[(1-1/4Q^2)\omega_r t \right] \right\} \qquad (2.17)$$

If a Q greater than five is assumed, this can be further reduced to:

$$Y_{(t)} \triangleq \sin \omega_r t \left\{ 1 - e^{\frac{-\omega_r t}{2Q}} \right\} \; ; \quad Q > 5 \qquad (2.18)$$

The response time for this filter to rise to roughly 63% of its final output is:

$$\gamma_f = 2Q/\omega_r \qquad (2.19)$$

From eq 2.12:

$$Q = \omega_r/B_f \qquad (2.20)$$

The filter response time then becomes:

$$\gamma_f = 2/B_f \qquad (2.21)$$

From eq 2.21, it can be seen that the filter response time is a function of its bandwidth. If a worst case response time of one-half the ramping time is assumed, eq 2.21 can be combined with eq 2.8 and 2.10 to yield the minimum bandwidth attainable in the described system.

$$t_{min} = \frac{2R_{max}}{C} = \frac{2}{B_f} \qquad (2.22)$$

Thus:

$$B_f = \frac{c}{R_{max}} \tag{2.23}$$

The range resolution of the system can be related to the frequency resolution by:

$$\frac{\Delta R_{fm}}{R_{max}} = \frac{B_f}{\omega_{dmax}} \tag{2.24}$$

Using eq 2.11 and eq 2.23, we find that:

$$\Delta R_{fm} = \frac{2c}{B_{fm}} \tag{2.25}$$

where B_{fm} is in rad/s. It should be noted that if the advanced system described earlier were to be used here, an extremely narrow-band filter would not respond properly to a continuous sequence of target returns due to the fact that these returns would not be phase coherent with each other. Range resolution is thus a function of maximum difference frequency, which is limited by system bandwidth. It will be shown in section 2.8 that the reduction in noise is also proportional to the minimum filter bandwidth attainable.

2.6 RANGE RESOLUTION WITH DISCRETE SIGNAL PROCESSING

Frequency analysis of the target signals may also be performed digitally. Developments in the field of dedicated processors make possible systems which would have the capability of providing indications of all ranges without requiring many analogue filter networks. Although systems which would give a real-time indication of range through discrete frequency analysis are quite expensive, this type of processing is

presently utilized in a new FMCW based radar system [20]. Although present-day prices for fast digital processing networks are too high to be considered for low-cost sonar systems, it is interesting to note the resolution attainable by frequency analysis techniques. Assume that the largest frequency which exists at the multiplier output is ω_{dmax}, (eq 2.11). If this signal is to be successfully sampled, the sample frequency must be at least twice the highest frequency present [69]. The sampling period is:

$$T_s = \frac{2\pi}{2\omega_{dmax}} = \frac{\pi}{\omega_{dmax}} \qquad (2.26)$$

where ω_{dmax} is in rad/s. The number of samples in any time T will then be:

$$N_s = \frac{T_R}{T_s} = \frac{\omega_{dmax} T_r}{\pi} \qquad (2.27)$$

If the discrete Fourier transform (DFT) is used to calculate the spectrum, the number of discrete frequencies (real and imaginary) available from the calculation will be equal to the number of samples. If these components are placed into the more common amplitude/phase format, the number is halved, and the total becomes:

$$N_s = \frac{\omega_{dmax} T_r}{2\pi} \qquad (2.28)$$

The frequency divisions, will be:

$$\Delta F = \frac{\omega_{dmax}}{N_s} = \frac{\omega_{dmax}\, 2\pi}{\omega_{dmax}\, T_r} = \frac{2\pi}{T_r} \qquad (2.29)$$

And range resolution is:

$$\Delta R_{fm(discrete)} = \frac{\Delta F}{\omega_{dmax}} = \frac{2\pi}{T_r \omega_{dmax}} = \frac{2\pi c}{4R_{max}} \cdot \frac{2}{B_{fm}} = \frac{\pi c}{B_{fm}} \qquad (2.30)$$

which is approximately equal to that obtainable from analogue filtering. However, digital processing could allow the magnitudes to be calculated which would eliminate the phase problems associated with the continuous return system.

However, there are additional considerations such as 'windowing' the sampled function, and the frequency blurring which occurs due to the difference between actual frequencies present and the frequencies represented by discrete transform [69]. These will reduce the resolution somewhat.

2.7 TARGET TRACKING

Although multiple targets can be identified using multiple bandpass filters, or by analyzing digital output, tracking a single target in a cluttered environment is more difficult and would require complex processing of all filter outputs (either digital or analogue). If the bandpass filter approach is used, a single filter's resonant frequency could be changed so that it would track a specific target. However, all tracking techniques would require a 'hill climb' technique to ascertain in which direction the frequency was changing. Such techniques would be complex and difficult to implement.

The approach which will be discussed in this section involves modifying the FMCW system in the following manner. Design one bandpass filter which has a resonant frequency ω_r and servo control the ramping rate such that a target of the expected range produces this difference frequency. When target range changes, a measure is made of the difference frequency deviation from bandpass filter center frequency, and

the ramping rate adjusted so as to drive the difference frequency back to ω_r. This approach has been used in the design of radar altimeters [7,68]. As here, the design goal was to reduce noise effects in the system by reducing the system bandwidth. The filter also excludes clutter, i.e., other targets not being tracked.

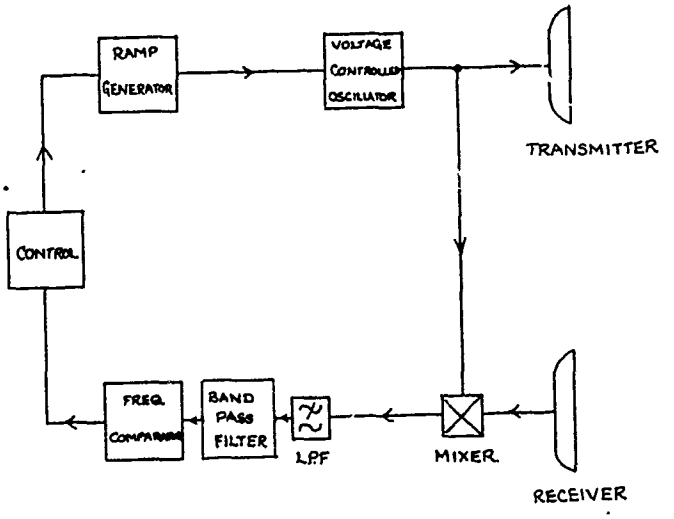

FIGURE 2.5 FMCW Tracking System

A block diagram of the tracking FMCW system is shown in figure 2.5. The frequency analysis stage which follows the multiplier stage has been replaced by a frequency comparator containing the bandpass filter as described. The output of the frequency comparator stage is a voltage which is proportional to the deviation between the filter center frequency and the incoming difference frequency. This voltage is used to drive a control unit which causes the ramping generator to adjust to the correct ramping rate. The overall system is now a frequency-locked system and can be described by the appropriate equations.

This modified system no longer produces ranging information as a function of filter output, and range must be extracted from either the ramping control voltage or from a count of the transmitter output. The ramping rate is a function of the control voltage:

$$k \propto V_c \tag{2.31}$$

In the constant frequency system, range is inversely proportional to ramping rate.

$$r = \frac{\omega_d c}{2k} \tag{2.32}$$

Since range is inversely proportional to ramping rate, it is therefore also inversely proportional to control voltage. Although range can be calculated by evaluation of eq 3.32, there is an alternate method of obtaining range. The number of cycles produced at the VCO output during one ramping operation are:

$$N_T = \int_0^{T_R} \frac{(\omega_o + kt)\,dt}{2\pi} = \frac{\omega_o T_R + \frac{k}{2} T_R^2}{2\pi} \tag{2.33}$$

Since

$$T_R = \frac{B_{fm}}{k} \quad ; \quad k = \frac{\omega_d c}{2r} \tag{2.34}$$

then

$$N_T = \frac{r}{2\pi c} \cdot \frac{B_{fm}}{\omega_d} \left\{ 2\omega_o + B_{fm} \right\} \tag{2.35}$$

and since ω_o , ω_d , B_{fm}, and c are constants (for the purpose of this analysis) the number of counts per ramp is directly proportional to range.

2.8 IMPROVEMENT IN NOISE PERFORMANCE

In an FMCW system, the amount of noise reduction afforded by the addition of bandpass filters is proportional to the ratio of filter bandwidth over transducer bandwidth. Thus, for an FMCW system with input bandwidth B_{fm} and output bandwidth B_f, the r.m.s. noise is reduced by a factor of:

$$\beta = \frac{B_f}{B_{fm}} \qquad (2.36)$$

if input noise of constant spectral density is assumed. The output SNR is:

$$SNR_{out} = SNR_{IN} \cdot \frac{1}{\beta} \qquad (2.37)$$

Therefore, the ultimate system SNR is a function of the width of the final bandpass filter. Since this filter bandwidth is limited by the system bandwidth, the ultimate system SNR is also limited. This is potentially a limiting factor with the use of FMCW systems.

2.9 CONCLUSIONS

Given a ranging system of determined bandwidth, an FMCW ranging algorithm can be implemented which will yield theoretically identical results with a pulse system with respect to range resolution. However, the system bandwidth reduction which can be obtained in an FMCW system

through filtering allows an improvement on S/N ratio which is directly proportional to the ratio of filter bandwidth to system bandwidth. The maximum amount of bandwidth reduction possible is limited due to the fact that accurate target information may only exist for a given time, which sets a limit on the minimum filter bandwidth. Either digital or analogue methods may be used for extracting target information. Digital processing, while offering potential advantages, would be much slower than analogue processing in providing target tracking information. This, of course, assumes the use of domestic or industrial digital systems, not high-speed advanced systems such as those used in military hardware.

Single target tracking with enhanced noise immunity can be obtained by servo-controlling the ramping rate so as to keep the target difference frequency within the range of a narrow-bandpass filter. The system has limits on the amount of noise reduction which can be obtained, but does offer promise of usefulness in areas where the input SNR is such that a pulse system would be greatly degraded. Chapter Three contains details of the construction, testing, and evaluation of a Tracking FMCW system and contrasts the performance with that of a basic FMCW system.

CHAPTER THREE

A TRACKING FREQUENCY MODULATION CONTINUOUS WAVE RANGING SYSTEM

Chapter Two concluded that while usable amounts of improvement in S/N ratios could be achieved by FMCW techniques, the range resolution and overall S/N ratio were still limited by the frequency resolution possible with a signal available for only a brief period of less than one frequency sweep. However, the amount of S/N improvement which could be gained seemed to indicate that an actual tracking FMCW system should be constructed and tested under high- noise conditions. The tracking FMCW system described below is modeled on the block diagram shown in figure 2.4. It is designed to track targets located at ranges of from 10 to 25 cm.

The basic system operation is as follows. The ramping generator causes the transmitter VCO to produce the frequency sweep described in Chapter Two. The echo signals are multiplied by the transmitter input waveform and the difference frequencies are extracted. These difference frequencies are compared with a reference frequency, with only the difference frequency close to the reference frequency having any real effect. Any deviation between these two frequencies is used to change the ramping rate in a manner that drives the difference frequency towards the reference frequency. In this experimental system, the reference frequency is 5 kHz.

Chapter 3 is divided into two sections: Section I deals with general details of the electronics used in constructing the tracking system. Section II deals with the testing of the completed system. Testing consists of ranging tests to verify proper system operation, and high-noise tests in which the system's immunity to external noise is evaluated. The high-noise tests are accomplished by attaching the transducers to a welding robot and recording the range output during welding.

SECTION I - FMCW TRACKING SYSTEM, CIRCUIT DETAILS

The tracking FMCW system block diagram is shown in figure 3.1. It consists of a ramping generator, VCO, transmitter, transmitting/receiving transducers, receiving amplifiers, frequency changer (multiplier), bandpass filter/frequency comparator, low-pass filter, and proportional plus integral control.

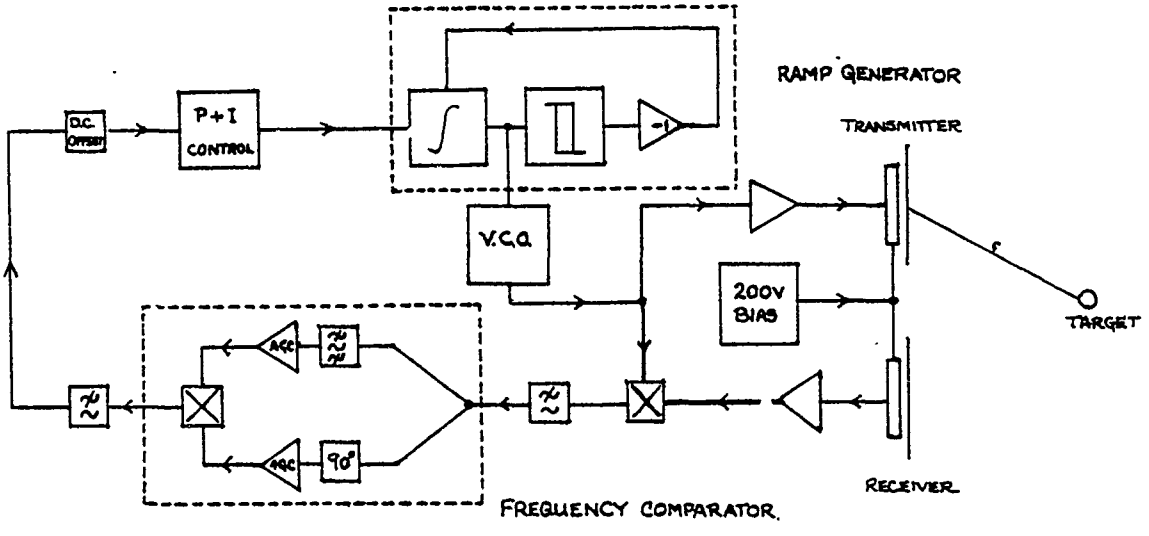

FIGURE 3.1 FMCW Tracking System

Appendix A contains the schematic diagrams of the system as described below. A2 contains the VCO, transmitter, high-voltage dc bias supply, receiving preamplifier, and multiplier sections. A3 contains the frequency comparison circuits. A4 contains the proportional plus integral controller and the ramping circuits. A5 contains the counter/display circuits.

3.1 VCO AND TRANSMITTER

An XR-2207 integrated circuit serves as the VCO. The output frequency is controlled by the current through one of four timing pins any one of which is user selectable through the use of two binary keying inputs. As configured in appendix A, the frequency output is determined by the current flowing from control pin 6. This current is varied by the control voltage provided from the ramping generator. A control voltage of zero volts causes a VCO output of approximately 87 kHz; four volts causes approximately 45 kHz. VCO output is centered on 4.5 volts.

The transmitting stage consists of two transistors and is a conventional complimentary symmetry design with approximately unity gain. The step-up transformer at the transmitting stage output increases the voltage of the signal to be transmitted by a factor of approximately fourteen for use by the transmitting transducers.

3.2 TRANSMITTING/RECEIVING TRANSDUCERS/HIGH-VOLTAGE POWER SUPPLY

The transmitting/receiving transducers used in the PMCW system are electrostatic types designed by L. Kay and previously manufactured by Ultra Electronics, LTD, of London. The units used in this thesis are fabricated at the Oxford Department of Engineering Science and shall be referred to as Oxford transducers throughout the remainder of this

thesis. The general construction of the transducer is shown in figure 3.2. The transducer diaphram is a plastic film (trade name: Melinex) with a metallized coating on the outer side. The metal backing plate, together with the metallized diaphram, form the two surfaces across which the signal is applied. The basic design features a grooved backing plate, with grooves of 0.51 mm spacing. The rings on the backing plate raise the transducer operating frequency by creating vibration nodes at each point in which the backing plate contacts the diaphram, thus reducing the effective diaphram width to that of the groove spacing.

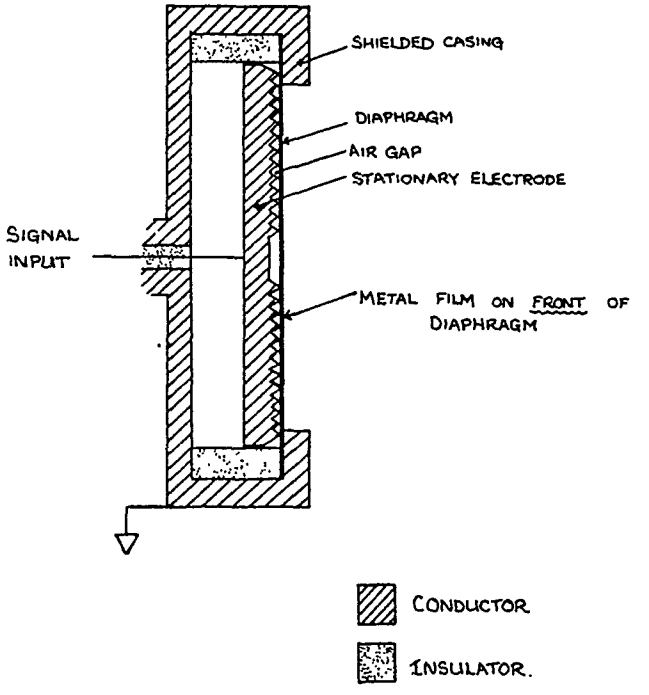

FIGURE 3.2 Oxford Electrostatic Transducer

Electrostatic transducers, with the exception of electret types, require a constant dc bias for proper operation. The following analysis applies for the transducer when used as a transmitter. The force exerted on a transducer diaphram of area A (if fringing effects are neglected) is [37,46]:

$$F = \frac{V^2 \varepsilon A}{2d^2} \qquad (3.1)$$

V; VOLTAGE BETWEEN TRANSDUCER PLATE & METAL FILM
ε; DIALECTRIC CONSTANT.
d; ELECTRODE SPACING.

where v is the voltage between the transducer plate and the metal film, ξ is the dialectric constant, and d is the electrode spacing. The force is proportional to the square of the input voltage. An ac input signal produces a forcing function which is a rectified version of the input. This effect is compensated by adding a high-voltage dc bias (V_b) to the input signal.

$$F = k(V_b + V_s)^2 \quad ; \quad k = \frac{\xi A}{2d^2} \tag{3.2}$$

$$F \propto V_b^2 + 2V_b V_s + V_s^2 \tag{3.3}$$

If $V_b \gg V_s$, the dominant time-varying term in equation 3.3 is $2V_b V_s$, and the output waveform does not suffer from rectification as before. In the receiving mode, a constant charge is maintained between the backing plate and the diaphragm. Any force changes incident on the diaphragm produce displacements which are translated into potential changes at the transducer output because displacement changes the capacitance.

The Oxford transducers produce reasonable transmit/receive waveforms when driven by 60Vpp signals (maximum) and biased at 220 volts. Laboratory tests showed that exceeding either limit caused increased distortion. All tests using electrostatic transducers follow these operating limits. Frequency response tests on all transducers utilized in this thesis are located in Appendix E.

The biasing voltage is provided by the power supply shown in Appendix A. The supply consists of a 555 timer wired as a 100kHz oscillator with approximately 50% duty cycle. The oscillator controls the transistor which switches current through the step-up transformer. The transformer output is rectified, filtered, and sent to the

electrostatic transducers.

3.3 RECEIVER/AMPLIFIER

The receiving amplifier is divided into two sections: One section is located in the transducer module, and serves as one-half of a cascode gain stage. The other section is located on the main component board and serves as the other half of the gain stage followed by a voltage follower. The cascode circuit allows the transistor in the transducer module to 'see' a low-impedance load, which reduces the effects of both cable and collector-to-base capacitance, increasing the high-frequency response. Circuit gain is approximately 140 at ultrasonic frequencies.

3.4 FREQUENCY CHANGING (MIXING)

The frequency-changing is done by the MC 1496 balanced multiplier ic. The multiplier has provisions for balanced inputs for both input signals, and balanced outputs for the product. The multiplication is accomplished by allowing one input to control the current sources of a differential amplifier (the other input), thus causing the gain to vary as a function of the current source control voltage. The balanced output is converted to unbalanced form via one section of the 324 quad op-amp. The signal available at the op-amp output consists of the sum and difference frequency terms as listed in equation 2.5. This signal is then passed to the frequency comparison section.

3.5 FREQUENCY COMPARISON

The frequency comparison section takes advantage of the fact that a bandpass filter output has zero phase shift at its center frequency, and lags or leads the input as the input frequency goes higher or lower than

the filter's center frequency. The method of producing a dc error signal from an input frequency is shown in figure 3.3. The mixer output is sent to a bandpass filter which has its center frequency the desired difference frequency. The mixer output is also sent through a phase shifter which shifts the phase of the difference frequency by 90 degrees. The difference frequency used in this system was 5 kHz and the filter bandwidth was 1 kHz.

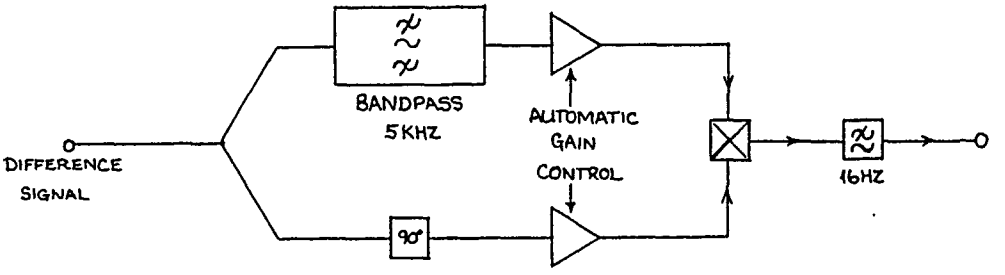

FIGURE 3.3 Frequency Comparison Section

Both signals are then passed through automatic gain control(AGC) stages in order to limit the magnitude of inputs to the analog multiplier. Following multiplication, the signal is low-pass filtered so as to leave only a term which will be a function of the difference between the filter center frequency and difference frequency. Equations 3.4, 3.5, 3.6, and 3.7 represent bandpass, phase shift, multiplier, and low-pass filter outputs. The filter output consists of a dc term which represents the difference in frequency between the incoming signal and the filter center frequency.

$$f_{BPF}(t) = A\cos(\omega_i t + \alpha) \qquad (3.4)$$

where α is the frequency dependent phase shift mentioned earlier.

$$f_{PS}(t) = B\cos(\omega_i t + 90°) \tag{3.5}$$

$$M(t) = \frac{AB}{2}\left\{\cos(2\omega_i t + \alpha + 90°) + \cos(\alpha - 90°)\right\} \tag{3.6}$$

$$f_{LPF}(t) = \frac{AB}{2}\cos(\alpha - 90°) = \frac{AB}{2}\sin\alpha \tag{3.7}$$

Two automatic gain control stages have been inserted between the filter and phase shift outputs and the multiplier input. This was required due to the fact that the MC 1496 multiplier places tight constraints on the input amplitude of the signal. The gain control stages insure that the input signal meets these requirements. The MC 1496 multiplier is used for the analogue multiplication, and is followed by a current to voltage converter stage which also provides an unbalanced output. The low-pass filter has a -3dB point located at approximately 16 Hz. The filter output is sent to the controller input.

3.6 RAMPING RATE CONTROLLER

The ramping rate controller consists of input buffer stage to isolate the previous passive filter followed by an inverter stage wired as shown on page A4. The transfer function of the inverter stage consists of a term which is directly proportional to the present value of the input signal, and a term which is proportional to the value of the integral of past input values. Equation 3.8 is the controller transfer function. The component values chosen for the controller stage were not chosen to maximize controller gain or to provide optimum integrator time constants, they were chosen to provide a workable first attempt at system control. The controller output is scaled and offset by the following

stage. The positive/negative voltages output from the controller stage are converted into negative voltages for use by the ramping generator.

$$\frac{V_o}{V_i} = -\left\{\frac{sC_1R_1+1}{sC_1R_2}\right\} = -\left\{\frac{R_1}{R_2} + \frac{1}{sC_1R_2}\right\} \qquad (3.8)$$

PROPORTIONAL TERM

INTEGRAL TERM

3.7 RAMP GENERATOR

The ramp generator consists of three 324 stages: integrator, comparator, and inverter. The integrating stage accepts the controller input and produces a positive voltage ramp until its output voltage exceeds the reference voltage of the comparator stage (approximately 4 volts). When this voltage is exceeded, a transistor discharges the integrating capacitor, the comparator is reset, and the integrating process begins again. The output of the integrating stage is also sent to the VCO input to provide the VCO ramping control voltage. Ramp output ranges from 0 to approximately 4.2 volts.

3.8 RANGE READOUT

As shown in Chapter Two the control voltage varies inversely with range and cannot be directly used as a measure of range. Direct range measurements require an actual count of the transmitter cycles during one ramp cycle. During ranging operation, the ramping is continuous, and the counter outputs would change too rapidly to be seen. Also, the ramp frequency varies from approximately 89 to 222 Hz for targets located in the range from 100-250 cm, requiring an interface to cause only every 100th ramp to be counted. The interface/controlling circuitry performs the following functions: counts the transitions of the comparator section of the ramping generator and marks each one- hundred counts,

holds the counter input active during the hundredth count ramp, and latches final count to the output display when the count is complete. This method of range readout is obviously a compromise. A more accurate system would count over many ramping periods and average the results.

SECTION II - FMCW TRACKING SYSTEM RANGING TESTS

3.9 FMCW TRACKING SYSTEM TESTS - LOW NOISE

The FMCW system was range tested using a 19.5 mm disc as target and noting both control voltage and counter output as a function of target distance. Table 3.1 lists ramp control voltage vs range system test result, and Figure 3.4 shows the results in graph format. The ramp control voltage follows the inverse range relationship shown in eq 2.32.

RANGE (cm)	RAMP CONTROL VOLTAGE
80	-3.69
90	-3.29
100	-3.04
110	-2.78
120	-2.55
130	-2.37
140	-2.23
150	-2.07
160	-1.95
170	-1.84
180	-1.73
190	-1.65
200	-1.58
210	-1.50
220	-1.44
230	-1.39

Table 3.1 - FMCW Tracking System, Ramp Control Voltage vs Range

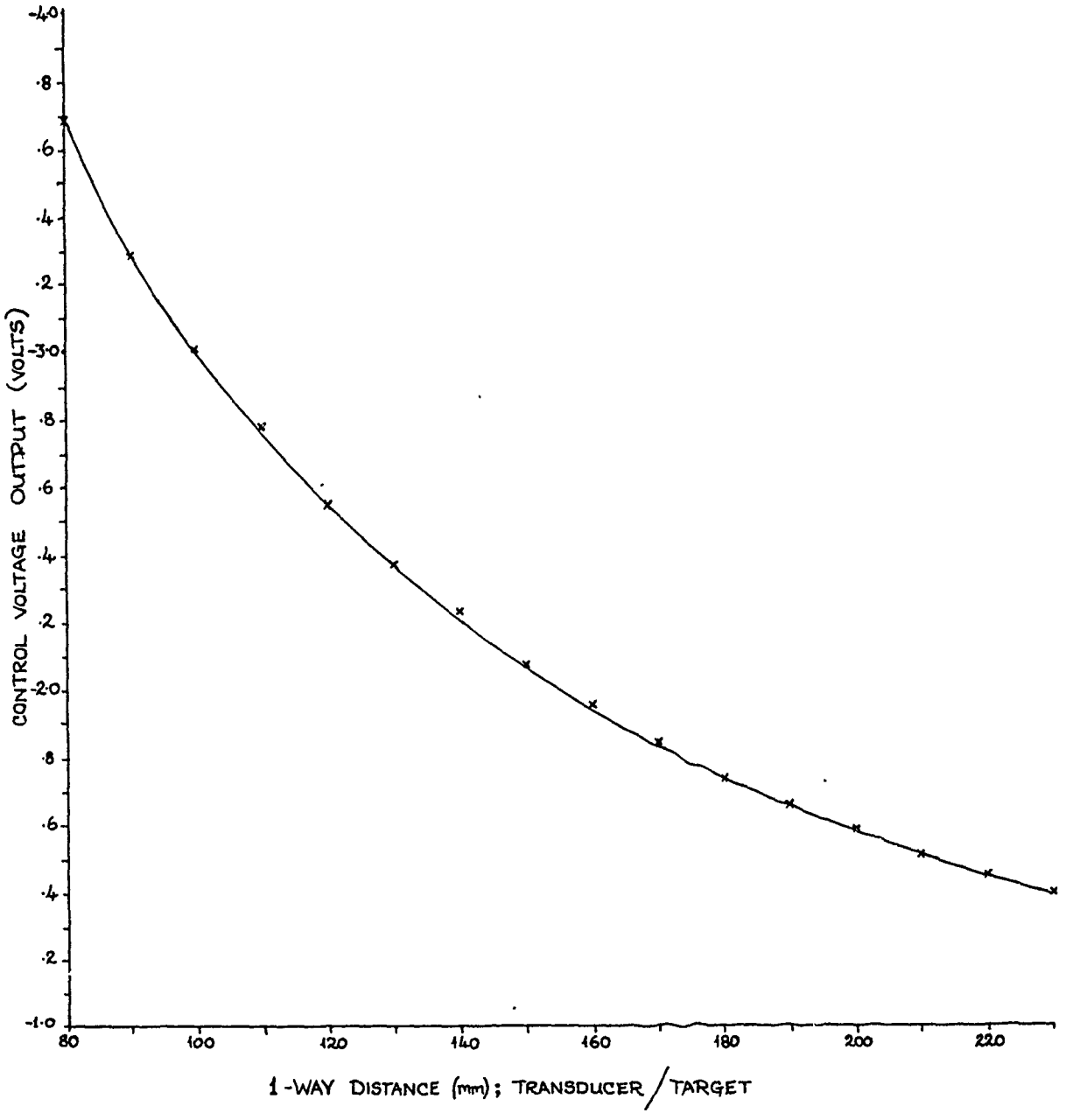

FIGURE 3.4 F.M.C.W. TRACKING SYSTEM, RAMP CONTROL VOLTAGE VS. RANGE

Theoretical count values were obtained by substituting system parameters into equation 2.35. The relationship obtained for the number of counts (C) as a function of range r (in cm) is:

$$N = 32.3r \qquad (3.9)$$

where B_{fm} =240.65 krad/s, ω_d = 31.42 krad/sec, and ω_0 =571.14 krad/s. The experimental system uses a negative ramp. That is, $\omega_0 > \omega_1$. Therefore, the sign of the B_{fm} term in equation 2.35 is negative for this system.

Theoretical and actual test values are contained in Table 3.2. The agreement between theoretical and actual count ranged from within 1% for the 10-15 cm range to 7% for the 25 cm range. While these figures indicate that the system is operating correctly, they contain far too much error to be used as an accurate measuring system. The counter output varied $\pm$ 3 counts while performing ranging on a stationary target. This variation could be reduced by attention to the ramping generator, VCO, and loop characteristics. As the circuit is designed, the ramping generator is not immune to small variations in the power supply, thus introducing ramp nonlinearities as a function of power supply voltage. Also, the VCO operates asynchronously from the ramping circuit, introducing another source of count variation. Finally, the loop gain chosen for the test system was done in a very informal manner. Closer attention to all stage gain parameters would allow a higher loop gain. In addition, the frequency comparator stage was an obvious first attempt, and its design could be improved so as to provide a more linear operation at the center of the filter bandpass. However, the system operation was judged sufficient to allow the prototype system to be tested for noise

effects.

RANGE (cm)	COUNT (theoretical)	COUNT (measured)
7.5	242	255
10.0	323	327
12.5	404	400
15.0	485	479
17.5	565	555
20.0	646	627
22.5	727	693
25.0	808	752
27.5	888	856

Table 3.2 - FMCW Tracking System, XMTR Count vs Range

3.10 FMCW TRACKING SYSTEM TEST - HIGH NOISE

The FMCW system was installed on an ASEA IRB-6 industrial robot and adjusted to measure distance to a flat-plate target which was to be MIG (metal, inert-gas) welded. The control voltage output was used as a range indicator for this test, as the goal of the test was an evaluation of the noise-immune properties of the system. The transducer module was attached to the welding torch as shown in figure 3.5, and the robot was programmed to move the torch in the route shown in figure 3.6. The ramping rate control voltage was used to determine noise immunity. The ramping rate control signal was attached to the y-axis of the chart recorder and the control voltage was recorded as a function of time.

A typical test result is shown in figure 3.7. The first portion of the output shows a 'dry run' in which the robot/transducer assembly was moved over the targets, but the current to the welding torch was not activated. In the second portion of the graph welding current is applied,

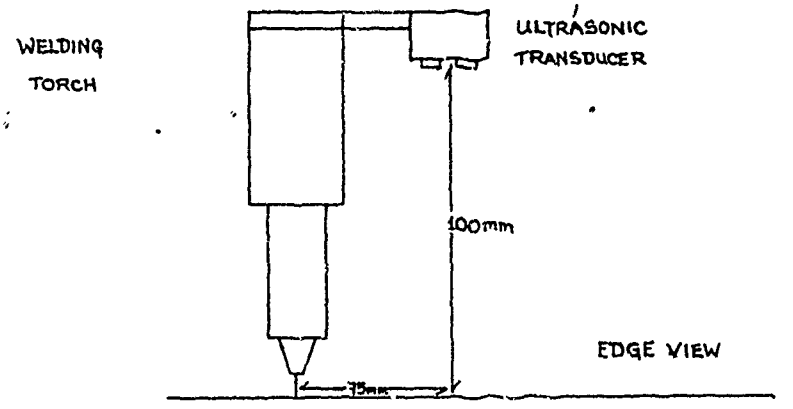

FIGURE 3.5 F.M.C.W TRACKING SYSTEM NOISE TEST, TORCH SET UP.

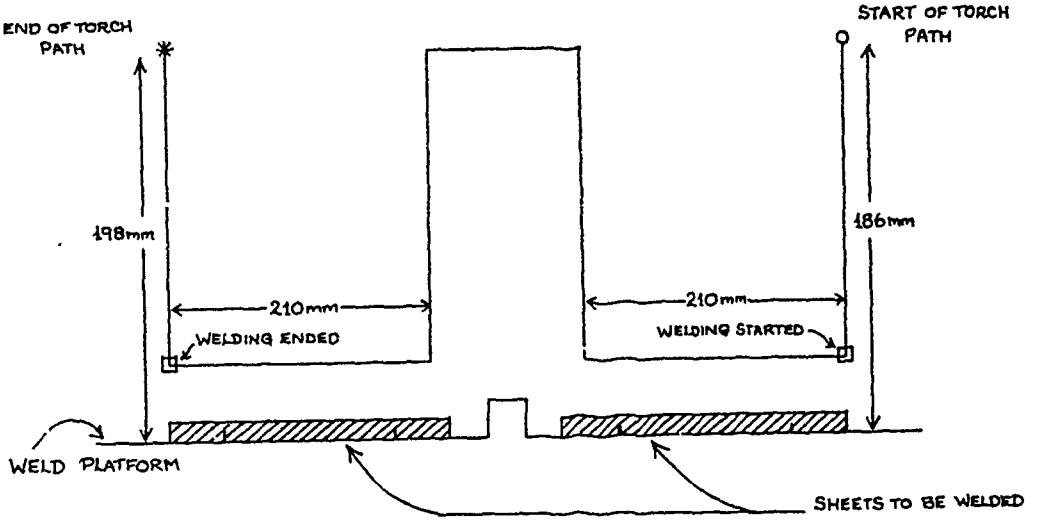

FIGURE 3.6 F.M.C.W. TRACKING SYSTEM NOISE TEST, TORCH ROUTE.

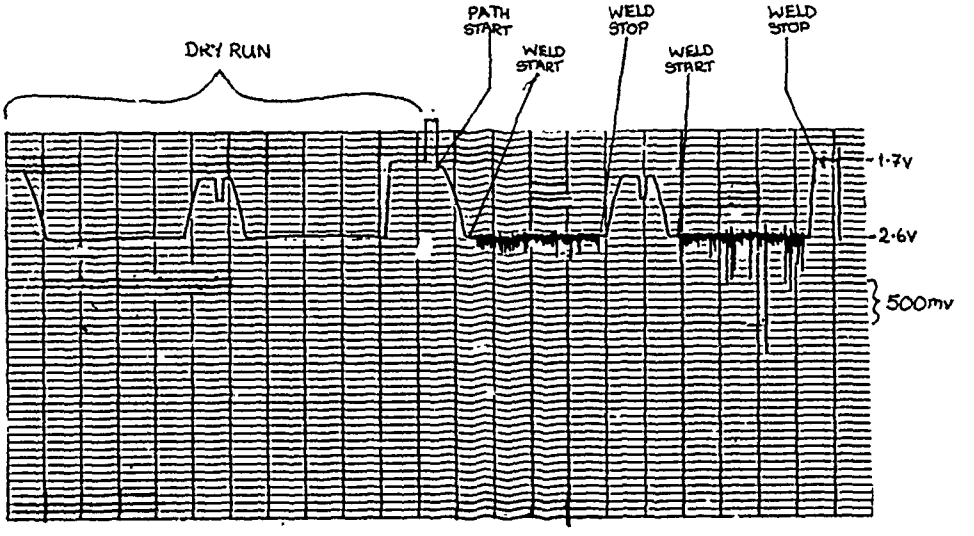

FIGURE 3.7 F.M.C.W TRACKING SYSTEM NOISE TEST.

the metal pieces were welded, and the ramping control voltage was recorded as before. The welding inteference detected on the second portion of figure 3.7 is noticible, with approximately 300mv peaks on sheet one, and occasional 600-1000 mv peaks on sheet two. Contrast this performance with figure 3.8, which is the range output of a conventional FMCW system used in a similar test. The conventional FMCW system used a fixed ramping rate, and obtained range values by converting a zero-crossing count of the difference frequency into a voltage proportional to range. When welding is started, ranging information is completely destroyed by the noise. The ranging information provided by the tracking system, while degraded, is still useful, though not accurate enough to provide more than very low-tolerance ranging information.

3.11 CONCLUSIONS

The results of the low-noise and high-noise tests indicate that an FMCW tracking system is potentially superior to conventional FMCW systems when both are used in high noise environments. Although comparable noise reduction could be obtained in a conventional FMCW systems through narrow bandpass filters, many filters would be required to track a target which changes range. In addition, tracking would involve complex circuitry in addition to the many filters required. The FMCW tracking system contains only one bandpass filter, and target tracking is an integral part of its design.

The ultimate bandpass limitations mentioned in Chapter Two played an important part in the decision to halt development of the FMCW Tracking System, and explore alternate methods of noise-immune ranging. However, the present system performance and accuracy could be improved by

attention to the following details:

1. Linear Ramping rate: Non-linearities in the ramp produce additional frequency modulation, and affect ramping time. The present ramping generator is suceptible to power supply fluctuations, and also to noise in the ramp control voltage.
2. Redesigned frequency comparator section with attention given to producing a linear output function for frequencies close to the center frequency.
3. Adjusting loop gain so that it is at a value which is closer to optimum. The present system was a first attempt at establishing workable loop gains. Also, adjusting the integrator time constant to provide more optimum control characteristics.
4. Lowering the cutoff frequency of the low-pass filter following the frequency comparison stage. The present cutoff of 16 Hz was much higher than needed.

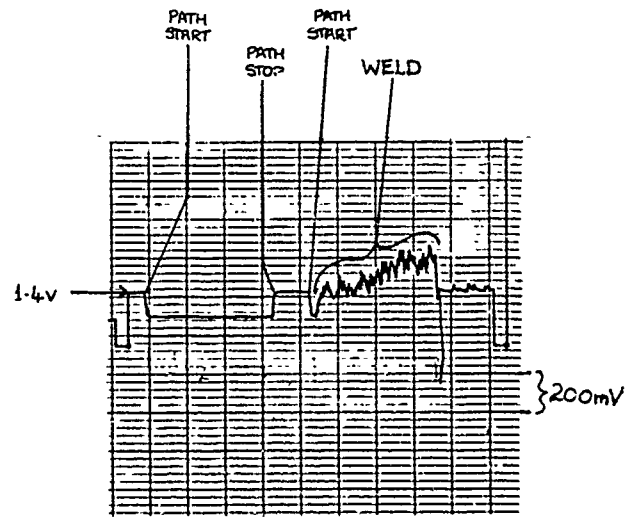

FIGURE 3.8 CONVENTIONAL FMCW. NOISE TEST

CHAPTER 4

RANDOM SIGNAL CORRELATION

Random signal correlation offers potential advantages over pulse and FMCW systems discussed in previous chapters. The advantages lie in the fact that the random nature of the transmitted signals allows 100% duty cycle to be attained, while the correlation of the received signal with delayed versions of the transmitted signal allows the system to operate as a matched filter system; that is, it will maximize the ratio between peak signal power and r.m.s. noise power. Both of these features will allow system SNR to be much higher than for a simple pulse-echo system. Further, there is no theoretical limit to the improvement in SNR available at the output of the integrator, provided one is prepared to wait long enough, and also if the target is stationary.

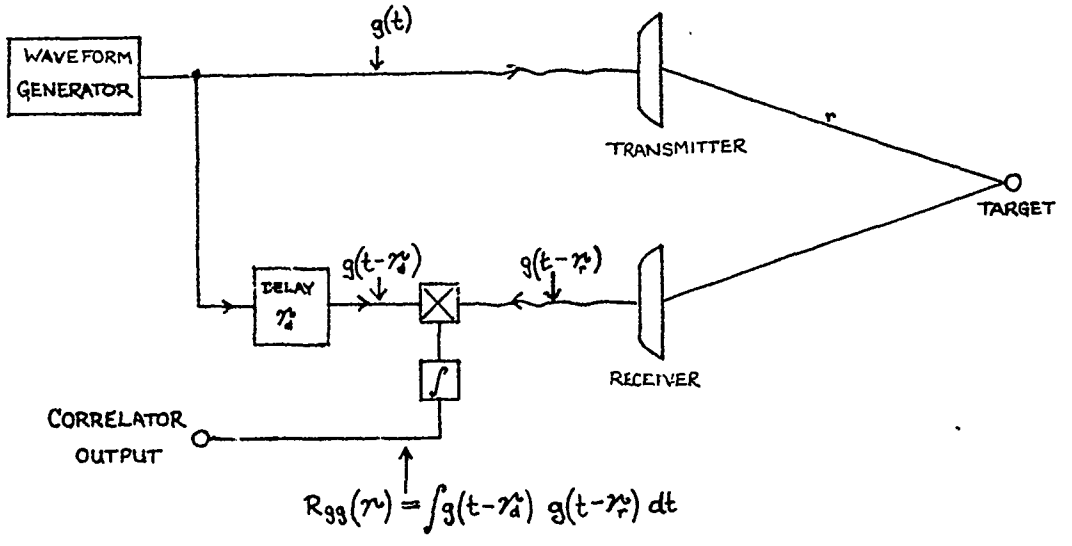

FIGURE 4.1 Random Signal Correlation System

4.1 BASIC CORRELATION SYSTEM OPERATION

The basic random signal correlation system is shown in figure 4.1. In this system, a random signal is transmitted and reflected from the target. The reflected signal is received and multiplied by a delayed version of the transmitted signal. The multiplier output is then summed by the integrator. The integrator will produce a maximum output when the system delay is equal to the target delay. The expression for the cross correlation of two signals is:

$$R_{gg}(\gamma_d, \gamma_r) = \frac{1}{2T}\int_{-T}^{T} g(t-\gamma_d)\, g(t-\gamma_r)\, dt \qquad (4.1)$$

or:

$$R_{gg}(\gamma_\Delta) = \frac{1}{2T}\int_{-T}^{T} g(t')\, g(t'-\gamma_\Delta)\, dt' \quad ; \quad t' = t-\gamma_d\,, \quad \gamma_\Delta = \gamma_r - \gamma_d \qquad (4.2)$$

For purposes of this analysis, all amplitudes have been normalized to one. However, in a real system, received amplitudes will obviously be a function of transmitted signal amplitude, range and target reflectivity. Since the integrator output would theoretically rise without limit when presented with a continuous signal and a target at the correct range, the integrator can be approximated by a low-pass filter which will give a 'short-time' average of the multiplier output. This filtered output can be expressed as:

$$R_{gg}(t, \gamma_\Delta) = \int_{-\infty}^{\infty} g(t-\gamma)\, g(t-\gamma-\gamma_\Delta)\, h(\gamma)\, d\gamma \qquad (4.3)$$

where $h(\gamma)$ is the low-pass filter impulse response.

4.2 GENERATION OF LONG PERIOD SIGNALS WITH SUITABLE CORRELATION FUNCTIONS

A correlation system requires a reference signal which has a precisely definable correlation function, yet which has a period long enough that the correlation function does not repeat itself so often that it cannot be used for ranging. One type of reference signal fulfilling these requirements is pseudo-random binary sequences.

It is possible to configure digital shift registers so that they produce signals which will act somewhat like random noise for purposes of cross-correlation. Such digitally generated sequences are most often referred to as Pseudo-Random Binary Sequences (PRBS). They are also called linear recursive, and binary shift sequences [64]. The simplest method of generating a PRBS is to use a binary shift register which utilizes modulo-2 addition (no carry) of selected cells with the sum being fed back into the shift input in the manner shown in figure 4.2. The register is pre-loaded with a number other than all zeroes and then is clocked at the desired rate.

A binary register of length m has the capability of holding 2^m different states, or values, within the register before any particular combination is repeated. If the values in a binary shift register are combined in a certain way and the resulting value fed back into the register input, it is possible to cause the shift register to attain a number of states which is one less than the maximum number of states. This number is called the maxlength [27] and it is equal to:

$$M = 2^m - 1 \qquad (4.4)$$

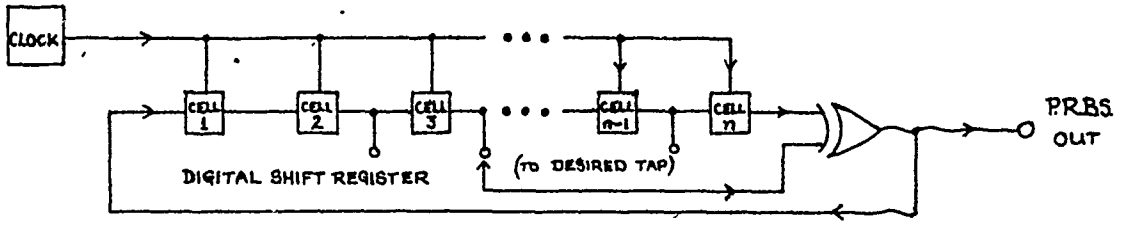

FIGURE 4.2 PRBS. GENERATOR.

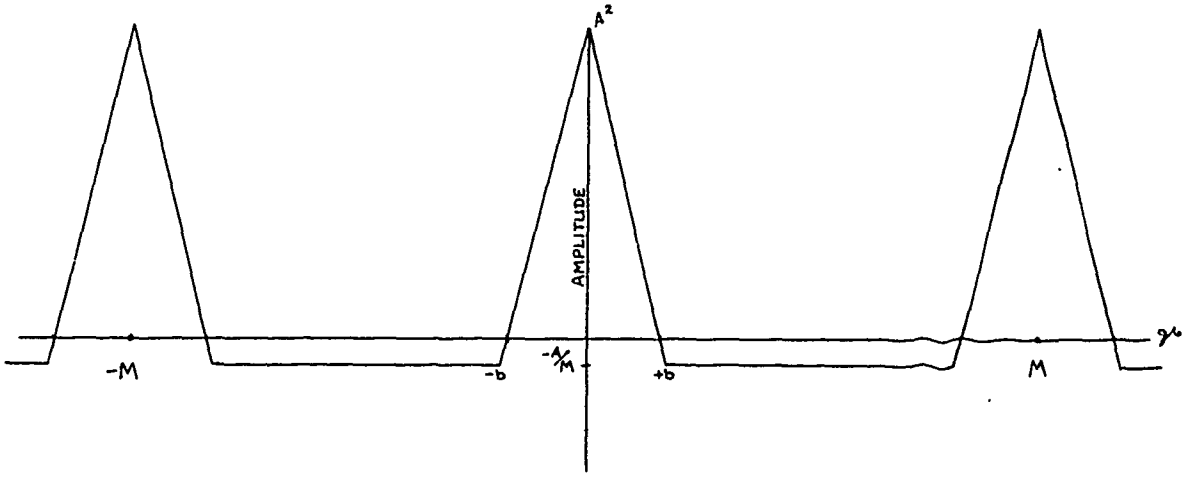

A; AMPLITUDE OF EACH BIT
b; BIT LENGTH (SEC).

FIGURE 4.3 PRBS AUTO-CORRELATION FUNCTION

The reason that the maxlength differs from the maximum number of states is due to the nature of the feedback system chosen. Note from figure 4.2 that the all-zero state could never change once entered. A proper choice of feedback taps will allow a shift register to attain all possible states except for the all zero state before repeating. Horowitz [27] contains a short listing of feedback connections which will produce maxlength sequences from shift registers. PRBS sequences have an auto-correlation function shown in figure 4.3. This correlation function is true only for continuous transmission of the random signals. If transmission is truncated, the correlation function develops sidelobes which are called 'self noise' [19]. There are special pseudo-random codes which do not display self-noise when transmitted in bursts. Among these are Barker Codes [63] and Golay Codes [42]. Since the system described in this thesis transmits continuously, the problem of self-noise will not be considered.

4.3 SPECTRA OF DIGITALLY GENERATED NOISE

The correlation function shown in figure 4.3 is valid only if the signals which are transmitted and received are not changed in any way by the ranging system. If the transmitted signal is not to be degraded seriously, the system bandwidth must be equal to or greater than the signal bandwidth. Therefore, the power spectra of PRBS noise must be investigated.

Since the auto-correlation function is the Fourier transform of the power spectral density [70], the PRBS spectrum can be evaluated from figure 4.3. It can also be directly evaluated from the PRBS sequence by taking the Fourier transform of the sequence. Although, strictly

speaking, a periodic function is described by a Fourier Series, the random binary sequence can be hypothesized to be non periodic and of arbitrary length 2T, with bit length b. This hypothesis allows the Fourier transform description of the sequence:

$$F(j\omega)=\frac{1}{\sqrt{2T}}\int_{-\infty}^{\infty} f(t)e^{-j\omega t}dt = \int_{-T}^{T} f(t)e^{-j\omega t}dt \qquad (4.5)$$

where $\sqrt{2T}$ is a normalizing factor to make amplitude independent of length.

Since f(t) consists of 2T/b discrete periods where the amplitude is ±A, equation 4.5 can be altered to the following:

$$F(j\omega)=\frac{1}{\sqrt{2T}}\sum_{i=-T/b}^{T/b}\int_{t_i-b/2}^{t_i+b/2} A_i e^{-j\omega t}dt \qquad (4.6)$$

where $A_i = \pm A$ as appropriate, and t_i = bit centre.

$$F(j\omega)= \left\{\sum_{i=-T/b}^{T/b} bA_i e^{-j\omega t_i}\right\} \frac{\sin \omega b/2}{\omega b/2} \qquad (4.7)$$

Since the value of A is random, the bracketed term can be written as:

$$\left\{\sum_{i=-T/b}^{T/b} A_i e^{-j\omega t_i}\right\} = \sqrt{\frac{2T}{b}}\ A e^{j\phi(\omega)} \qquad (4.8)$$

where the root term is the expected amplitude of 2T/b terms of amplitude ±A and random phase where $\phi(\omega)$ is a random phase function. Equation 4.7 becomes:

$$F(j\omega) = A\sqrt{\frac{2T_b}{2T}}e^{j\phi(\omega)}\frac{\sin \omega_b/2}{\omega_b/2} = A\sqrt{b}\ e^{j\phi(\omega)}\frac{\sin \omega b/2}{\omega b/2} \qquad (4.9)$$

Since f(t) is in fact periodic, the actual spectrum will consist of

discrete frequencies spaced at integer sub-intervals of the register clock frequency f_c as shown in equation 4.10 [27].

$$F_N = \frac{f_c N}{M} \qquad N = 1, 2, 3.... \tag{4.10}$$

The power spectrum is $F^2(j\omega)$ and the envelope of the discrete spectrum is shown in figure 4.4.

Note that the half-power point is located at approximately 45% of the clock frequency, and that the main portion of the signal energy lies within the first zero crossing of the power spectrum, which is located at the clock frequency. Thus, a system of bandwidth equal to or greater than ω_c will pass the PRBS pulses with essentially no distortion.

4.4 METHODS FOR ALTERING THE CORRELATION FUNCTION

While a ranging system having the correlation function shown in figure 4.3 would allow range to be calculated, additional time and complexity is required in order to resolve the ambiguity caused by the fact that a given cross- correlation value may be produced by one of two delay values, as is shown in figure 4.5. In order to resolve this ambiguity, the ranging system would be required to change the relative delay time in some manner and note the results. This could be time consuming.

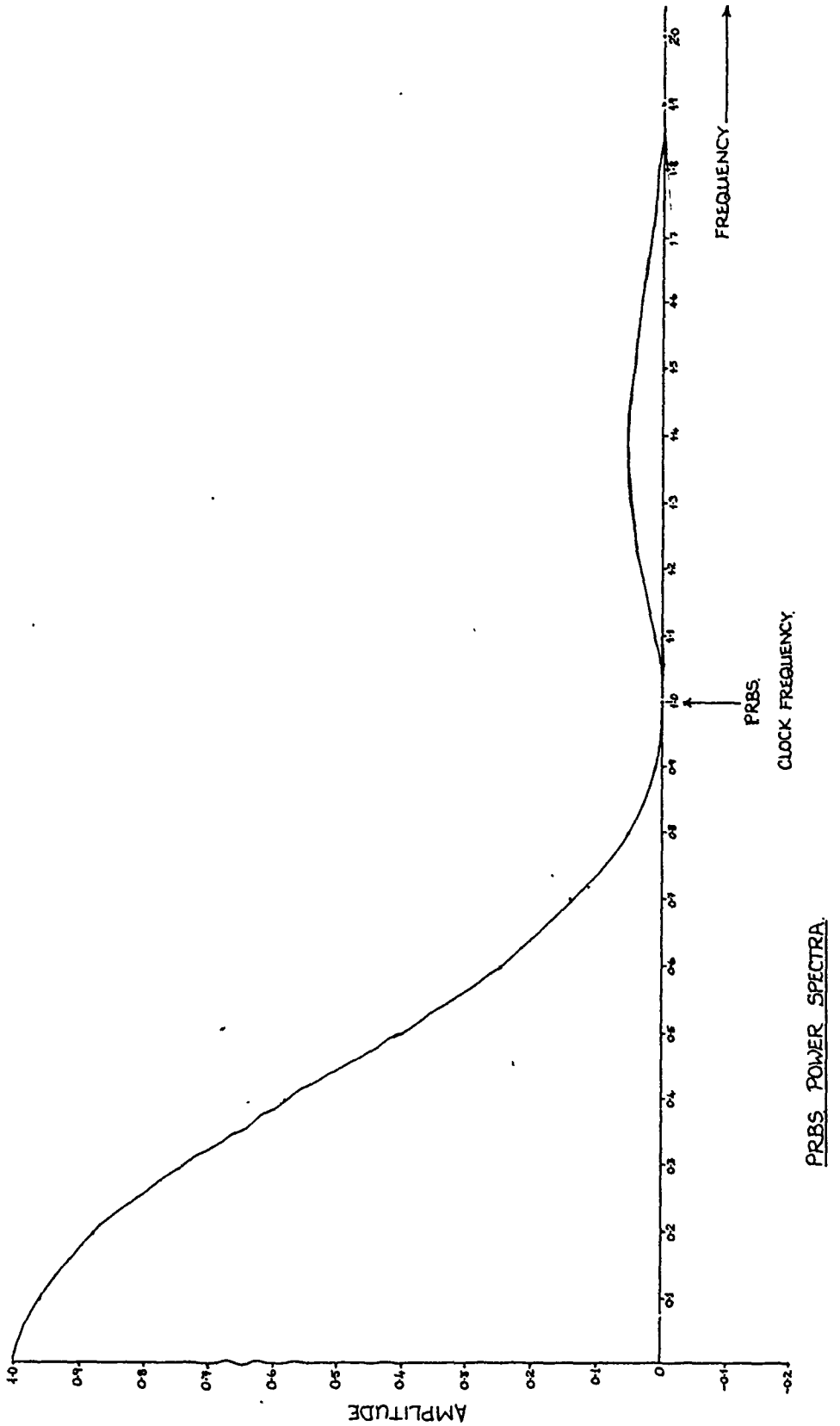

FIGURE: 4.4 PRBS POWER SPECTRUM, ENVELOPE

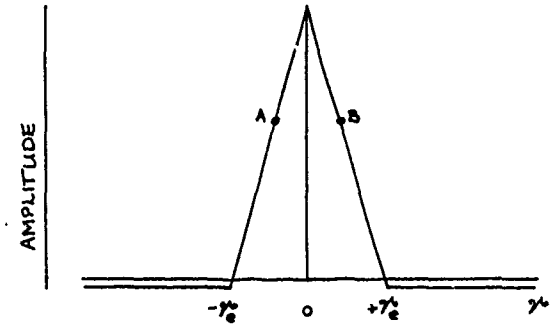

POINT A CORRELATION FUNCTION FOR ERROR OF $-\gamma_e'$.
POINT B CORRELATION FUNCTION FOR ERROR OF $+\gamma_e'$.

FIGURE 4.5 Ambiguities in the Auto-Correlation Function

If cross-correlation is to be used for control purposes, a more desirable function would be that shown in figure 4.6. With this modified function, a positive range error will produce a correlation output of one polarity, and a negative range error will produce a correlation output of the opposite polarity. This modified function is an 'odd' function, that is: $f(-\gamma')=-f(\gamma')$. Like this, it could be used as a direct input to the corrective circuitry. In order to achieve this modified correlation function, either the transmitted or the delayed comparison signal must be changed in some manner.

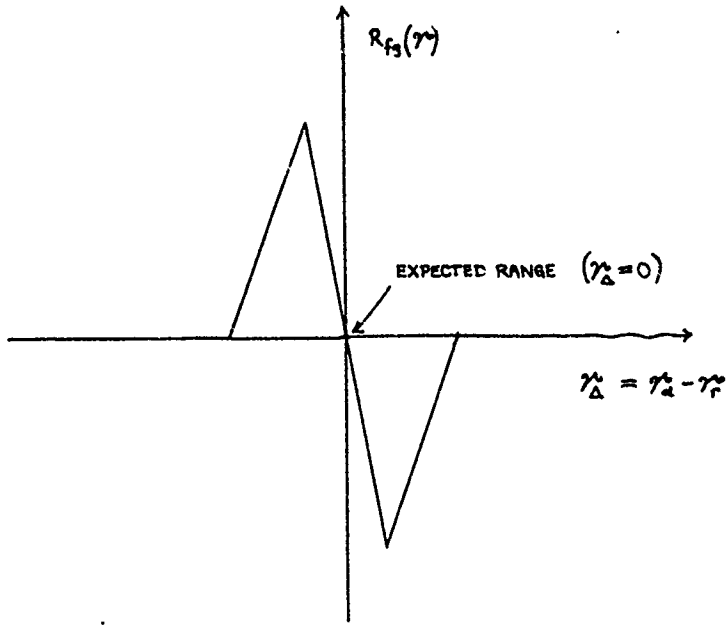

FIGURE 4.6 Desired Cross-Correlation Function

One method of determining the form of signal modification needed to produce a cross-correlation function such as that of figure 4.6 is to examine the cross-spectral density of the correlation function. Let f(t) and g(t) be two signals which are to be cross-correlated. As before, these signals will be random, not necessarily identical, and of arbitrarily long period 2T. The signals then each have Fourier transforms which we will define in a slightly inconventional way as:

$$F(j\omega) = \frac{1}{\sqrt{2T}} \int_{-T}^{T} f(t) e^{-j\omega t}\, dt \qquad (4.11)$$

$$G(j\omega) = \frac{1}{\sqrt{2T}} \int_{-T}^{T} g(t) e^{-j\omega t}\, dt \qquad (4.12)$$

The ($\sqrt{2T}$) term is added as a normalizing factor and will become clear in the following text. The time functions f(t) and g(t) can be expressed as the inverse Fourier transform of their respective frequency functions:

$$f(t) = \frac{\sqrt{2T}}{2\pi} \int_{-\infty}^{\infty} F(j\omega) e^{j\omega t} d\omega \qquad (4.13)$$

$$g(t) = \frac{\sqrt{2T}}{2\pi} \int_{-\infty}^{\infty} G(j\omega) e^{j\omega t} d\omega \qquad (4.14)$$

Referring to equation 4.2:

$$R_{fg}(\nu) = \frac{1}{2T} \int_{-T}^{T} f(t)\, g(t-\nu)\, dt \qquad (4.15)$$

$$= \frac{1}{2T} \int_{-T}^{T} g(t) \left\{ \frac{\sqrt{2T}}{2\pi} \int_{-\infty}^{\infty} F(j\omega) e^{j\omega(t-\nu)} d\omega \right\} dt \qquad (4.16)$$

Rearranging the integration order of eq 4.16, we find:

$$R_{fg}(\nu) = \frac{1}{2\pi} \int_{-\infty}^{\infty} F(j\omega) e^{-j\omega\nu} \left\{ \frac{\sqrt{2T}}{2T} \int_{-T}^{T} g(t) e^{j\omega t} dt \right\} d\omega \qquad (4.17)$$

$$= \frac{1}{2\pi} \int_{-\infty}^{\infty} F(j\omega)\, G(-j\omega)\, e^{-j\omega\nu} d\omega \qquad (4.18)$$

This is an expression for the cross spectral density of the two functions. Since the correlation function $R_{fg}(\nu)$ is real,

$$R_{fg}^{*} = R_{fg} \qquad (4.19)$$

where * denotes the complex conjugate. We can then say:

$$R_{fg}(\nu) = R_{fg}^{*}(\nu) = \frac{1}{2\pi} \int_{-\infty}^{\infty} F(-j\omega)\, G(j\omega) e^{j\omega\nu} d\omega \qquad (4.20)$$

Thus, the cross-correlation function $R_{fg}(\nu)$ is the inverse Fourier transformation of the product of the two spectral densities (or the cross spectral density) of the two random functions. Conversely, the cross spectral density function must be the Fourier transfo.. of the

cross-correlation function.

$$S_{fg}(j\omega) = \int_{-\infty}^{\infty} R_{fg}(\tau) e^{-j\omega\tau} d\tau \qquad (4.21)$$

where

$$S_{fg}(j\omega) = F(-j\omega)\, G(j\omega) \qquad (4.22)$$

The desired shape of $R_{fg}(\tau)$ is odd, as in figure 4.5. Re-writing eq 4.21 in sinusoidal form:

$$S_{fg}(j\omega) = \int_{-\infty}^{\infty} R_{fg}(\tau) \left\{ \cos \omega\tau - j \sin \omega\tau \right\} d\tau \qquad (4.23)$$

If $R_{fg}(\tau)$ is odd, the $\cos(\omega\tau)$ term drops out, and the equation may be reduced to:

$$S_{fg}(j\omega) = 2j \int_{0}^{\infty} R_{fg}(\tau) \sin \omega\tau \, d\tau = F(j\omega)\, G(j\omega). \qquad (4.24)$$

Equation 4.24 gives a method for determining the required cross-spectral density function knowing the general shape of the required cross-correlation function. Since $S_{fg}(jw)$ is imaginary for all w, the two functions $F(j\omega)$ and $G(j\omega)$ must be ninety degrees out of phase with each other throughout the frequency domain. In other words, an odd cross-correlation function will be obtained if the two signals to be cross-correlated have the following frequency relationship:

$$\text{Arg } F(j\omega) - \text{Arg } G(j\omega) = \pm 90^{\circ} \qquad (4.25)$$

Given one waveform, there are many ways of obtaining this phase shift in a related waveform. Among them are:

1. Differentiate or integrate an odd number of times.

2. Hilbert transform

3. Phase modulation

4. Time shifting

Items one and two produce ninety degree phase shifts by their very nature. Items three and four can, under certain conditions, also create the desired phase shift. The method selected must provide not only a phase shift, but must also shift the spectrum such that the signal to be transmitted is located in a usable portion of the transducer bandpass.

Since the cross-correlation function relies on the cross- spectral density of f(t) and g(t), there must also be large areas of overlap if significant energy is to be located within the overlap region. As was shown earlier, the basic PRBS power spectrum starts at almost 0 Hz and contains the majority of its energy in the band below clock frequency. This signal is therefore not suited for transmission in the ultrasonic region unless the clock frequency is made much greater than the transducer operating frequency. However, if this is done, the bandwidth of the transmitted signal will be too great for undistorted transmission. The next section will examine methods for raising the PRBS spectrum to the ultrasonic region while simultaneously shifting the phase by the required ninety degrees.

4.5 METHODS OF PRBS FREQUENCY/PHASE SHIFTING

Method one, that of differentiating or integrating an odd number of times, will produce the required phase shift. It will also change the PRBS spectrum, emphasizing higher frequencies in the case of differentiation, and lower frequencies in the case of integration. However, the spectral changes are not sufficient for operating in the unltrasonic range, and these methods were judged to be unsuitable for further development. Method two, the Hilbert Transform, while providing the required phase shift, does not shift the frequency, and is also difficult to implement. It was also discarded. The remaining methods show some promise.

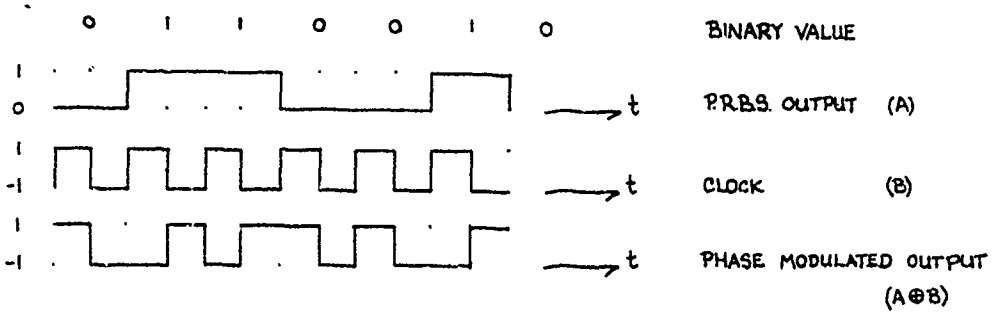

FIGURE 4.7 PRBS Phase Modulation

Method three, phase modulation, refers to a specific form of modulation by the PRBS signal in which each bit of the original sequence is replaced by one complete cycle of either positive or negative phase [63]. For example, for a 'one' (or positive) output of the PRBS shift register, the phase-modulator output is (+1,-1), while for 'zero' (or negative) PRBS output, the output would be (-1,+1). A sample of a PRBS

and phase-modulation by a square wave of the same frequency as the PRBS clock is shown in figure 4.7. The PRBS output is represented as digital (0,1) values, but the phase modulator output is represented as bipolar (+1,-1) outputs which would be sent to a transmitting transducer.

If a PRBS of amplitude ± A is multiplied by the clock frequency of amplitude B, equation 4.12 can be modified as follows:

$$G(j\omega) = \frac{1}{\sqrt{2T}} \sum_{i=-T/b}^{T/b} \left\{ \int_{t_i - b/2}^{t_i} \frac{A_i}{A} B e^{-j\omega t} dt + \int_{t_i}^{t_i + b/2} -\frac{A_i}{A} B e^{-j\omega t} dt \right\} \qquad (4.26)$$

$$= \frac{1}{\sqrt{2T}} \frac{B}{A} \sum_{i=-T/b}^{T/b} A_i \frac{e^{j\omega t_i}}{-j\omega} \left\{ 2 - e^{j\omega b/2} - e^{-j\omega b/2} \right\} \qquad (4.27)$$

$$G(j\omega) = jB\sqrt{b}\, e^{j\phi(\omega)} \frac{\sin^2(\omega b/4)}{\omega b/4} \qquad (4.28)$$

$\sqrt{2T}$; NORMALIZING FACTOR.

where $\phi(\omega)$ is a random phase function as in eq 4.8. As can be seen from equation 4.28, the phase has been shifted by ninety degrees compared with the PRBS spectrum, and the phase-modulated spectrum lies around the carrier frequency. This does not present a problem as long as the transducers are able to pass the signal bandwidth, which is now twice that of the original PRBS bandwidth. The power spectrum of a phase-modulated PRBS signal is shown in figure 4.9.

Method four, time shifting modulation, makes use of the time-shifting theorem of Fourier analysis. A signal shifted in time retains the same spectrum, but undergoes a shift in phase as shown in equation 4.29.

$$\mathcal{F}\left\{x(t-t_o)\right\} = X(j\omega)\, e^{-j\omega t_o} \qquad (4.29)$$

where $\mathcal{F}$ denotes the Fourier transform.

Consider a shift register as shown in figure 4.8, having a shift time of bit length b and with the summing amplifier connected to cells (i) and (i-1).

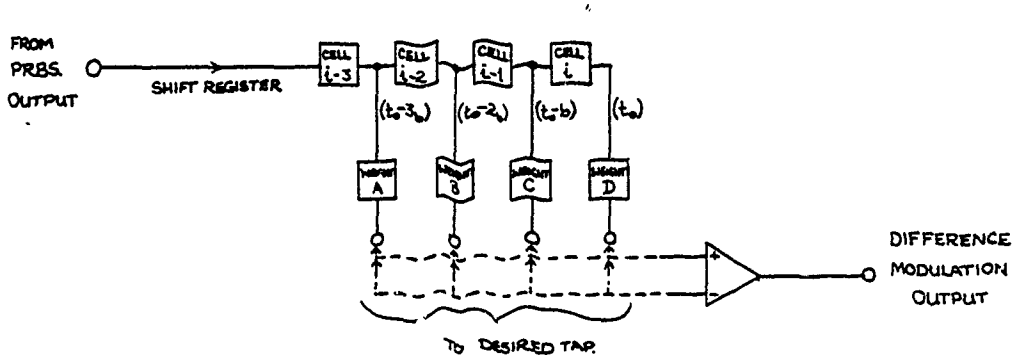

FIGURE 4.8 Time-Shift Modulation

If the zero time shift reference is considered to be halfway between the registers, the resulting output can be expressed as follows:

$$g(t) = f(t + b/2) - f(t - b/2) \tag{4.30}$$

The frequency function is then:

$$G(j\omega) = F(j\omega) e^{j\omega b/2} + F(j\omega) e^{-j\omega b/2} \tag{4.31}$$

$$= F(j\omega) \left\{ 2j \sin \omega b/2 \right\} \tag{4.32}$$

As can be seen in equation 4.32, the phase has been shifted by ninety degrees. Again, the spectrum has been altered. Signals of medium frequency are little affected, but low and high frequency signals will be attenuated. The power spectrum of the function defined by eq 4.32 is shown in figure 4.9. As can be seen from reference to figure 4.9 which shows the power spectra of a PRBS signal, the phase-modulated and one

specific time-shift modulated PRBS power spectra, these two methods do indeed shift the PRBS spectrum to a point where they may be usable by appropriate ultrasonic transducers. These methods will be utilized in the experimental cross-correlation system described in Chapter Five.

4.6 EFFECTS OF TIME-SHIFTING ON CROSS-CORRELATION FUNCTION

The cross-correlation function obtained from the time-shifting method described above will be a mathematically odd function as previously described. Its exact shape could be obtained by taking the inverse Fourier transform of the cross-spectral density of the original PRBS and the time-shifted PRBS, a difficult calculation. It could also be obtained by direct computer calculation of the correlation function. However, a third method will not only yield the cross-correlation function, but also will provide an insight into methods for creating many other cross-correlation shapes, which will prove to be of value in Chapter Six, dealing with advanced correlation systems.

Since the time-shifting system of figure 4.8 is linear, the effect is the same as that of adding the cross-correlation functions which would result from each tap. When the two cross-correlation functions are added, the final cross-correlation function is the superposition of the individual functions, as is shown in figure 4.10. Note that other shapes can be obtained by simply varying the positions of the taps, and also by varying the effect of each tap (the tap weighting). Figure 4.11 shows the calculated cross-correlation function for two separate tap selections. The spectra of the time-shift functions shown in figure 4.11 can be evaluated in a manner similar to that described in eq 4.30 through 4.32.

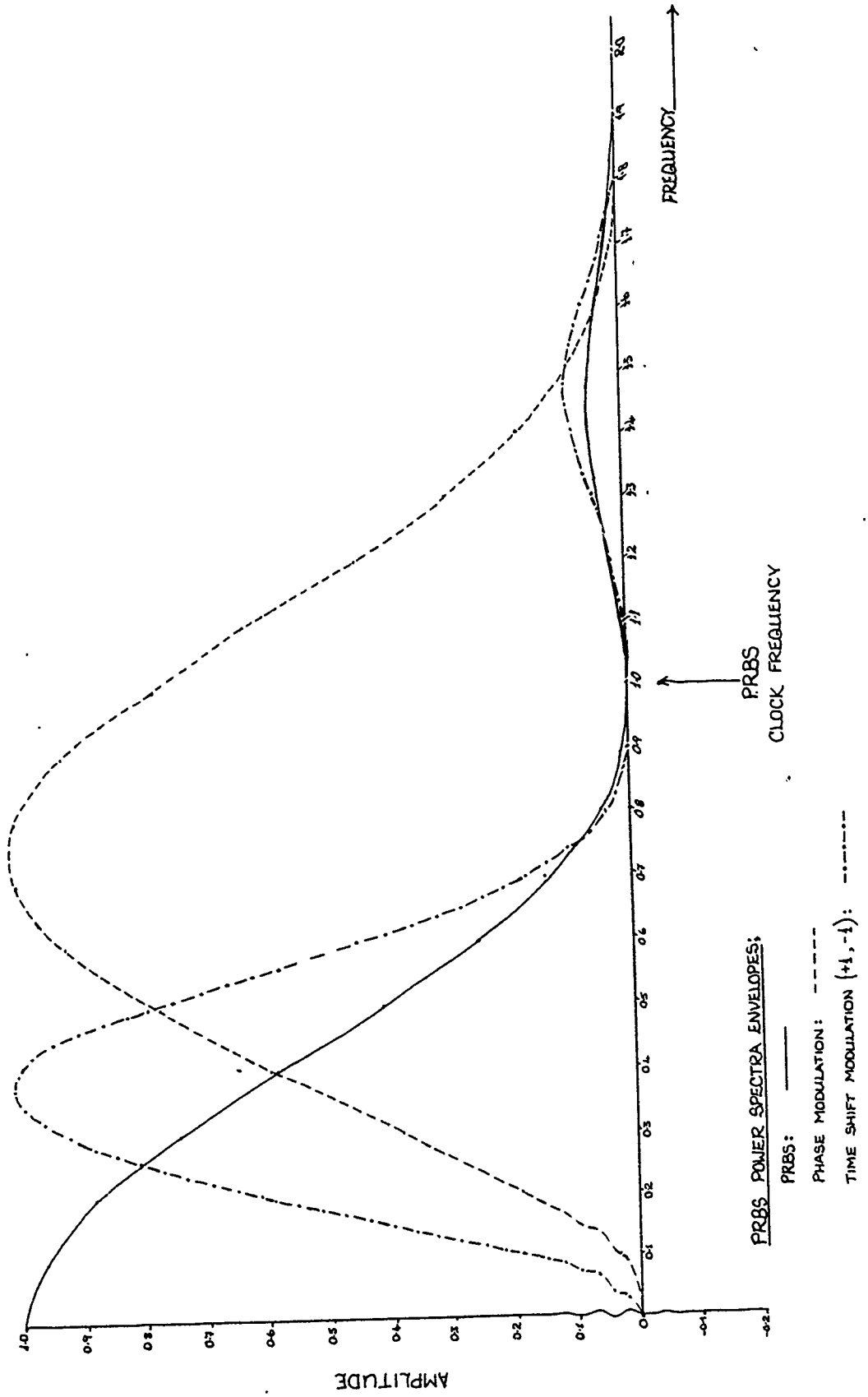

FIGURE: 4.9 PRBS, PHASE MODULATION, TIME SHIFT MODULATION POWER SPECTRA

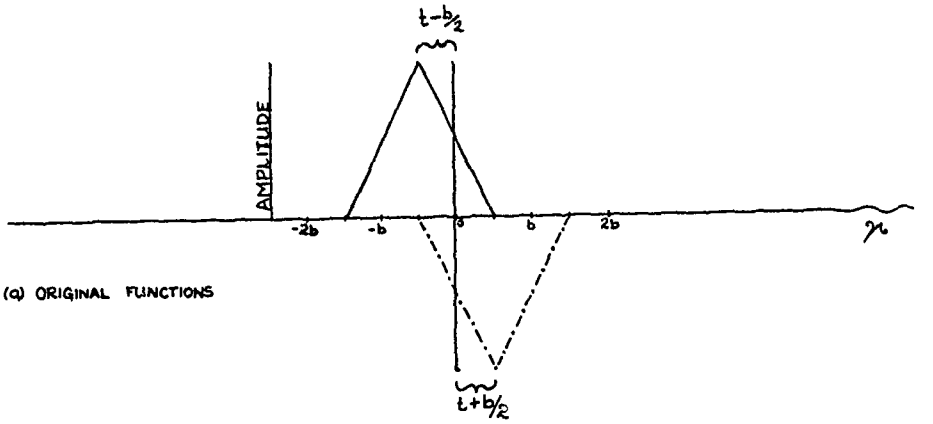

(a) ORIGINAL FUNCTIONS

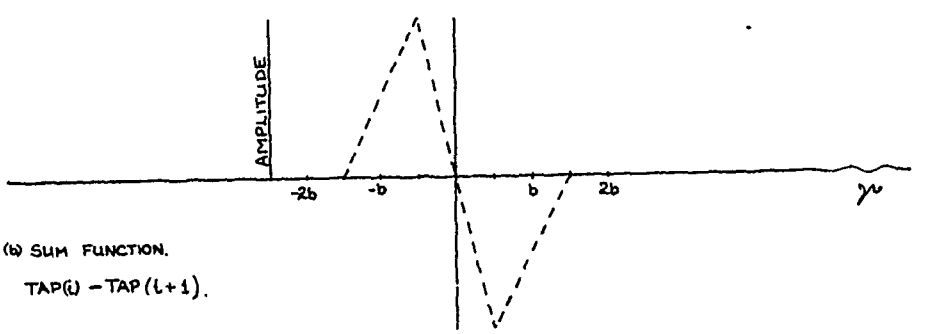

(b) SUM FUNCTION.

TAP(i) − TAP(i+1).

FIGURE: 4.10 CROSS CORRELATION FUNCTIONS, TIME-SHIFT MODULATION

$\left\{ \text{TAP}_i\,(\omega t^{tap} = +1)\,,\ \text{TAP}_{i+1}\,(\omega t^{tap} = -1) \right\}$

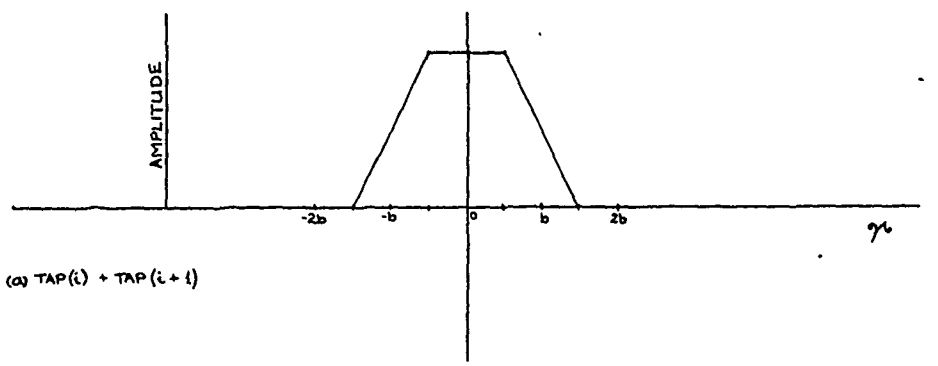

(a) TAP(i) + TAP(i+1)

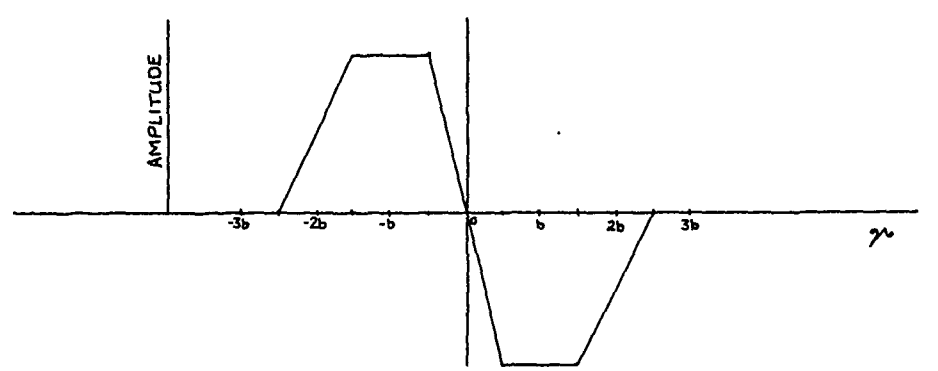

(b) TAP(i-1) + TAP(i-2) - TAP(i+1) - TAP(i+2)

FIGURE; 4.11 TIME-SHIFT CROSS CORRELATION FUNCTIONS.

4.7 RANGE RESOLUTION, RANDOM SIGNAL CORRELATION SYSTEM

The range resolution of a random signal correlation system is a function of the width of the correlation function. Targets located as distances such that the correlation functions would coincide would not be able to be differentiated by the control system. A reasonable assumption concerning the cross-correlation function shown in figure 4.3 would be that a target spacing of a distance equal to that traveled by sound in air during one bit time would be the minimum target resolution, since the original cross-correlation function is two bits wide. This is expressed in eq 4.33. The modified correlation function has a width of 2 bits in the case of phase-modulation and three bits in the case of time-shift modulation (see figure 4.10). Using the same reasoning as before, this yields a range resolution for a phase modulation system which is equal to that of the unmodulated PRBS system, and a range resolution for the time-shifted system which is larger by a factor of 1.5.

Figure 4.9 shows that there is a tight relationship between clock frequency , signal bandwidth, and center frequency. If a transducer has an extremely high centre frequency, the PRBS clock can be adjusted to provide signals around this frequency. However, the bandwidth will increase dramatically, and the transducers will distort the transmitted and received signals unless they are capable of handling this bandwidth. This link between PRBS bandwidth, modulated signal bandwidths, and transducer center frequencies and bandwidths will prove to be a problem with existing systems.

4.8 NOISE REDUCTION CAPABILITIES, RANDOM SIGNAL CORRELATION SYSTEM

Skolnik [64] shows that correlation systems are matched filter systems. As such, a correlation system will maximize the ratio between peak signal power and average noise power. Further, the nature of the PRBS signal is such that the correlation system provides target information continuously, as compared to the basic pulse system, which can provide information concerning each range resolution element only once per pulse repetition cycle [64]. Newhouse [51] has shown that the ultimate signal-to-noise improvement capability of a correlation system can be expressed as:

$$SNRE = B_c T \tag{4.33}$$

SNRE; SIGNAL-TO-NOISE RATIO ENHANCEMENT

Where B_c is the system input bandwidth and T is the time of integration, or time constant of the low-pass filter. Elias [15, 16], Newhouse [50,51], Chapelon [11], and others have demonstrated signal-to-noise ratio enhancement values of over 10,000 using these types of systems. As such, the potentials of a correlation system seem sufficient to merit closer consideration. It seems as if this particular method of providing both matched filtering and 100% duty cycle will provide one of the best chances of achieving a usable signal from a system designed to be operated in the presence of noise and clutter.

4.9 CONCLUSIONS

The results of this chapter can be summarized as follows. Correlation systems offer a potentially useful method of providing high signal-to-noise ratios along with high duty cycles. Digital generation of pseudo-noise is the most efficient and economical method. Such a

noise source is stable, easily delayed, can be made arbitrarily long (if sufficient shift register length is available), and has a readily definable power spectrum. Cross-correlation functions of the type desired for control purposes require shifting the PRBS signal by ninety degrees and cross-correlating this modified signal with the unmodified one. In addition, ultrasonic transducer operating frequencies require shifting the PRBS spectrum to a position more efficiently usable by the transducers. For transducers whose centre frequency is approximately the same as that of the PRBS clock frequency, these considerations are met by two methods of signal modification: phase-modulation, and time-shifting modulation. Both of these methods shall be implemented in the experimental system which will be described in Chapter Five.

CHAPTER FIVE

AN EXPERIMENTAL CROSS-CORRELATING RANGING SYSTEM

Chapter Four showed that random signal correlation systems are able to increase the signal-to-noise ratio by a large amount through filtering and a high duty cycle. Further, it demonstrated methods of digitally generating suitable noise-like signals and how to modify these signals so that their cross-correlation functions would be of desired form. The modifying processes were termed phase-modulation and time-shift modulation. These methods are used in the experimental cross-correlating system described below. The system utilizes the same electrostatic transducers as did the FMCW system as well as another make of electrostatic transducer which was obtained after the FMCW experiments were completed. Both sets of transducers have nominal center frequencies of 60 kHz and -3dB bandwidths of approximately 20 kHz. This chapter describes system construction and testing, along with a modification designed to improve transducer frequency response. The experimental system described in this chapter will be referred to as a Type I System.

Systems similar to the type I system have been used extensively by researchers in the field of non-destructive testing [15,16,38,50,51], as well as in the field of medical ultrasonics [11,54]. Phase modulation, in particular, has been the primary means of placing the PRBS spectrum nearer to the transducer operating frequencies. Although these systems

are widely used and documented, few researchers have attained cross-correlation functions which resemble the theoretical ideal function shown in figure 4.3. This is due to the fact that the transducer bandwidths are not high enough to pass the PRBS signal without significant distortion. This chapter discusses a first attempt at an experimental cross-correlation system which has user selectable phase-modulation or time-shift modulation. The chapter covers general details of circuit construction, followed by correlation tests of the Type I system. Following the tests, a method is described and implemented which attempts to bring the transducer bandwidth more in line with what is needed to pass an undistorted signal. The results of the modified system are discussed.

The correlation tests use five pairs of Oxford transducers (as described in Chapter Three) and two pairs of Polaroid transducers. The Polaroid transducers are also electrostatic, and their operating characteristics are such that they are capable of being used in place of the Oxford transducers without any circuit modifications. As will be seen in the results section, the system performance is very much a function of the transducers used. Since both sets of transducers varied widely in their responses, it was felt that a realistic appraisal of system performance should include a representative cross-section of transducers taken from what was believed to be a typical production run. Frequency response tests of all transducers used are shown in Appendix E.

5.1 TYPE I CROSS-CORRELATION SYSTEM- LAYOUT AND OPERATION

The block diagram for the Type I system is shown in figure 5.1. This system is constructed in modules consisting of two plug-in circuit boards, transmitter/receiver chassis, and transducer module. The

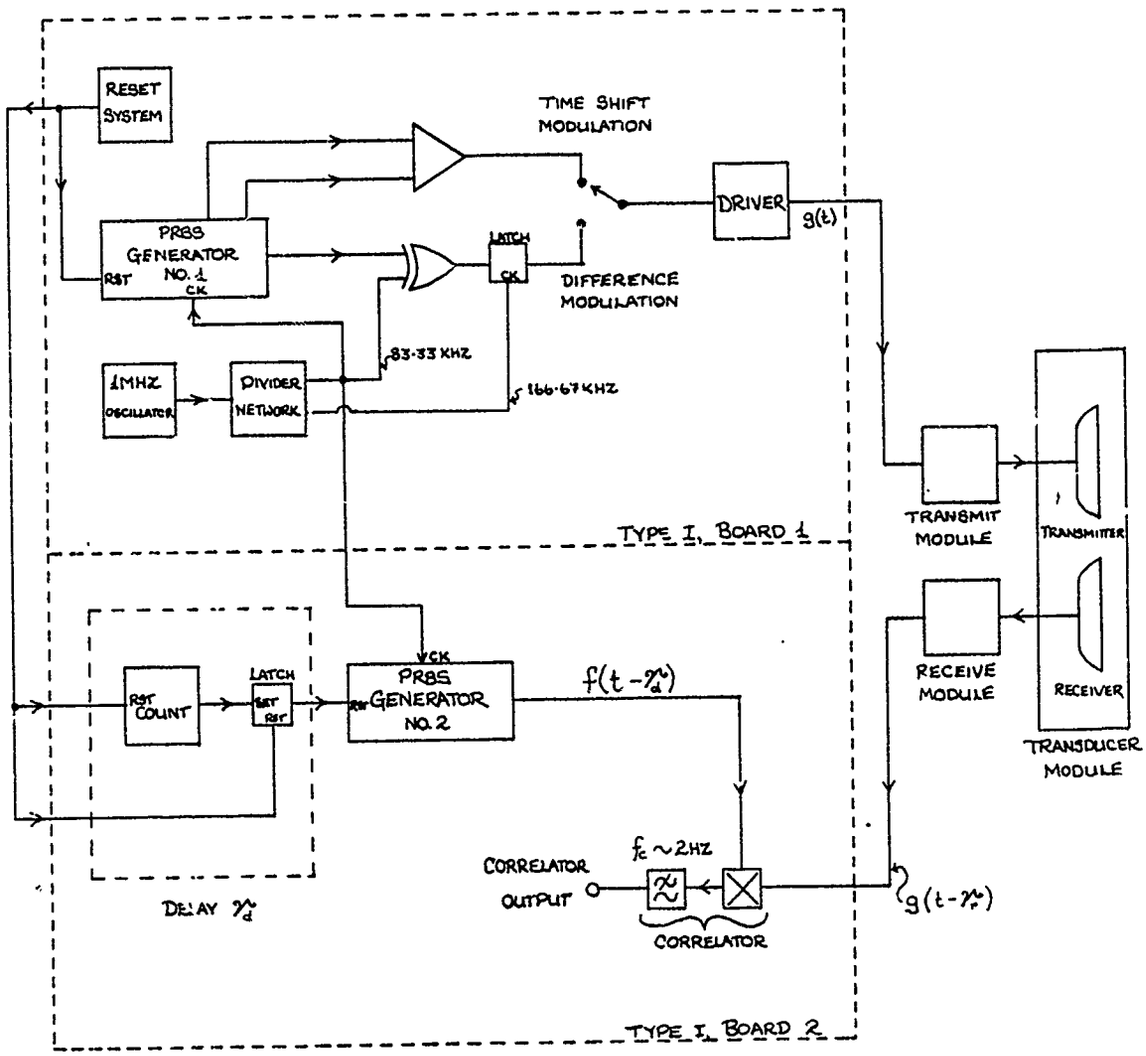

FIGURE : 5.1 TYPE 1 SYSTEM, BLOCK DIAGRAM.

schematic diagrams for the system are contained in Appendix B. Photographs of the components described in this chapter are also contained in Appendix B.

5.2 TYPE I SYSTEM, MASTER OSCILLATOR/DIVIDER STAGE, (BOARD 1)

Figure 5.2 shows the block diagram for board 1. It consists of a master oscillator, divider stages, PRBS generator, time-shift and phase modulation circuitry, and a transmitter driver stage. The master oscillator uses a single transistor (2N3904) whose switching rate is controlled by the 1 MHz crystal. Use of crystal control allows the high clock frequency stability necessary for ranging and tracking. The oscillator output is fed to the first CMOS divider stage (4522) which is configured to divide by three, producing a 333.33kHz output. This is in turn divided by two by a 4027 JK flip-flop wired so as to toggle every other clock pulse. This arrangement was originally used in order to provide a 333 kHz signal for an earlier cross-correlation system. The system as finally developed had no need of the higher frequency signal; however, it was left in as wired. If rebuilt, the 4522 could simply be wired to divide by six. The 166.67 kHz output is again divided by two, producing an 83.33 kHz output which is used by the PRBS generator and the phase modulation system. The 167 kHz output is needed in order to remove switching problems from the phase modulation system. This will be explained in a subsequent section.

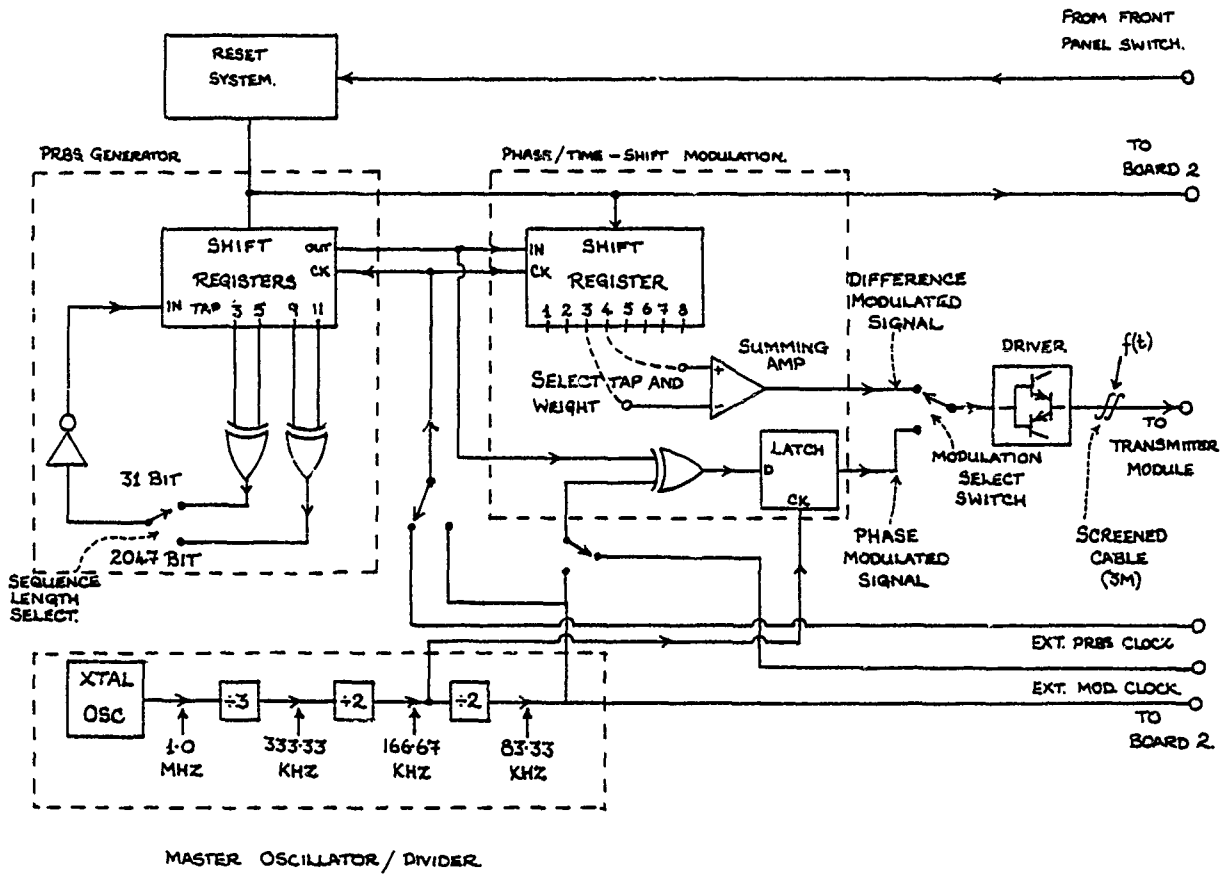

FIGURE 5.2 Type I System, Board 1

5.3 TYPE I SYSTEM, PRBS GENERATOR, (BOARD 1)

The PRBS generator stage uses two 4015 8-bit shift registers wired as described in Chapter Four. The maximum length of a binary sequence produced by a feedback register is a function of the shift taps selected. Further, there are certain shift register lengths which will allow a maximum length sequence to be generated by using only two feedback taps [27]. The taps selected for the experimental system are taps 3 and 5,which produce a 31 bit sequence, and taps 9 and 11 which produce a 2047 bit sequence. The 31 bit sequence was ideal for circuit checking on an oscilloscope due to the short repetition time, while the 2047 bit

sequence was used for all correlation tests. It provides for a maximum range of roughly 421 cm, which is calculated using the following relationship:

$$R_{max} = \frac{2047c}{2f_c} \qquad (5.1)$$

where c at 20 degrees Celcius is approximately 343 m/sec [28]. Increased range can be obtained by selecting other feedback taps. Each tap pair is summed modulo-2 (EX-OR) and the inverted sum outputs are switch selected to be fed back to the shift register input. The inverting stage is necessary to allow the system to have an all zero state from which to start. The all zero state is normally excluded, since once entered can never be left. However, the addition of the inverter stage makes the all one state the excluded state. This revision allows the RST function on the shift registers to return them to the all zero state, thus making system start up and delay timing easier.

The shift register clocking rate was 83.33 kHz, which provided a PRBS bit rate of 83.33 kilobits/second, with a bit length of 12 microseconds. The PRBS power spectrum thus produced contains the majority of its energy in the band below the clocking frequency, and has a half-power point at approximately 38kHz.

5.4 TYPE I SYSTEM, PHASE MODULATION/TIME SHIFT MODULATION, (BOARD 1)

The phase modulation section consists of an EX-OR gate which has the PRBS signal as one input and the PRBS clock as the carrier input. This produces a signal whose phase (with respect to the clock) is either inverted or noninverted, depending upon the logic value of the PRBS signal. This system is modified to include a latch at the EX-OR output.

This modification is included in order to eliminate switching transients which occur twice each clock cycle. These transients are due to the difference in switching speeds between the 4015 shift registers and the 4070 EX-OR gate. The 167 kHz signal is used to latch the EX-OR output after it has stabilized. This provides a clean output signal from the phase modulator. As shown in Chapter Four, the phase modulator output spectrum will be twice the bandwidth of the original PRBS signal, but will not be symmetrical about the phase modulation frequency.

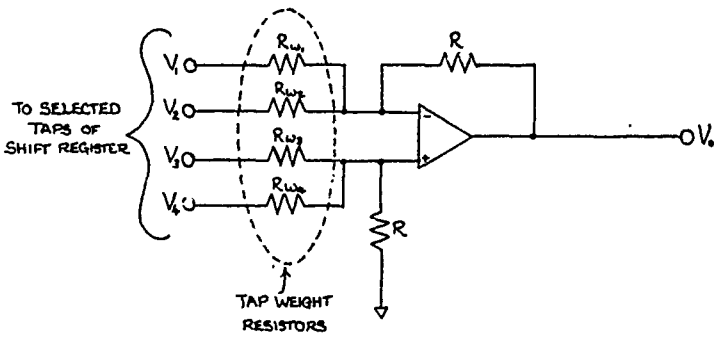

FIGURE 5.3 Type I System, Time-Shift Modulator, Board 1

The time shift modulation section consists of an LF 351 high speed op-amp which is wired as shown in figure 5.3. The weight given to each tap is a function of the resistance used to connect the tap with the amplifier input. The time shift input signals are taken from an additional 4015 shift register, and correct choice of resistor values will provide desired weights for each input, with a maximum of eight inputs allowed. In normal practice, however, only two taps are used, with weighting values of plus/minus one. These values produce the desired phase shift necessary for the desired cross-correlation function. The additional shift register was not strictly necessary, as desired time delays could be obtained by tapping the PRBS generator shift registers.

However, it was added so that an additional delay would be provided for the time-shift modulation system, making comparison tests easier.

The output of either the phase or the time shift modulator is selected by SPDT switch and sent to the transistor driver stage, which provides a high-current, low impedance source to drive the transmitter stage, located in a separate enclosure. Two level controls are installed in order to balance the phase and difference modulation outputs. Tests of the transducers showed that both types (Polaroid and Oxford) exhibited reduced performance when fed by signals in excess of 4.4 volts (pp) at the transmitter module input. Since the difference modulation output could range from +15 to -15 volts, while the phase modulated output went from 0 to +15 volts, the adjustments insured that the peak-to-peak value of the driver output remained the same when the modulation mode was switched. The driver outputs are ac coupled to the actual transmitter input. Since the PRBS signals are continuous, this serves the purpose of making either the phase-modulated or the time-shift modulated signal seem as if it were a bipolar signal.

5.5 TYPE I SYSTEM, TRANSMITTER MODULE, TRANSDUCER MODULE, RECEIVER MODULE

The transmitter section is housed, along with the power supply, in a separate chassis in the interest of modularity. As can be seen from the schematic on page B-6 it has minor changes from the design used in the FMCW system. The FMCW design utilizes triangular waves, and showed little distortion of the input waveform. However, the phase or difference modulated PRBS inputs were square waves with fast rise times. These signals were severely distorted by the existing transmitter design. The transmitter circuits were modified by the addition of an LF 351

op-amp as the transistor driver stage, and negative feedback with compensation was used to alter the stage frequency response. This modification produced low distortion waveforms at the transducer input.

The transducer module used in the Type I PRBS system is almost exactly as that used in the FMCW test system. An additional 560 ohm resistor has been added to the emitter circuit in order to reduce the gain to approximately forty at ultrasonic frequencies. This was required in order to reduce the effects of overload when high level noise signals were sent to the analog switches used in the cross-correlation circuitry, since overload conditions affect the correlation circuitry in a very different manner than the did the FMCW circuitry.

The receiver module consists of only two transistors as used in the FMCW system. One transistor is wired in the common base mode as one-half of a cascode pair, as before. The other is configured as an emitter follower which provides a low-impedance source for sending received signals through the shielded cable to the cross-correlator circuitry.

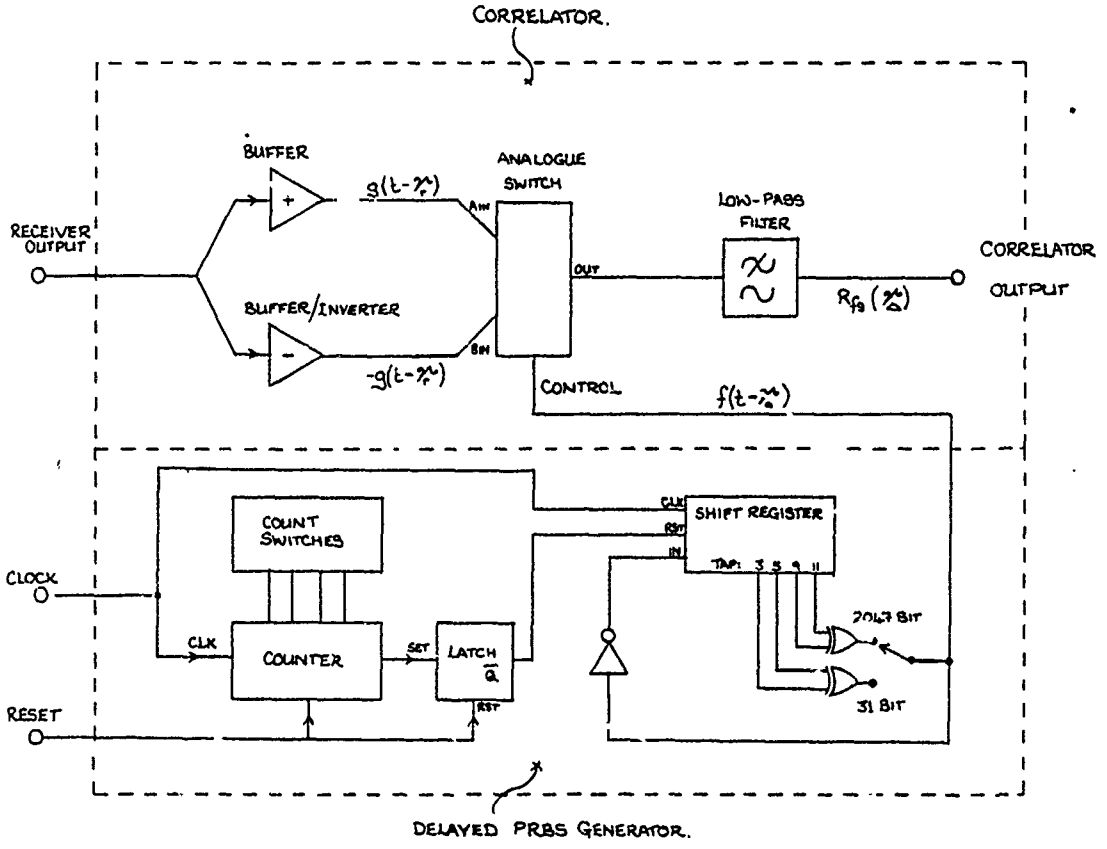

FIGURE 5.4 Type I System, Delayed PRBS/ Correlator , Board 2

5.6 TYPE I SYSTEM, DELAYED PRBS (BOARD 2)

A requirement for any cross-correlating system is a delayed version of the original (or modified original) signal. Methods of obtaining the necessary delay may be either electrical,mechanical or acoustical [51]. Since this system uses a digital reference signal, a delayed signal could be provided simply by passing the original signal through shift registers clocked at the bit rate. However, this method requires a number of registers which increases linearly with the delay time required.

The delay method adopted for use was that used by Chapelon [11] and Elias [16] in their work with cross-correlation systems. The method works as follows. Since a PRBS is uniquely determined by the feedback taps, it follows that two shift registers which have identical feedback taps will produce identical signals. If one of the registers is initialized at time t0, and the other initialzed at a later time t1, the output of the latter shift register will be identical to the former, but delayed in time by an amount equal to (t1-t0). This method is able to provide delays of arbitrary magnitude.

The delay system used on the Type I system consists of 4522 decimal divide-by-n counters which may be cascaded. Two 4522 counters are used in this design, and the count is switch selectable from 1 to 100. When the system reset signal is logic high, the shift registers in both the transmitter and receiver boards are set to zero. When the reset signal returns to logic low, the transmitter register begins to generate pseudo-noise. The receiver shift registers are held in the zero state until enabled by a signal from the counters. If the clock frequency to the counters is f_c, and the counters have been programmed to count until n, the time delay between transmitter and receiver shift registers may be calculated as:

$$\gamma_d = \frac{n}{f_c} \qquad (5.2)$$

The clocking frequency used for the counters is the same as that for the shift registers: 83.33 kHz. Thus, each count represents a time delay of 12 microseconds. If the velocity of sound in air is c, the target range for correlation will be:

$$r = \frac{\gamma_d c}{2} \qquad (5.3)$$

The block diagram for the delayed PRBS generator along with the correlator is shown in figure 5.4.

5.7 TYPE I SYSTEM, CROSS-CORRELATION, (BOARD 2)

The correlation circuits are relatively simple and consist of signal buffer/inverters, analog multiplication, and low-pass filtering. Two signals have to be multiplied, as in the FMCW system. However, in the case of the PRBS, one of the signals is digital. This leads to a simplification in the multiplier circuitry. Since the digital signal can be regarded as either a plus or minus value, the delayed PRBS output is used to switch either a non-inverted or an inverted version of the analogue signal to the filter stage. The received signal is passed through a dc blocking capacitor and fed to a pair of LF 351 op-amps which provide non-inverted and inverted signal inputs to the 4053 triple analogue switch. The digital control signal causes either the inverted or non-inverted input signal to be selected and presents it to the low-pass filter. The low-pass filter is a standard Sallen-Key second-order design [39], and has a bandpass of approximately 2 Hz, and damping factor of approximately 0.8. As mentioned in Chapter Four, the low-pass filter stage is a substitute for an integrator stage and allows for continuous reception of the transmitted signal without the consequent unlimited rise in correlation value. Narrower bandwidths are, or course, possible. However, the speed with which the system can react to changes in range is a function of filter bandwidth, among other things, as will be shown in Chapter Nine.

5.8 TYPE I SYSTEM, CROSS-CORRELATION TESTS

There are three main options for obtaining the relative time delays necessary to obtain the cross-correlation function: hold the target at a constant range and vary the delay time of the system delay, use discrete signal processing techniques, or hold the system delay constant and vary the target range. The first method involves placing a target at a given distance, setting the system to a desired delay time, and recording the filter output. Following this, the delay system could be set to the next delay time increment, and the filter output recorded. This would be continued until cross-correlation values for all delay times of interest were recorded. Obviously, this would be a time-consuming technique. The time signal can also be converted into digital format and the cross-correlation computed using digital techniques. However, digital techniques would introduce an additional delay which might prove unacceptable for purposes of real-time control, besides adding expense.

The third method, and the method chosen for the experiment, is to mount the transducers on a fixed reference point, attach the target to the movable bar which serves as platform for a marking pen on an X-Y recorder, connect the correlator output to the Y axis input, and cause the recorder to move slowly in the x direction. This method is far simpler to accomplish, and it does not require the additional circuitry. The experimental set-up is shown in figure 5.5.

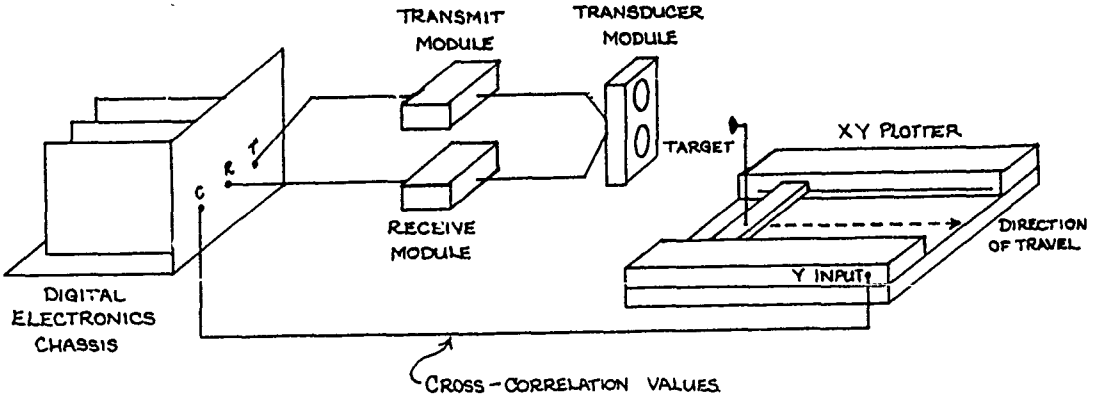

FIGURE 5.5 Type I System, Test Set-Up

As configured, the chart recorder output (y-axis) is a record of the cross-correlation values for the target for all distances through which the recorder platform travels (x-axis). In practice, the delay system was set to provide an appropriate delay, the recorder internal ramping generator was switched on, and the correlation values were recorded.

5.9 TYPE I SYSTEM, CROSS-CORRELATION TEST RESULTS

The Type I system cross-correlation tests were carried out on the system as described above. The relevant system parameters are contained in Table 5.1.

PRBS bit rate	: 83.33 kbit/sec
PRBS bandwidth (-3dB)	: 37.5 kHz
Phase modulation frequency	: 83.33 kHz
Modulated PRBS bandwidth	: 75 kHz
Target	: 19.5 mm disc
Preset expected range	: 26.5cm
Cross-correlation function width	: 0.816 cm (phase mod)
	: 1.224 cm (time-shift mod)

TABLE 5.1 - TYPE I SYSTEM TEST PARAMETERS

The width of the theoretical cross-correlation function is 2 bits for the phase-modulated signal and 3 bits for the time-shift modulated signal. The PRBS clock frequency listed in the table above yields a bit time of 12 microseconds. The correlation function widths stated in the table are obtained by calculating the distance sound will travel in the time of 2 (or 3) bit lengths. The actual target range for cross-correlation will be one-half the theoretical values due to the nature of the experimental test set-up. That is, a movement of one centimeter of the target will produce a total range change of 2 cm.

A typical cross-correlation run is shown in figure 5.6. These cross- corrrelation values were obtained for a single pair of transmit/receive transducers. Both phase and time-shift modulation correlation values are shown. As can be seen, the cross-correlation function is not at all like the theoretical function shown in figure 4.6, in that it is oscillatory and has a much greater width. However, it closely resembles figure 5.7 which illustrates typical results obtained

by Chapelon [11], Elias [16], and Ferguson [19]. Note, however, that the Type I System transmits continuously and, as such, does not suffer from the sidelobe problems seen in figure 5.7. In all cases, these results are due to the fact that the system bandwidth is less than that of the PRBS being fed through it. The resulting function then resembles the system impulse response [11]. Since the PRBS signal has a bandwidth of approximately 35 kHz, the transducers need 70 kHz bandwidths to successfully carry both sidebands of the transmitted signal. Tests on available transducers (Appendix E) show an average transducer transmit/receive bandwidth of approximately 20 kHz.

If the Type I System is to produce the desired cross-correlation function, the transducer bandwidth must be increased, or the some method must be developed which would break the direct relationship between transducer frequency range and PRBS bandwidth. The decision was made at this point to attempt to increase transducer bandwidth. It seemed possible that altering the transducer response through equalization might enhance the transmit/receive bandwidth sufficiently for use with the Type I System.

5.10 TRANSDUCER EQUALIZATION

Transducer frequency response tests (Appendix E) showed marked variation in response of selected transmit/receive pairs. As can be seen by reference to the two frequency response plots shown in figures 5.8 and 5.9, the tested transducer pairs display a rising response above 20 kHz, peaking roughly at 60 kHz for figure 5.8 and 75 kHz for figure 5.9. The response then drops off at roughly the same slope as the rise. None of the transducers show a usable response below 20 kHz, and only a few show any usable response above 100 kHz. Preliminary tests utilizing a 50 kHz

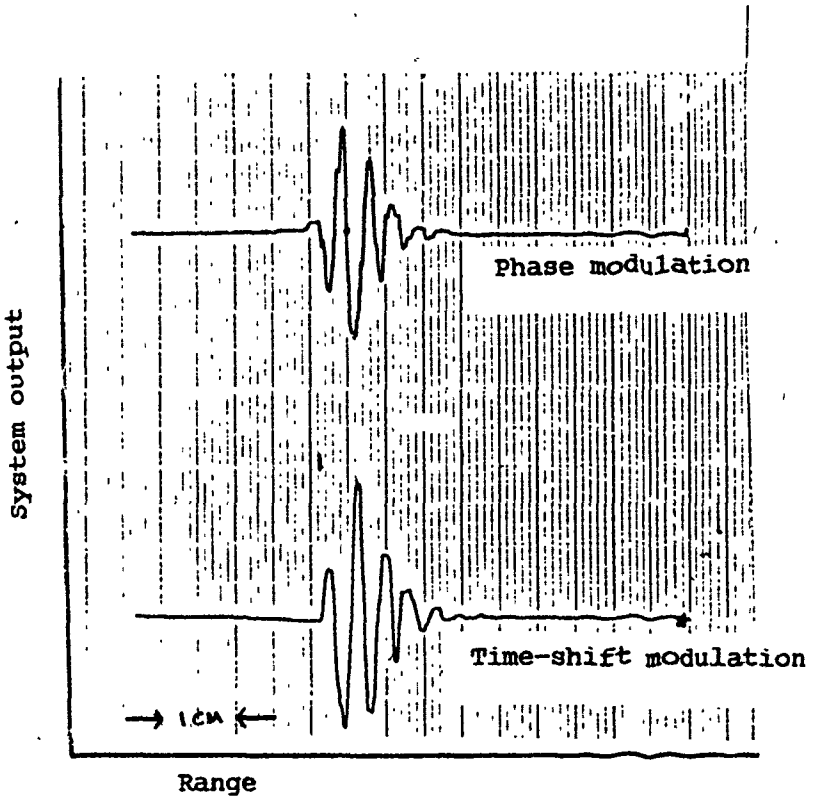

FIGURE: 5.6 TYPE 1 SYSTEM, EXPERIMENTAL RESULTS.

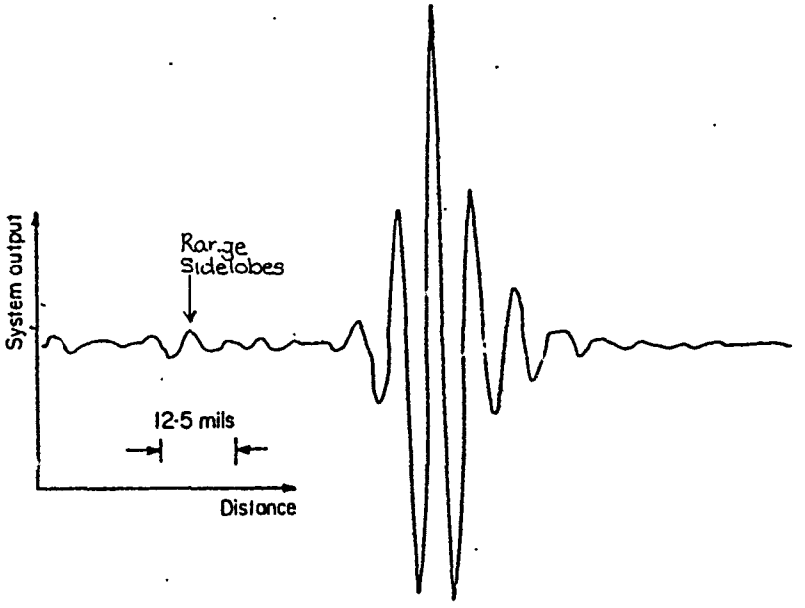

Detection of 1 mil (25·4 μm) gold wire in water at 15 cm.

NEWHOUSE, 1977

FIGURE; 5.7 EXPERIMENTAL RESULTS (REF 51, P127).

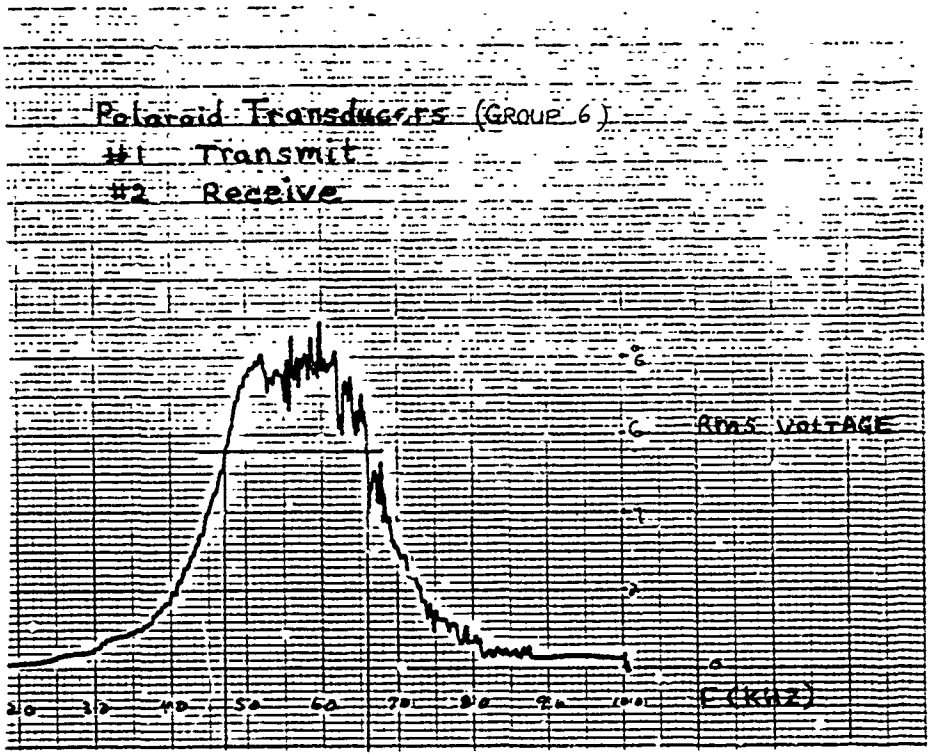

FIGURE: 5.8 POLAROID TRANSDUCERS – FREQUENCY RESPONSE TESTS

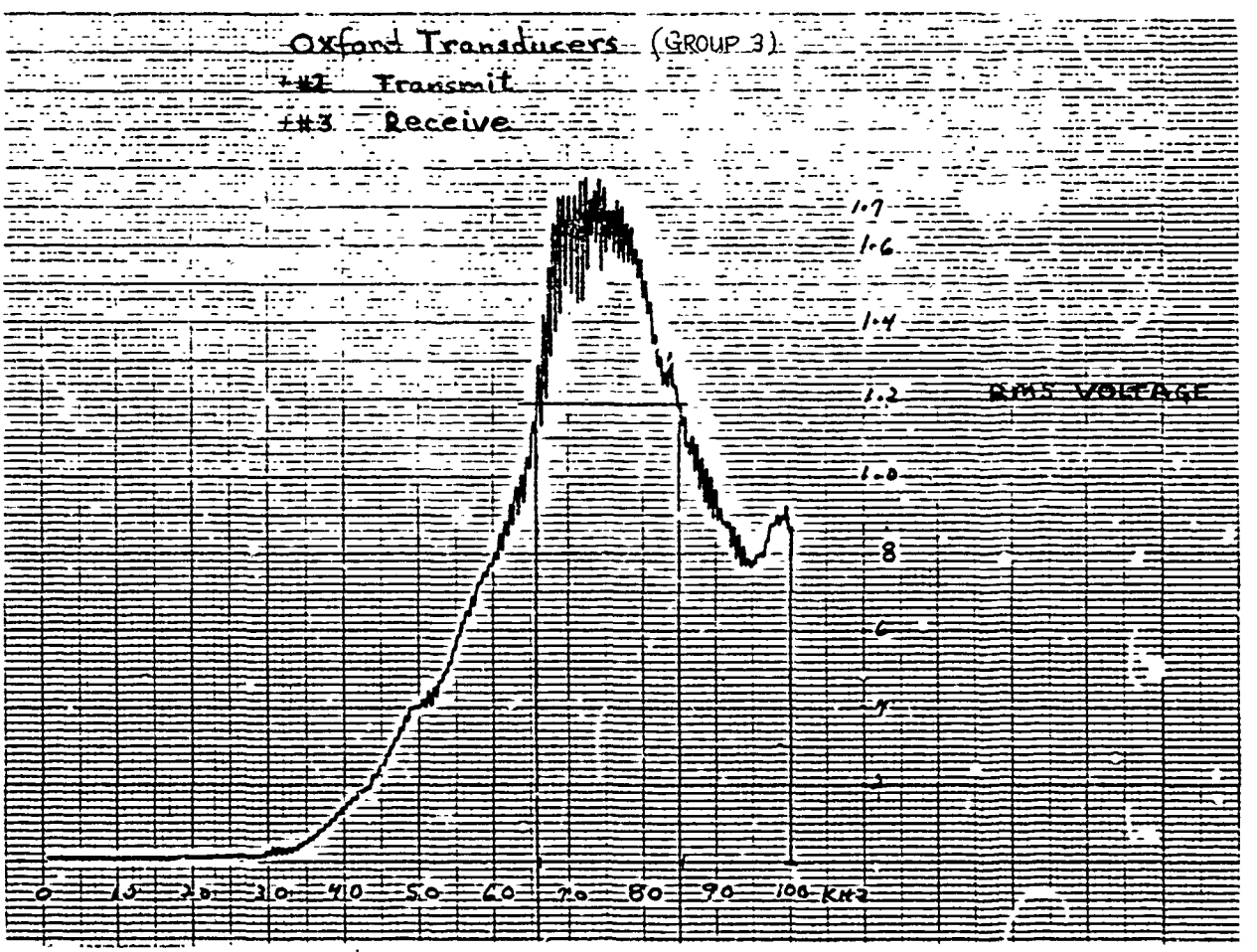

FIGURE: 5.9 OXFORD TRANSDUCERS – FREQUENCY RESPONSE TESTS

2 cycle pulse for a transmitted reference signal showed that the transmit/receive system was effectively acting as if the transducers were producing received signals which seemed to be higher order derivatives of the transmitted signal. Such responses seemed to correspond to the reference by McLachlan [46] indicating that the pressure response of a transducer would be a function of the second derivative (or acceleration) of its position. An equalization network was constructed which acted as an integrator in the frequency regions of interest (above 20 kHz). The equalizer was simply a single-pole low-pass network followed by a buffer, allowing multiple stages to be cascaded.

The equalizer circuits were inserted into the receive chain, following the emitter follower output, and cross- correlation tests were reaccomplished. The equalizer tests were run in four stages: no equalization, 40dB, 60 dB, and 80 dB/decade respectively. Figures 5.10 and 5.11 show two correlation runs which were done with pairs of Oxford and Polaroid Transducers, respectively. These particular examples were chosen as representative of the best and worst results. As can be seen, the particular pair of Oxford transducers used in figure 5.10 show considerable improvement, with the time-shift modulation cross-correlation function approaching ideal shape and width. Appendix C contains the complete cross- correlation tests with and without equalization for all transducers tested, both Oxford and Polaroid. The transducer pair which showed the most improvement was that whose performance is shown in figure 5.10. These were Oxford transducers exhibiting a rising response from approximately 40 kHz and which was still rising at 100 kHz, the limit of the test. Obviously, this response curve was well suited to the single slope equalization applied to them.

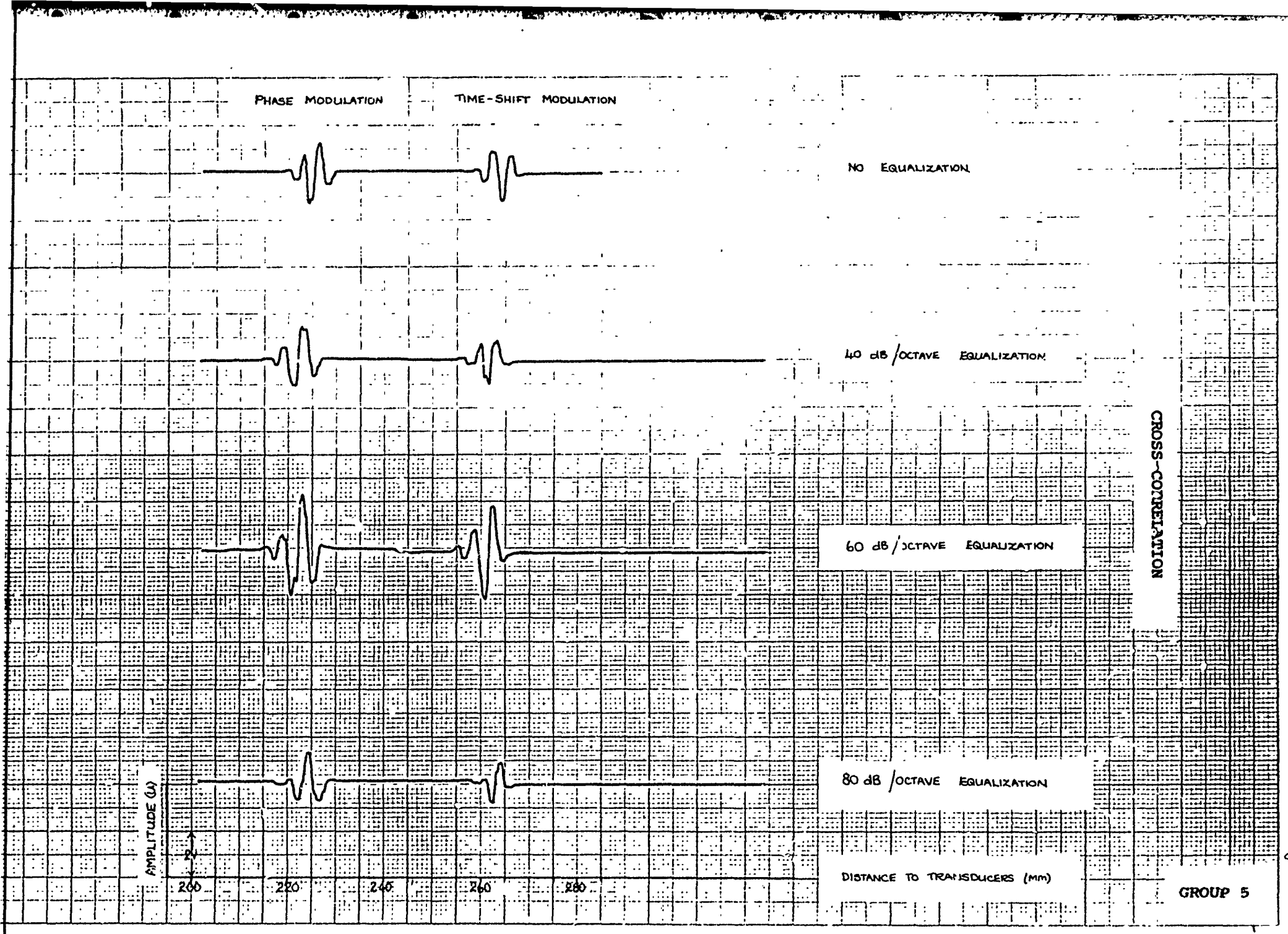
PHASE MODULATION
TIME-SHIFT MODULATION
NO EQUALIZATION
40 dB/OCTAVE EQUALIZATION
60 dB/OCTAVE EQUALIZATION
80 dB/OCTAVE EQUALIZATION
CROSS-CORRELATION
AMPLITUDE (V)
2V
200
220
240
260
280
DISTANCE TO TRANSDUCERS (mm)
GROUP 5

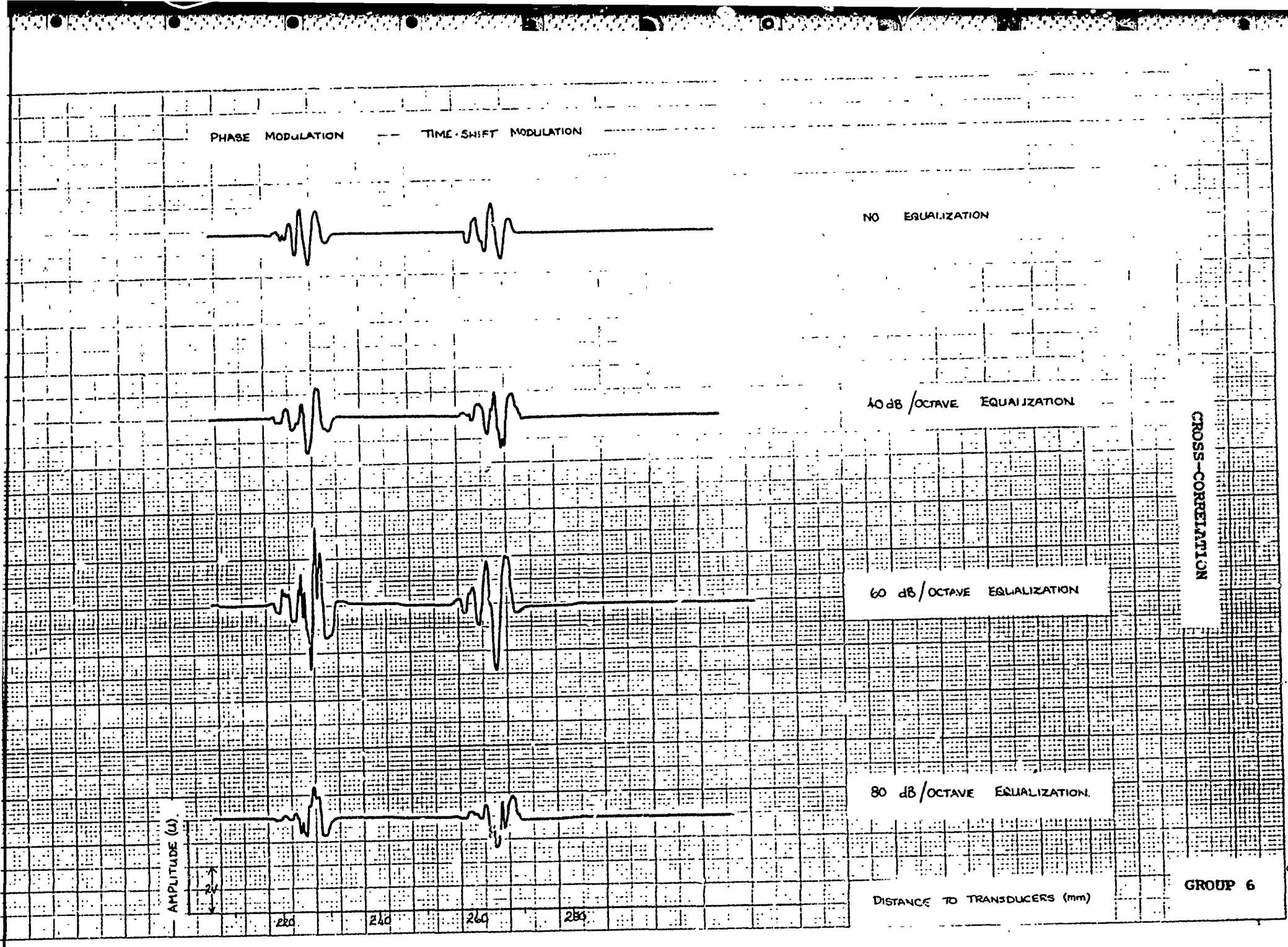
PHASE MODULATION
TIME-SHIFT MODULATION
NO EQUALIZATION
40 dB/OCTAVE EQUALIZATION
60 dB/OCTAVE EQUALIZATION
80 dB/OCTAVE EQUALIZATION
CROSS-CORRELATION
AMPLITUDE (V)
2V
220
240
260
280
DISTANCE TO TRANSDUCERS (mm)
GROUP 6

However, this particular response (and equalized cross-correlation function) was unique. The remainder of the transducer pairs had the peaked response curves described earlier. A more suitable equalization system for these transducers would produce an equalizer response similar to that shown in figure 5.12. Ideally, the transducer equalizer response curve would be an inverse curve of the transmit/receive frequency response curves found in Appendix E. This would, in theory, produce a flat frequency response in the area of the modulated PRBS, thus allowing the system to produce the desired cross-correlation functions.

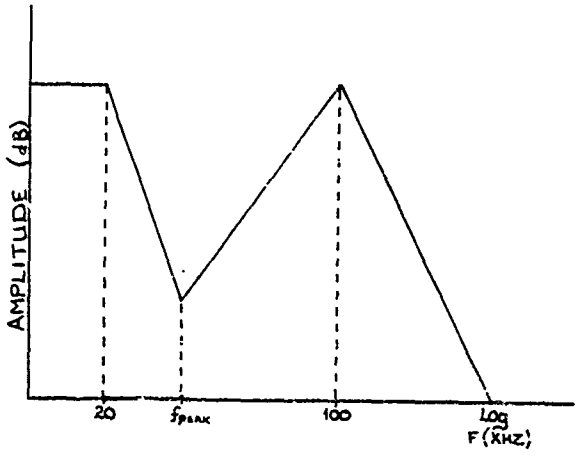

FIGURE 5.12 AN IMPROVED TRANSDUCER EQUALIZER RESPONSE

Although the above results showed that there was much improvement to be gained through equalization, the decision was made to discontinue research into this particular area for the following reasons: the extreme variability in transducer frequency response (even among those produced at roughly the same time) would require individual matching of equalization systems to transducer responses. Additionally, experience during this period of research indicates that these types of transducers also show effects of aging; that is, they exhibit changes in response and sensitivity. This makes the job of proper equalization even more

difficult. Unless transducer response and aging characteristics could be more tightly controlled, the equalization system would need to be modified as the transducers aged or whenever they were replaced.

5.11 SUMMARY

A Type I Correlation system was designed and tested using both Oxford and Polaroid transducers. Preliminary cross-correlation tests indicated that the PRBS bandwidth was too wide for the transducers, thus producing cross-correlation functions as in figure 5.6 instead of the ideal function shown in figure 4.6. Attempts to improve the results through equalization were marginally successful in that certain transducer pairs produced superior results, most did not. Although the equalization system could have been further developed to more closely match individual transducer responses, a decision was made to devote efforts to methods which would allow a degree of independence between transducer bandwidth, transducer center frequency, and PRBS bandwidth. The theoretical systems which are considered are discussed in Chapter Six.

CHAPTER 6

CARRIER CORRELATION SYSTEMS

Chapters Four and Five discussed the theoretical and actual performance of basic correlation systems which transmitted modulated versions of pseudo-noise and cross-correlated the received signal with delayed versions of the unmodulated signal. The purpose of modulation was twofold: first, to alter the pseudo-noise spectrum so that it would produce a desired cross-correlation function; and second, to move the transmitted spectrum to a point which would be more usable by the transducers. However, these systems, called Type I systems in this thesis, did not demodulate the received signal. That is, they did not attempt to restore the received signal to the spectrum which it had before transmission. The result is that, in order for the technique to be successful, considerable spectral overlap must exist between the two signals to be cross-correlated. This created a tight link between the bandwidth of the transmitted PRBS signal and its center frequency. Matching these variables with those of the transducers proved to be a difficult problem.

This chapter discusses a modulation/demodulation technique which will allow the transmitting frequency range to be independent of the pseudo-noise spectrum (with the stipulation that the modulated pseudo-noise bandwidth be within the capabilities of the transducers.) Of

course, the signals to be cross-correlated must still retain the phase relationship discussed in Chapter Four if they are to produce the desired cross-correlation function. The modulation/demodulation techniques discussed here are separate from, and independent of, any phase shifting techniques used for cross-correlation function modifications.

6.1 MODULATION TECHNIQUES

Given a signal of known bandwidth, there are two main methods of moving the signal information to the area around a higher, or carrier, frequency: amplitude modulation and angle modulation. These terms refer to the parameters of the carrier frequency which are controlled by the information (or input) signal. The basic equation for a general modulated carrier is given as [70]:

$$\chi_c(t) = A(t)\cos\left[\omega_c t + \theta(t)\right] \qquad (6.1)$$

where A(t) is the amplitude function, ω_c is the carrier frequency, and $\theta(t)$ is the phase function. If A(t) is caused to vary as the information bearing signal, the modulation is termed amplitude modulation. If $\theta(t)$ is caused to vary, the modulation is termed frequency or more properly, angle modulation. The general term of amplitude modulation is further sub-categorized into headings of amplitude modulation (AM), double sideband (DSB), and single sideband(SSB), these terms being a function of whether or not the carrier is transmitted along with both signal sidebands (AM), and whether or not one (SSB) or both (DSB) sidebands of the modulated information signal are transmitted without a carrier. There are two main categories of angle modulation: phase and frequency modulation. These terms describe whether or not $\theta(t)$ or its derivative is varied as a function of the

information signal. The goal of this Chapter is not to fully explain each modulation technique. It is, rather, to choose a method which would be most likely to succeed under the conditions of operation described in Chapter One, namely, the location and tracking of specified targets under conditions of clutter and noise. Thus, the modulation technique chosen will be the one which shows minimum suceptibility to degradation when operated under the described conditions.

The mathematical analysis of the effects of noise and multiple signals upon each of the types of modulation listed above is complex and quite lengthy, and will not be covered in this thesis. Zeimer [70], and Schwartz [61], contain excellent discussions of the matter. Zeimer concludes that angle modulation techniques are capable of excellent performance in the presense of noise, provided that the noise is kept below a given threshold. Once noise exceeds this threshold, the system performance decreases dramatically, with the effect that the system is no longer usable. In addition, angle modulated systems are also very sensitive to the effects of multipath propagation. Signals from large targets would 'swamp' signals from small targets. That is, the signals from the smaller targets would not be able to be detected in the presence of these larger returns. As such, angle modulation systems must be eliminated from consideration since the problems of noise and clutter are precisely those which are to be overcome in this thesis.

Amplitude modulation is left as a possibly useful technique, but which form would yield useful results? The first amplitude modulation technique, AM, involves transmitting a continuous carrier wave along with the information-bearing signal. This technique allows a relatively simple demodulation system, known as envelope detection, to be used. However, envelope detection is also suceptible to the threshold effect

[70]. Since envelope detection is unusable, carrier components are not needed, which leaves DSB and SSB. Both offer the same potential performance in the presence of noise. However, SSB uses half the transmitted bandwidth as DSB. That is, a modulated information-bearing signal of bandwidth BW will require 2BW if DSB is used, and BW if SSB is used. However, circuit complexity is increased in order to generate SSB, as opposed to DSB. Therefore, a decision was made to utilize DSB modulation.

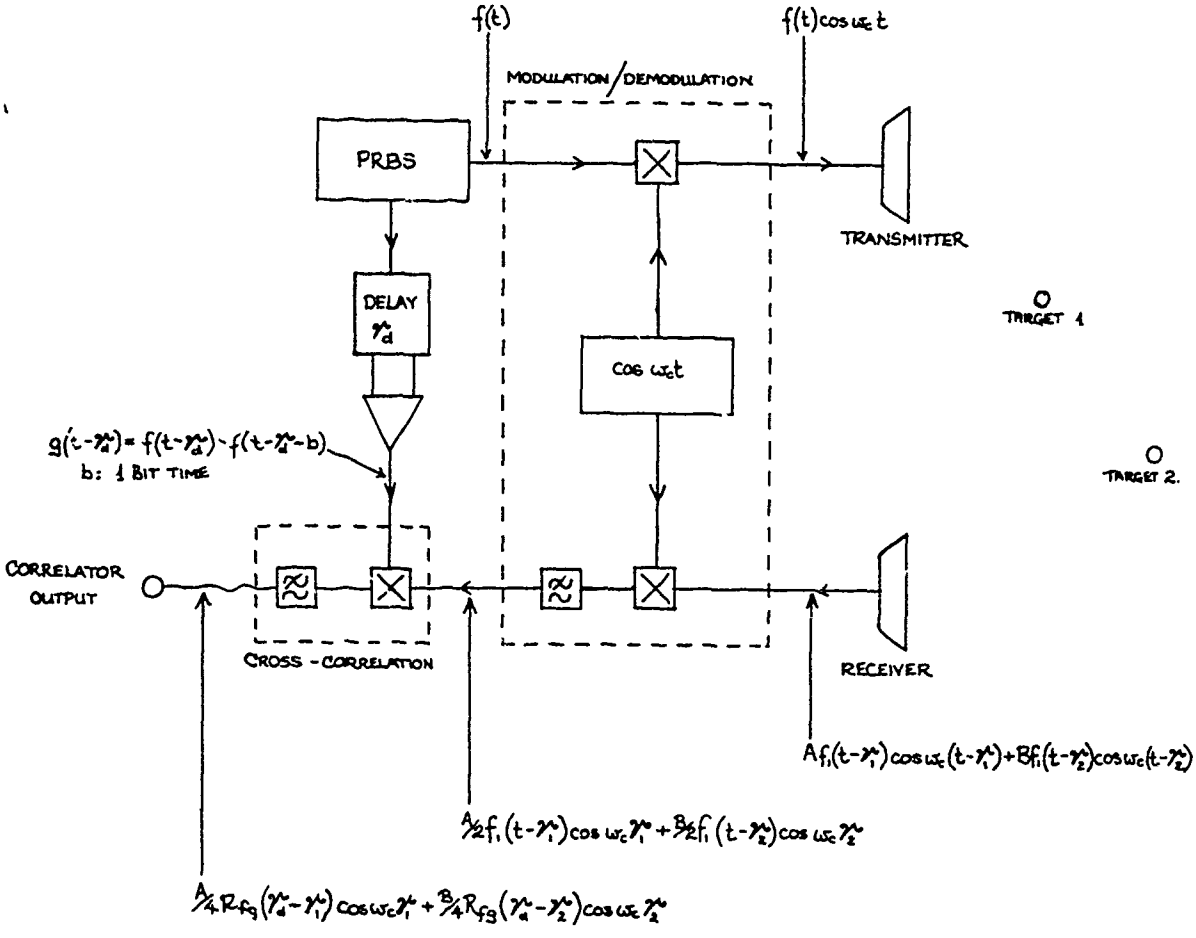

FIGURE 6.1 DSB Correlation System with Coherent Demodulation

6.2 A DSB CORRELATION SYSTEM WITH COHERENT DEMODULATION

The basic set-up for a DSB modulating system is shown in figure 6.1. In this system, the PRBS output is modulated by a carrier of frequency ω_c and transmitted. The received signals are demodulated by multiplying them by the same carrier (hence the term coherent demodulation) and then low-pass filtering the multiplier output. This output is then cross-correlated with a modified version of the delayed PRBS, in order to produce the desired cross-correlation function. For purposes of the following discussion, assume that two targets are within the maximum range and that the system is continuously transmitting a modulated PRBS signal. The transmitted, received, and demodulated signals are shown in equations 6.2, 6.3, and 6.4, respectively.

$$f_T(t) = f(t)\cos\omega_c t \tag{6.2}$$

$$f_R(t) = A f_T\left(t-\gamma_1'\right)\cos\omega_c\left(t-\gamma_1'\right)+B f_T\left(t-\gamma_2'\right)\cos\omega_c\left(t-\gamma_2'\right) \tag{6.3}$$

$$f_D(t) = \frac{A}{2} f_T\left(t-\gamma_1'\right)\left\{\cos\left(2\omega_c t-\omega_c\gamma_1'\right)+\cos\omega_c\gamma_1'\right\}+\frac{B}{2} f_T\left(t-\gamma_2'\right)\left\{\cos\left(2\omega_c t-\omega_c\gamma_2'\right)+\cos\omega_c\gamma_2'\right\} \tag{6.4}$$

where A, B, γ_1' , and γ_2' are the amplitudes and time delays of return signals from two targets at different ranges. As before, the low-pass filter removes the sum frequency terms and the filter output is:

$$f_{LPF} = \frac{A}{2} f_T\left(t-\gamma_1'\right)\cos\omega_c\gamma_1' + \frac{B}{2} f_T\left(t-\gamma_2'\right)\cos\omega_c\gamma_2' \tag{6.5}$$

Note that the filter output now consists of the original PRBS sequence, but scaled by the constant determined by the cos term. Following multiplication by the delayed PRBS , the filtered output is:

$$f_c(t) = \frac{A}{4} R_{fg}(\gamma_d - \gamma_1)\cos \omega_c \gamma_1 + \frac{B}{4} R_{fg}(\gamma_d - \gamma_2)\cos \omega_c \gamma_2 \quad (6.6)$$

The output now consists of the correlation term (a dc value for a stationary target) multiplied by the cos term , also dc. Note, however, that the cos term will be zero for targets at distances such that the argument attains odd multiples of pi/2, even though there might be a non-zero correlation function for targets at that distance. Thus, coherent demodulation as drawn in figure 6.1 will not operate in a satisfactory manner.

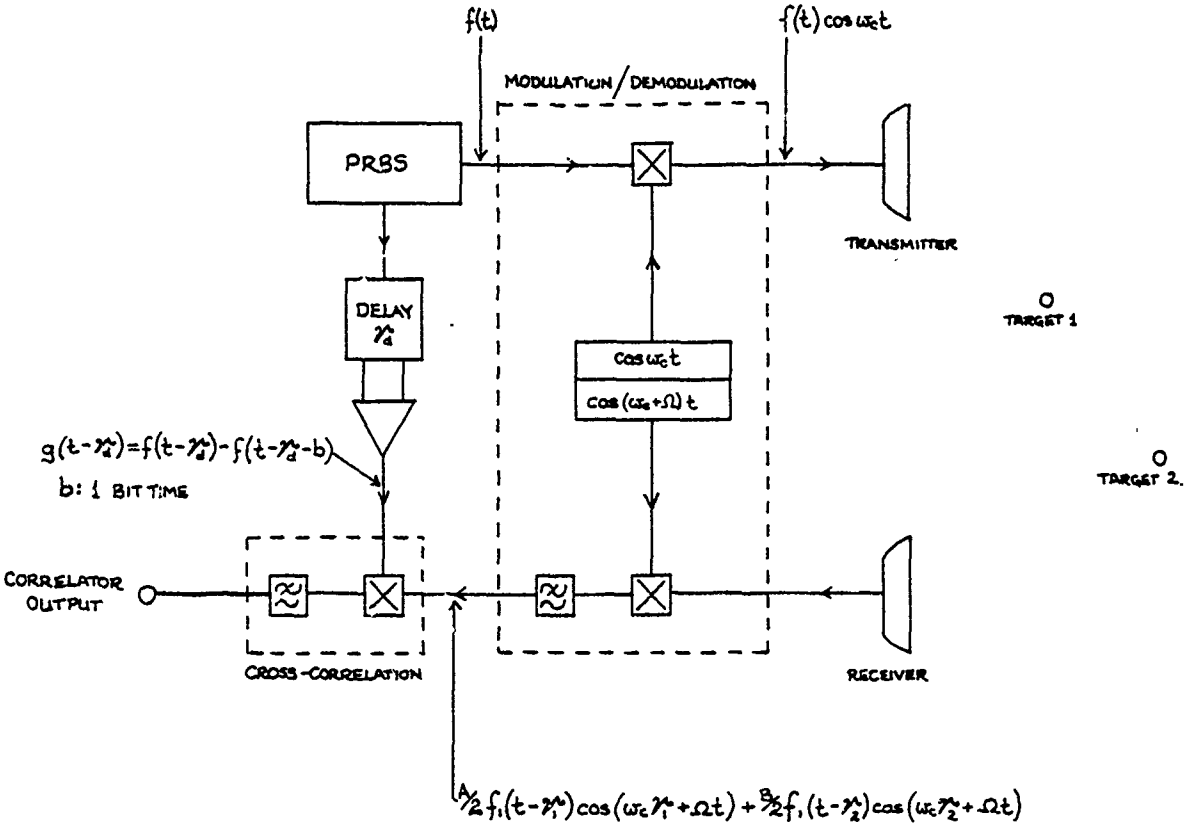

FIGURE 6.2 DSB Correlation System with Non-Coherent Demodulation

6.3 A DSB CORRELATION SYSTEM WITH NON-COHERENT DEMODULATION

One solution to this problem is to provide two versions of the demodulating carrier, one lagging the other by ninety degrees. This has been done by Lam [38] in an ultrasonic PRBS flaw-detection system. However, this method requires additional circuitry following the correlator in order to provide a correct correlation amplitude [38]. While this approach remains a perfectly viable one, it was discarded because of the difficulties of distinguishing between positive and negative position error.

An alternate solution to the problem of null points is to change some parameter such that targets which are at the null points mentioned previously can be observed. One way of doing this is to use a demodulating carrier that is slightly offset in frequency from the modulating carrier. Assume a system such as that shown in figure 6.2 which is identical to figure 6.1 except for the change in demodulating frequency. This changed demodulating frequency is expressed as:

$$f_d(t) = \cos(\omega_c + \Omega)t \tag{6.7}$$

This would produce a demodulator output (after filtering) of:

$$f_{LPF} = \frac{A}{2} f_T(t-\gamma_1') \cos(\omega_c \gamma_1' + \Omega t) + \frac{B}{2} f_T(t-\gamma_2') \cos(\omega_c \gamma_2' + \Omega t) \tag{6.8}$$

and a correlator output of:

$$f_c(t) = \frac{A}{4} R_{fg_1}(\gamma_d' - \gamma_1') \cos(\omega_c \gamma_1' + \Omega t) + \frac{B}{4} R_{fg}(\gamma_d' - \gamma_2') \cos(\omega_c \gamma_2' + \Omega t) \tag{6.9}$$

The correlator output is now modulated by a cos term of frequency Ω.

This system, as described, will produce a correlator output if a target is located within the proper distance, that is, if the correlation function was non-zero at that particular delay time. However, the output of the correlator would no longer be dc; it would be a sinusoid whose amplitude would be a function of the cross-correlation function at that particular range. This method of demodulating with a carrier offset in frequency allows the receiving system to readily detect target motion. Target motion will produce changes in the sinusoid period which can be used to determine target velocity. Such a system using non-coherent demodulation is used by Shiozaki [62] in a system which exploited the Doppler resolution capabilities of the system. The effects of target motion are discussed in greater detail in Chapter Nine, dealing with secondary effects.

Figure 6.3 shows a typical correlator output for the system as shown in figure 6.2. The correlator output is now ambiguous. There is no way in which the sign of the correlator output can be determined from this signal alone; that is, a sinusoid of amplitude A may be produced by either a positive or negative tau. This problem negates the advantage of the altered cross-correlation function. A solution to the problem lies in providing an appropriate reference signal of frequency Ω which will allow the relative phase of the correlator sinusoid to be determined.

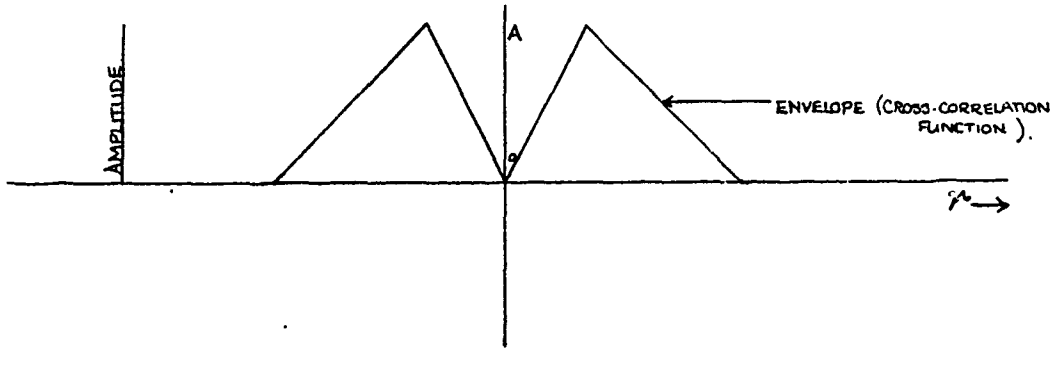

FIGURE 6.3 Envelope of Sinusoidal Correlation Function (see text)

A first try at a solution to this problem might be to provide a reference sinusoid of the same frequency as the correlator output, but which would not change its phase (relative to the correlator frequency) whenever the target is moved. Obviously, this signal could not be internally generated, as the received signal would then change phase as the target changes range. One possible solution lies in the interesting properties of the time-shifting modulation system discussed in Chapter Four.

Section 4.5 discussed the ease with which cross-correlation functions could be 'constructed' through the appropriate choice of tap positions and tap weights. Specifically, figure 4.10a illustrated the tap connections required to produce the desired cross-correlation function. However, figure 4.11a shows another cross-correlation function which has the same time-width as the desired function, but does not change sign when tau passes through zero. These two figures are shown again in figures 6.4a and 6.4b, respectively. If the system shown in figure 6.2 is modified to add another correlator stage, and if this correlator stage has a separate time-shift modulated signal as its input, the block diagram would be as in figure 6.5. The two correlator outputs each contain a sinusoid of frequency Ω, with the amplitudes following the envelopes depicted in figure 6.4a and 6.4b. As can be seen, R_{fg_1} changes sign at tau=0, R_{fg_2} does not. The cross-correlation function R_{Rfg_2} can thus serve as the needed reference function for R_{Rfg_1}. This system, the DSB system using twin correlators fed by different time-shifted reference signals, will serve as a model for the experimental DSB system described in Chapter Seven. Its operation is explained further in the next section.

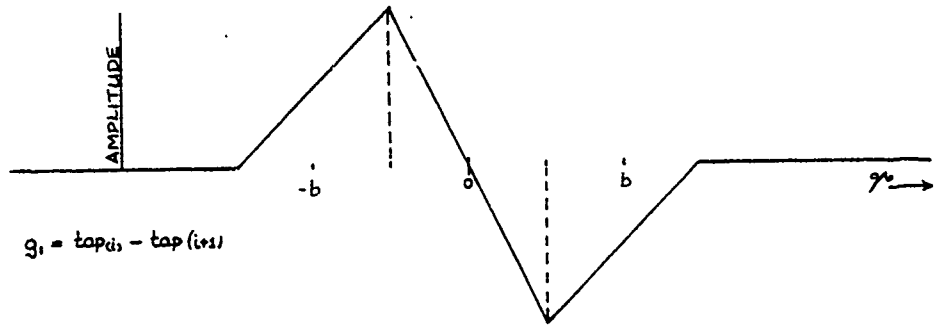

a) R_{fg_1}; $g_1 = tap_{(i)} - tap_{(i+1)}$

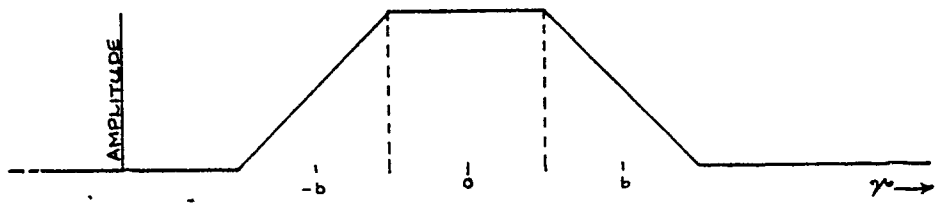

b) R_{fg_2}; $g_2 = tap_{(i)} + tap_{(i+1)}$

Figure 6.4 Cross-Correlation Functions

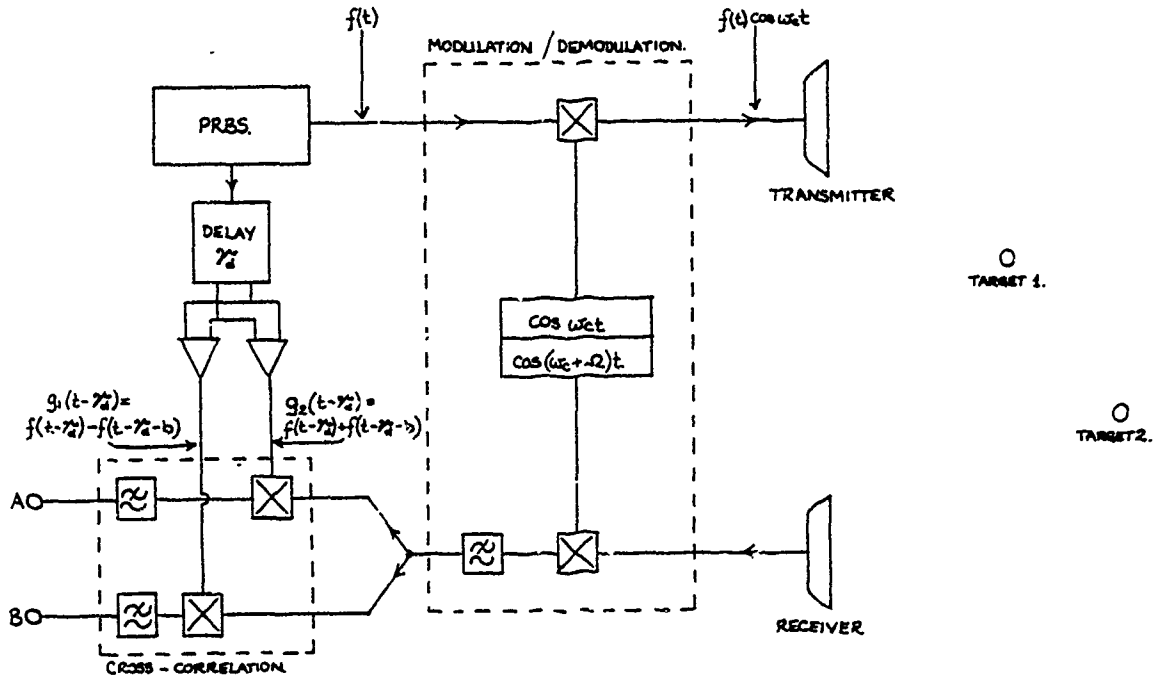

CORRELATOR OUTPUTS

$$A(t) = \tfrac{1}{4} R_{fg_2}(\gamma_d - \gamma_1) \cos(\omega_c \gamma_1 + \Omega t) + \tfrac{3}{4} R_{fg_2}(\gamma_d - \gamma_2) \cos(\omega_c \gamma_2 + \Omega t)$$

$$B(t) = \tfrac{1}{4} R_{fg_1}(\gamma_d - \gamma_1) \cos(\omega_c \gamma_1 + \Omega t) + \tfrac{3}{4} R_{fg_1}(\gamma_d - \gamma_2) \cos(\omega_c \gamma_2 + \Omega t)$$

FIGURE 6.5 DSB Dual Correlation System, Non-Coherent Demodulation

6.4 PROVIDING AN ACCEPTABLE OUTPUT FROM THE DUAL CORRELATORS

The MK III system shown in figure 6.5 has as its outputs (A and B) two sinusoids of frequency Ω which are in phase (or anti-phase) at all times, and which have amplitudes $R_{fg_1}(\gamma)$ and $R_{fg_2}(\gamma)$. These two signals must be combined in order to produce one single correlator output which is a function of range. This may be done in the following manner. Consider figure 6.6a. The inputs to the multiplier stage are A(t) and B(t), which are the outputs of the dual cross-correlator stages mentioned in the previous section. Assume that only one target having time delay γ_1 is within the correlation 'window', thus making $R_{fg_1}(\gamma_2)$ and

$R_{fg_2}(\tau_2)$ equal to zero. The expressions for the correlation outputs for the two cross-correlators are:

$$A(t) = R_{fg_2}(\tau_d - \tau_1)\cos(\omega_c \tau_1 + \Omega t) \quad (6.10)$$

and

$$B(t) = R_{fg_1}(\tau_d - \tau_1)\cos(\omega_c \tau_1 + \Omega t) \quad (6.11)$$

where the amplitudes have been normalized to one. After filtering, the multiplier output is:

$$M(t) = \frac{R_{fg_2}(\tau_d - \tau_1)\, R_{fg_1}(\tau_d - \tau_1)}{2} \quad (6.12)$$

While this method will work, it produces a final cross-correlation function for each target which is the product of two individual cross-correlation functions. This will produce enormous differences in cross-correlation magnitudes for small changes in received signal strength. A better arrangement is to place a sign function block into one of the multiplier inputs, where a sign function block has a signal as an input, and the sign of the signal as the output. The revised multiplier stage is shown in figure 6.6b. After filtering, the multiplier output becomes:

$$M(t) = \frac{2}{\pi} R_{fg_1}(\tau_d - \tau_1) \quad (6.13)$$

where the 2/pi term comes about as a result of the sign function. The correlator output is a function of only one cross-correlation function, and is therefore much less sensitive to changes in received signal

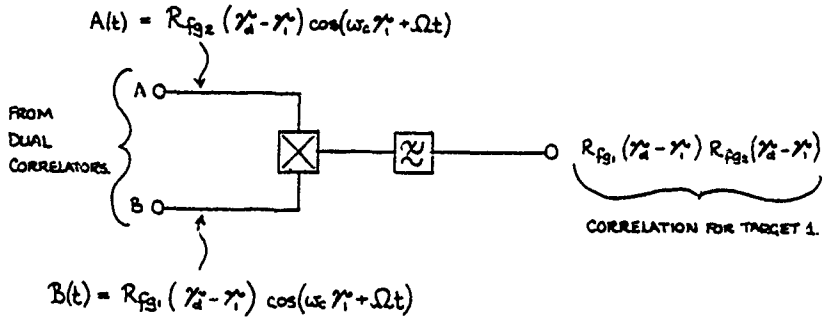

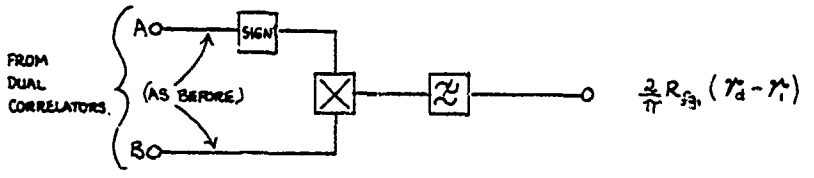

FIGURE; 6.6. COMBINING DUAL CROSS-CORRELATION FUNCTIONS.

strength.

6.5 CONCLUSION

Various means of modulation and demodulation have been considered for use in a carrier correlation system. All types of angle modulation methods, along with basic amplitude modulation, were rejected due to the suceptibility of the demodulator stages to noise when input signal-to-noise ratio was low (the threshold effect) and also due to the demodulator's inability to cope with a cluttered environment (multipath effects). The final method chosen was double-sideband modulation (DSB). It was chosen over single-sideband modulation (SSB) modulation due to its relative simplicity. Coherent demodulation of DSB signals was judged to be unsuitable due to the fact that there were ranges at which targets would not be detected due to phase shifts between the reference carrier and the reflected signals. Non-coherent demodulation allows targets to be detected without the effects of nulling. However, this method did not allow the absolute sign of the resulting correlation sinusoid to be determined, thus negating the advantages to be gained through using the modified cross-correlation function. The addition of a second correlator stage, which operates in parallel with the first correlator stage and uses a different time-shifted reference function as it input, allows the original cross-correlation function to be restored.

This theoretical system allows the PRBS bandwidth to be set independently of the carrier frequency, thus breaking the linkage which caused problems in the Type I system covered in Chapter Five. An experimental system has been constructed which uses the methods discussed in this chapter. Details of system construction and performance are

contained in Chapter Seven.

CHAPTER 7

AN EXPERIMENTAL CARRIER CROSS-CORRELATING RANGING SYSTEM

This chapter details the layout, construction, and testing of a double sideband (DSB) cross-correlating system which was developed in Chapter Six. The advanced system, referred to as a Type II system throughout the remainder of this thesis, generates a reference pseudo-noise (PRBS) signal, uses it to amplitude modulate a carrier of frequency ω_c, demodulates the the received signals with an asynchronous carrier of frequency $\omega_c + \Omega$, and cross-correlates the demodulated signals with two modified and delayed versions of the reference PRBS. The two cross-correlated outputs are then combined to form a single cross-correlation output.

7.1 SYSTEM LAYOUT

The Type II system consists of three digital/analogue circuit boards, separate transmitter and receiver chassis, and a transducer module. The transmitter and receiver chassis and the transducer modules are unchanged from the Type I system and will not be covered in this section. Refer to Chapter Five for information on these components. The master oscillator/PRBS generator/modulator board contains small changes from the Type I system. These changes are covered in the following section. The divider/frequency synthesis board and the

demodulator/correlator boards are completely changed from the Type I system and will be examined in more detail. The block diagram for the Type II system is shown in figure 7.1. Appendix B contains schematic diagrams for both the Type I and Type II systems.

7.2 TYPE II SYSTEM, MASTER OSCILLATOR/PRBS/MODULATOR, (BOARD 1)

The Type II system generator/modulator board (board 1) is the same as that used on the Type I system. However, the following modifications were made:

1. The internal divider system is disabled, and the 1 MHz clock signal is brought to the edge connectors for use by a revised divider system located on board 2.
2. The modulation switch is left in the Phase Modulation position, but the phase modulation clock is taken from board 2 (clock 1).
3. The PRBS shift register clock is obtained from board 2 (clock 2).

There is no block diagram of the Type II system board 1, as the changes from a Type I system to a Type II system are made through changes in switch positions on board 1. Refer to Chapter 5, figure 5.2 for the board layout. Figure 7.1 shows the signals which are derived from board 1 and sent to board 2 for further processing.

7.3 TYPE II SYSTEM, DIVIDER/FREQUENCY GENERATOR BOARD, (BOARD 2)

Board 2 contains all frequency synthesis circuitry, the delayed PRBS system, and the two time-shift modulation stages. Schematics for board 2 are on page B3. THE 1MHz signal from board 1 serves as a master clock

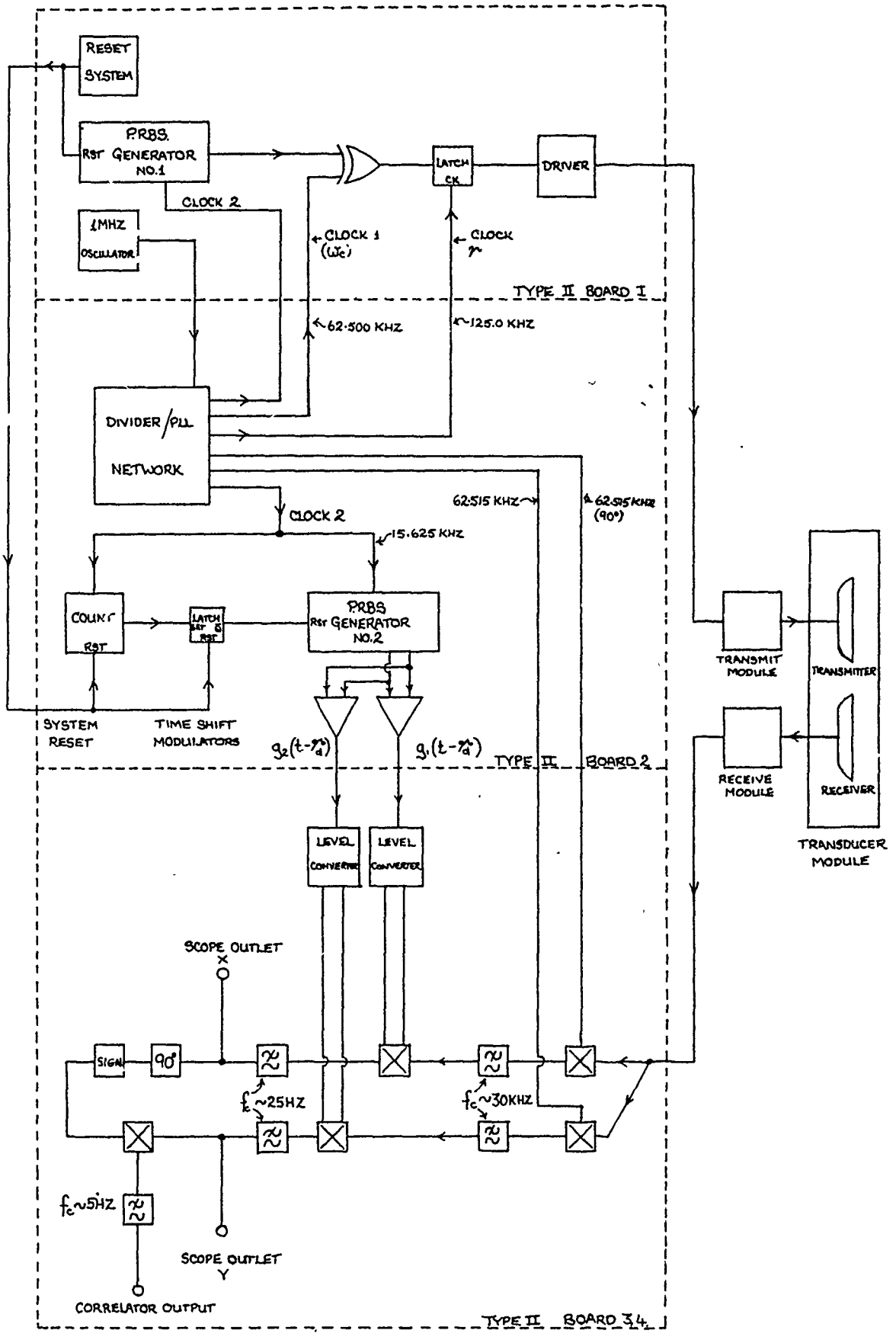

FIGURE; 7.1 TYPE II SYSTEM - BLOCK DIAGRAM.

signal for the divider circuitry contained on board 2. These dividers provide clock signals to the rest of the circuitry. Table 7.1 lists the various clocking signals provided by board 2. The block diagram is shown in figure 7.2.

Clocks 1,2, and r were obtained by standard divide by n techniques. However the clock 3 and 4 signals require a bit more sophistication. As shown in Chapter Six, the demodulating frequency must be different from the carrier frequency by some amount Ω. The Ω selected for the experimental circuit was 15 Hz, and it was obtained by dividing the 1 MHz clock by 8190, producing a frequency of 122.1 Hz. This served as the reference frequency for a phase-locked-loop network wired as a frequency multiplier so as to provide an output of 250.06 kHz. This signal was again divided in a manner so as to provide two separate 62.515 kHz signals, one shifted from the other by 90 degrees. These two demodulating signals are required because there are two parallel demodulator circuits in the demodulator/correlator board. This was a deliberate move which was designed to provide correlation outputs which could be viewed as a Lissajous figure on an oscilloscope during the preliminary development stages. This topic will be further discussed in the section dealing with the demodulator/correlator board.

clock 1: 62.500 kHz

clock 2: 15.625 kHz

clock 3: 62.515 kHz

clock 4: 62.515 kHz (shifted 90 degrees with clock 3)

clock r: 125.0 kHz

TABLE 7.1 - CLOCK SIGNALS AND FREQUENCIES (Type II, board 2)

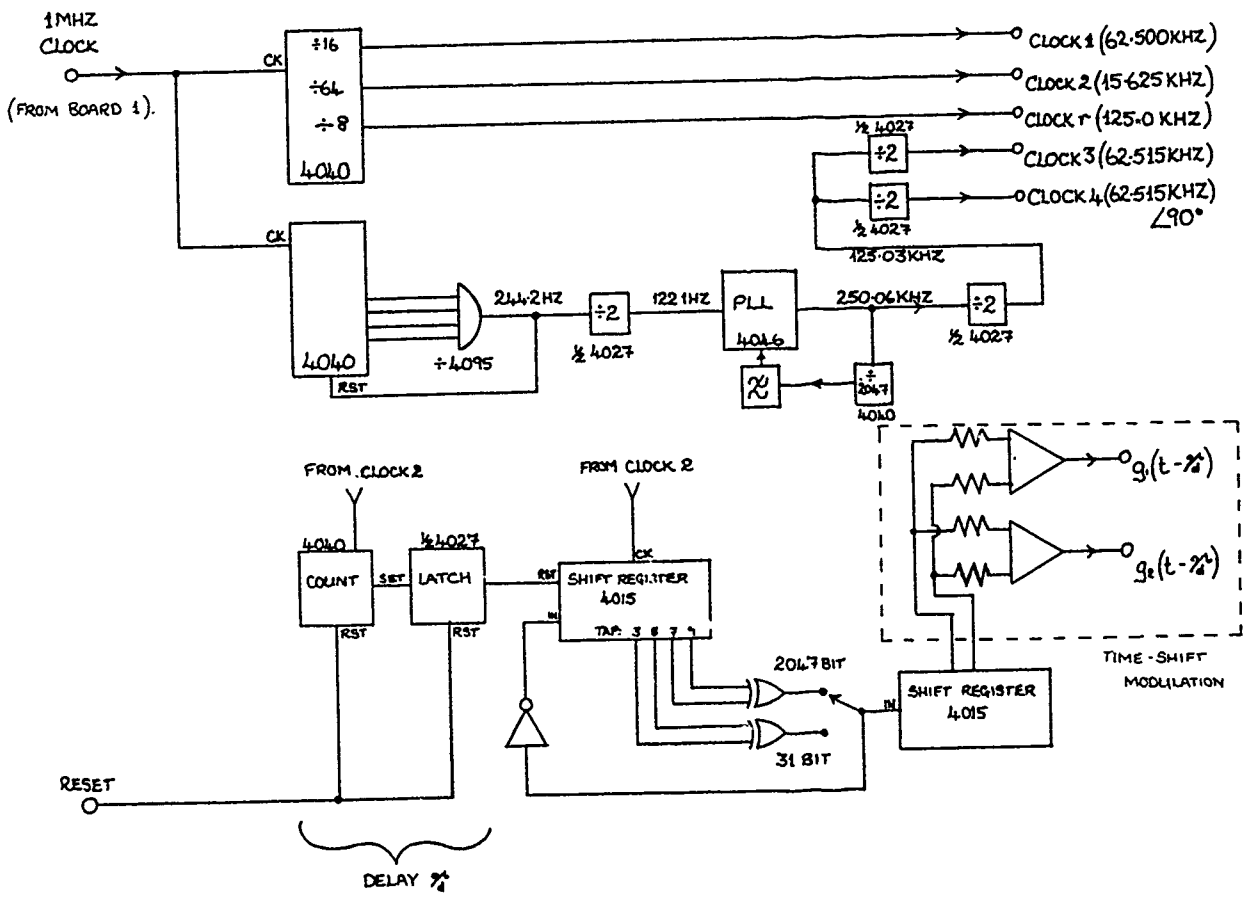

FIGURE; 7.2. TYPE II SYSTEM - BOARD 2 DIVIDER, FREQUENCY SYNTHESIS, DELAYED PRBS.

Board 2 also contains the delayed PRBS circuits. The delayed PRBS system works exactly as described for the Type Isystem. Upon receiving a reset signal, the second PRBS generator is reset and held in that state until allowed to start by a signal from the counter circuit. The delay circuitry was simplified with respect to Type I board 2 in that no switch selectable delays were provided. One 4040 binary counter serves as the delay counter, and delay times are selected by plugging the 4027 latch input into the desired binary count pin. For instance, a delay of 1024 counts will be provided if the latch is plugged into the divide-by-1024 output pin.

The time-shift modulation circuits are also contained on board 2. One circuit generates $g_1(t-\gamma_d^*)$ by taking the difference of two consecutive shift values of a 4015 shift register and the other circuit generates $g_2(t-\gamma_d^*)$ by taking the sum of the same two shift values, regarding the outputs as plus/minus one, not zero and one. The values of the weighting resistors around the appropriate op-amps are chosen so as to provide three-valued output signals of +15, 0, and -15 volts.

7.4 TYPE II SYSTEM, DEMODULATOR/CROSS-CORRELATOR (BOARD 3)

Board 3 contains all demodulating and correlating circuitry. The block diagram for board 3 is shown in figure 7.3.

DEMODULATION

The demodulating circuitry uses 4053 analogue switches to select either a non-inverted or inverted version of the incoming signal, the same arrangement as was used in the Type I Correlator. The multiplier output

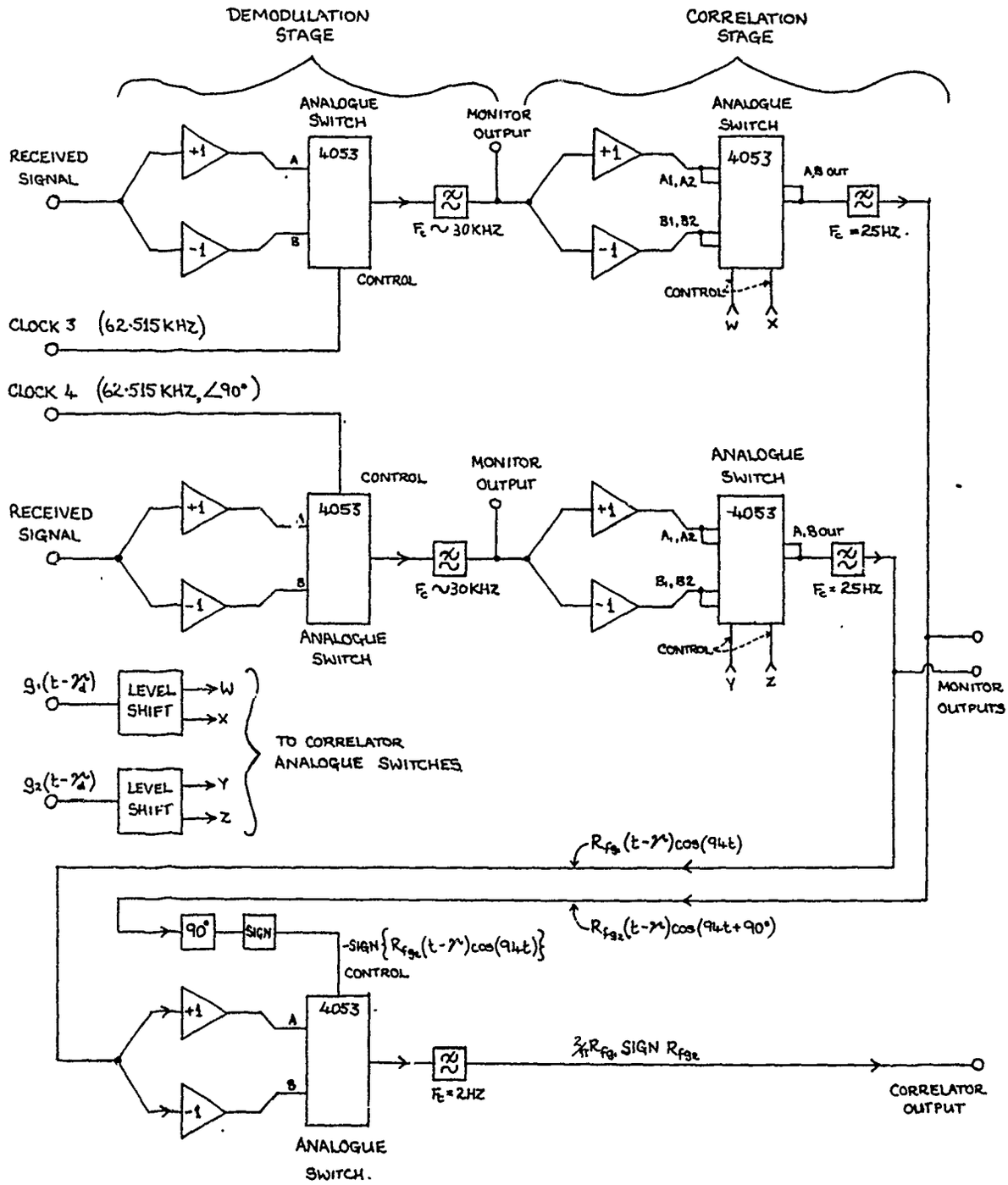

FIGURE; 7.3. TYPE II SYSTEM – BOARD 3 DEMODULATOR/CORRELATOR BOARD.

is filtered by a second order low-pass network which has a bandwidth of twice the PRBS clocking frequency. This was a much wider bandwidth than necessary and would of course be narrowed in further systems. Two demodulator circuits are contained on Board 3. These demodulator circuits are fed by the 62.515 signals: clock 3 and clock 4. The decision was made to build the prototype system with two separate demodulating sections. The received signal would be fed to both, but the demodulating carrier to one would lag the other by ninety degrees. Following demodulation, each signal is cross-correlated with one of the time-shift functions. The resulting sinusoids still retain the amplitudes of their respective cross-correlation functions, but the sinusoidal variation in each cross-correlation function will be out of phase by ninety degrees. This enables the two cross-correlation functions to be viewed on the XY inputs of an oscilloscope as Lissajous figures. Signals from targets at a range which produced a non-zero cross-correlation function would appear as ellipses with the spot rotating clockwise for targets beyond the preset range, counterclockwise for signals closer than the preset range, and a vertical line for targets precisely at the preset range. This arrangement allowed easier troubleshooting of the demodulator/correlator circuitry during the development stage. Following successful development, a decision was made to leave the modified system as designed, and add on a phase-shifting stage to the final multiplier circuit. This would produce a final correlator output as described in Chapter Six. Of course, a system designed anew would not need to contain this excess circuitry.

CORRELATION

The multiplier stages of the correlator stages differ from the Type I system in that the delayed PRBS signals g1 and g2 are the outputs of the time-shift modulator, and as such have three logic levels. It was necessary to design level shifting circuitry in order to allow this tri-level signal to switch the binary inputs of the 4053 analogue switch. This level shifting follows the truth table shown in table 7.2. The output voltage levels are +7.5 volts maximum due to limitations on the analogue switches. Input signals were also required to be less than +7.5 volts and larger than -7.5 volts.

g1, g2 voltage levels:	+15v,	0v,	-15v
(from board 2)			
Output A voltage level:	0v,	0v,	+7.5v
(on board 3)			
Output B voltage level:	+7.5v ,	0v,	0v
(on board 3)			

TABLE 7.2 LEVEL SHIFT TRUTH TABLE

The level shift outputs drive a pair of CMOS switches configured so that an input signal of 0 volts causes the switch output to be connected to earth through 2K2 resistors, +7.5 volts allows the non-inverted function to be selected, and -7.5 volts allows the inverted function to be selected. The multiplier outputs are then low-pass filtered by second-order Sallen-Key filters having a bandwidth of approximately 25Hz. At this stage, the correlator outputs should be dc values modulating a sinusoid at 15 Hz. However, target movement will produce changes in this

frequency (which will be covered in further detail in Chapter Eight). Therefore, a nominal value of 25 Hz was chosen for these filters, in order to allow target movement towards the transducers at speeds of up to 0.25 m/sec.

CORRELATOR MULTIPLICATION

The correlator multiplier uses a 4053 analogue switch, as did previous multiplier sections. As discussed earlier in this section, a ninety degree phase shift of one of the correlator outputs is required in order to provide system operation as described in Chapter Six. This phase shift was provided by a second-order low-pass filter which was designed to have a low damping factor (approximately 1.75). This caused the phase shift to vary slowly when the frequency was changed from the designed 15 Hz. However, as might be imagined, this modification was not an optimum one when targets were moving with respect to the transducers, but the prototype system did perform in a very satisfactory manner during dynamic tests. Following the phase shift, the signal was sent to a comparator stage, which performed the sign function mentioned in Chapter Six. The positive feedback resistors provided a 15 mv hysteresis, and the series capacitor in the positive feedback loop insured a rapid transition relatively unaffected by noise. The output of the comparator was then used to switch the control input of the 4053 analogue switch. The analogue switch selects either the inverted or the non-inverted $R_{fg_1}(t-\gamma)$ and connects it to the input of the second-order filter. This filter has a cutoff frequency of approximately 2 Hz, and it is this filter which determines the final SNR for the system.

7.5 CORRELATION TESTS, TYPE II SYSTEM

The Type II system was tested in the same manner as the Type I system; that is, placing the transducers in a fixed position, selecting a single PRBS delay time, and varying the distance to the target while simultaneously recording the correlator output. The system test parameters are listed in table 7.3.

PRBS Bit Rate	:	15.625 kbit/sec
PRBS bandwidth (-3dB)	:	7 kHz
Carrier frequency	:	62.500 kHz
Modulated PRBS bandwidth (-3dB)	:	15 kHz
Demodulator frequency	:	62.515 kHz
Target	:	19.5 mm disc
Preset expected Range	:	32.5 cm
Cross-correlation width	:	6.3 cm

TABLE 7.3 TYPE II SYSTEM TEST PARAMETERS

The theoretical cross-correlation function width is 3 bits and the time width of each bit is 64 microseconds. Sound, at 343 metres/sec, will travel approximately 6.59 cm during three bit times. Since the correlation system measures round trip time, the range width is halved to a range width of 3.3 cm for the test set-up. Two results of the experimental Type II cross-correlation function are shown in figure 7.4. As can be seen, the actual correlation functions closely resemble the theoretical function. The width is approximately 3.4 cm, vs the theoretical value of 3.3 cm. The Type II system experimental cross-correlation functions of all transducer pairs tested are shown in

Appendix D. All transducer pairs produced cross-correlation functions sufficient for purposes of control. In other words, the cross-correlation functions were reasonably close to the theoretical functions and would allow appropriately designed positioning circuitry (or algorithms) to reduce positional error to within system tolerances.

The Polaroid transducers exhibited an anomaly in the negative portion of the cross-correlation function (see Appendix D). This anomaly cannot readily be explained, but these transducers could still be used for control purposes as the cross-correlation function does not change sign at the points of anomaly.

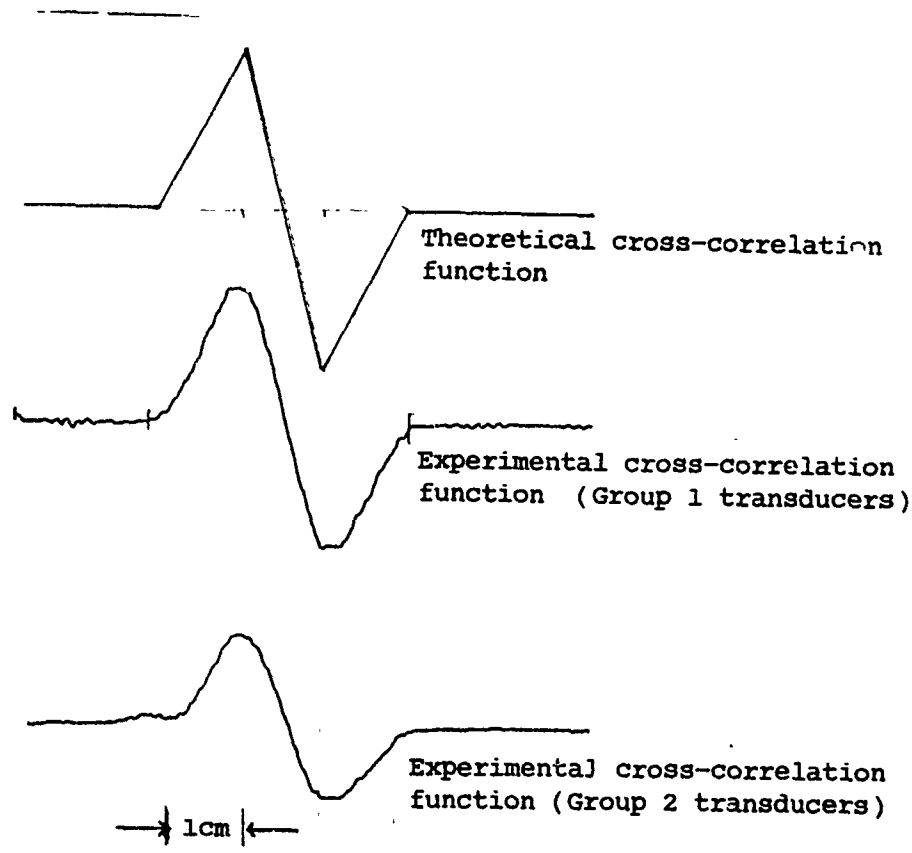

FIGURE 7.4 Type II System, Typical Cross-Correlation Function

7.6 WELDING NOISE TESTS, TYPE II SYSTEM

Due to the nature of the Type II system, the welding noise tests were conducted with the transducers placed so that they were at a fixed range from the target. The IRB-6 robot/welding set was then programmed to weld at distances from 30 to 40 cm from the transducers.

The system was tested using two correlator boards, one with a final bandpass of approximately 5 Hz, the other with a bandpass of approximately 2 Hz. Both outputs were recorded simultaneously while welding was performed. The correlator outputs had a range of plus/minus 6 volts for a range deviation of plus/minus 1.7 cm. Thus, using the 500 mv/div scale on the chart recorder (as was done for the FMCW weld tests), a relatively small range deviation would move the chart needle off-scale. However, the tests were done at the same recorder sensitivity to give a relative indication of the amount of noise reduction obtained. The system was adjusted so that the target (the welding sheet) was located at a range which produced the mid-point of the correlation function, providing a 0 volt output. Figure 7.5 shows the correlator outputs both with and without the welding noise added. As can be seen, the welding had almost no influence at all on the correlator output. The actual received signal input to the correlator boards was 0.5 vpp during periods of no welding, and 6 vpp during periods of welding, yielding an overall S/N average at the correlator inputs of approximately -21.6 dB.

7.7 SUMMARY

The Type II system performance was such that it was judged to be a success. The cross-correlation functions attained with the Oxford transducers was extremely close to the theoretical function, while the

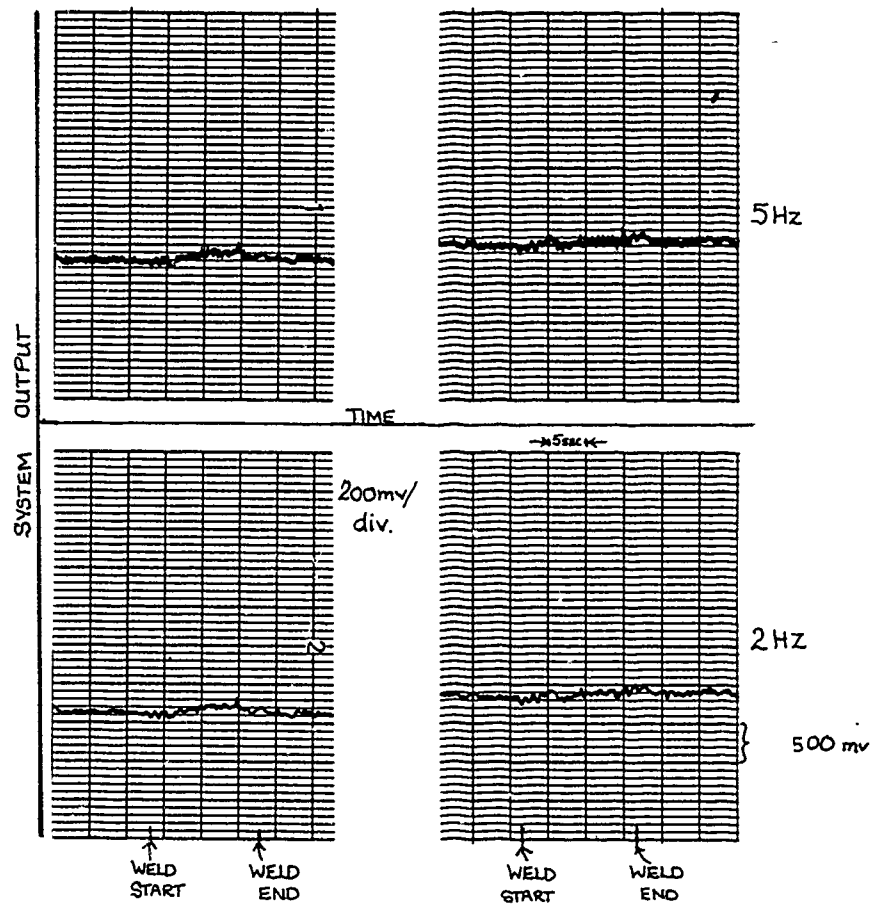

FIGURE : 7-5 TYPE II SYSTEM - WELDING NOISE TESTS

cross-correlation functions attained with the Polaroid transducers was acceptable, though they did show an unexplainable departure from the theoretical ideal (see Appendix D). This anomaly could perhaps be a function of the carrier frequency used, and might be removed by using a lower carrier. The success of system cross-correlation tests indicate that the design can be used for transducers which operate at a much higher center frequency.

The noise tests were judged to be completely successful. Welding noise was almost completely unnoticeable at the correlator outputs. This indicates that the system would be capable of providing range information even during periods of extremely poor signal-to-noise ratio. Strength of the target return signal will obviously affect the final signal-to-noise ratio, with small targets of low reflectivity showing more noise effects. However, the system will be able to compensate for the decreased signal-to-noise ratio if narrower bandwidth filters are used. This will, of course, result in a slower 'reaction time' for the correlator. The system performance was such that a decision was made to discontinue basic system development and use the time remaining to developing a preliminary tracking system. This tracking system is covered in Chapter Eight.

CHAPTER EIGHT

TRACKING TYPE II SYSTEMS

Chapters Four, Six, and Seven have discussed the theory and delelopment of a cross-correlation system which is capable of providing range information on targets which are buried in noise and clutter. However, the experimental system provides information concerning range only. This chapter covers additions to the experimental system which allow it to provide target azimuth information. Azimuth, in the context of this thesis, means the angle of the target under consideration with respect to the vertical axis (which is at right angles to the transducer plane). The modifications are incorporated into the experimental Type II system, and it is thus able to track selected targets. The modified system tracks targets in range and azimuth by using the correlator range-error information to control servos which physically move the transducers so that the range and azimuth error is reduced to approximately zero.

In addition, other modifications are suggested which will enable a system having stationary transducers to track moving targets. This system was not constructed due to time limitations.

8.1 A METHOD FOR DETERMINING TARGET AZIMUTH

Since the Type II system discussed in Chapters Six and Seven is capable of providing range error signals as a function of target deviation from an expected range, one method of determining the target azimuth from the transducer plane is to use two receiving transducers, spaced equally on either side of the transmitting transducer. A target at the correct distance and azimuth from the transmitter produces signals having equal range delays for each each receiver. Any target movement directly away from or towards the transmitter will produce equal changes in each correlator output; however, a movement lateral to the transducer plane will produce unequal range delays, and thus unequal correlator outputs. Such a system could be used to provide both target range and azimuth information.

8.2 BASIC CONFIGURATION

Consider a transducer array consisting of one transmitter and two receivers as shown in figure 8.1. In figue 8.1, a target located directly over the transmitting transducer at distance y will produce a range delay in either receiver which may be expressed as:

$$\gamma_{r_1} = \gamma_{r_2} = \frac{1}{c}\left\{ y + \sqrt{y^2 + d^2} \right\} \qquad (8.1)$$

where γ_{r_1} , γ_{r_2} are the signal travel times from transmitter to target, and from the target to back to the appropriate receiver.

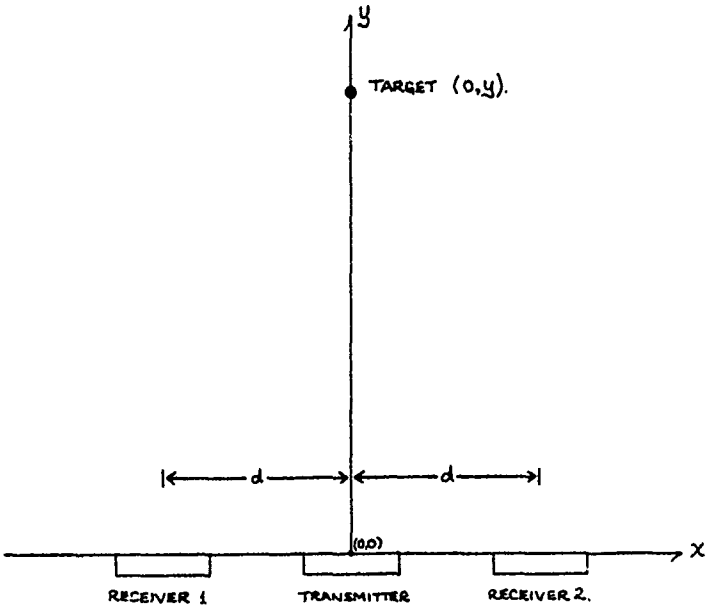

FIGURE 8.1 Ranging and Azimuth Set-Up with Two Receiving Transducers

Any target movement in the vertical (y) direction will produce equal changes in γ_{r1}° and γ_{r2}°. However, any target movement in the lateral (x) direction produces an increase in one range delay and a decrease in the other range delay. The actual times are calculated as follows.

$$\gamma_{r1}^{\circ} = \frac{1}{C}\left\{\sqrt{y^2+x^2} + \sqrt{y^2+(d+x)^2}\right\} \qquad (8.2)$$

$$\gamma_{r2}^{\circ} = \frac{1}{C}\left\{\sqrt{y^2+x^2} + \sqrt{y^2+(d-x)^2}\right\} \qquad (8.3)$$

The difference in each range delay, that is, the new range delay minus the old range delay, is calculated as:

$$\gamma_{r_1(OLD)} = \frac{1}{C}\left\{y + \sqrt{y^2+d^2}\right\} \simeq \frac{y}{C}\left(2+\frac{d^2}{2y^2}\right), \qquad x \text{ SMALL} \tag{8.4}$$

$$\gamma_{r_1(NEW)} = \frac{1}{C}\left\{\sqrt{y^2+x^2} + \sqrt{y^2+(d+x)^2}\right\} \simeq \frac{y}{C}\left\{1+\frac{x^2}{2y^2}+1+\frac{(d^2+2dx+x^2)}{2y^2}\right\} \tag{8.5}$$

$$= \frac{y}{C}\left\{2+\frac{(d^2+2dx+2x^2)}{2y^2}\right\}$$

$$\Delta\gamma_{r_1} = \gamma_{r_1(NEW)} - \gamma_{r_1(OLD)} = \frac{y}{C}\left\{2+\frac{(d^2+2dx+x^2)}{2y^2} - \left(2+\frac{d^2}{2y^2}\right)\right\} \simeq \frac{x}{Cy}\left(d+\frac{x}{2}\right) \simeq \frac{xd}{Cy}$$

$$|x| << D. \tag{8.6}$$

The actual correlator output is a sinusoid-like function of the range difference, and can be approximated by:

$$R(\gamma) \simeq A \sin\left\{\frac{2\pi}{P}\cdot\frac{xd}{Cy}\right\} \qquad ; \text{ FOR } \left|\frac{xd}{Cy}\right| \leq P/2 \tag{8.7}$$

where A is the amplitude of the cross-correlation function, and P is the period (a spatial period, not a time period). Using eq 8.7, the difference between the two correlator outputs can be expressed as:

$$R(\gamma_2) - R(\gamma_1) = A\left[\sin\left\{-\frac{2\pi}{P}\cdot\frac{xd}{Cy}\right\} - \sin\left\{\frac{2\pi}{P}\cdot\frac{xd}{Cy}\right\}\right] \simeq -\frac{4\pi A x d}{P y} \tag{8.8}$$

$$; \text{ FOR } \left|\frac{xd}{Cy}\right| \leq P/2$$

This difference signal can be fed to a circuit which controls the azimuth of the transducers. Any target movement in the positive or negative x direction will produce a positive or negative control voltage which would indicate to the controller the direction of rotation which would reduce the correlator output difference to zero.

The range error can be obtained from the sum of the correlator outputs. Note in the example given above that a target movement in the lateral (or x) direction will produce correlator outputs of opposite sign. A ranging controller which has as its input the sum of the two

correlator outputs will not correct for range error if a target is moved laterally, but would correct for error if there was any range (or y component) variation in the target movement. Thus, a system which produces the difference of the two correlator outputs can be used as an azimuth error system, while a system which produces the sum of the two correlator outputs can be used as a range error system.

8.3 TYPE II SYSTEM MODIFICATIONS TO ENABLE RANGE/AZIMUTH TRACKING

In order to provide target range/azimuth information as discussed in the previous section, the experimental Type II system described in chapter Seven was modified in the following manner:

1. Existing transmitting and receiving transducers were moved to a redesigned module, and an additional receiving transducer, with its required circuitry, was added.
2. An additional receiver cascode amplifier and voltage follower was added to the receiving module.
3. An additional correlator board was built and added to the system. The circuitry was identical to board 3. Additional circuitry was added to provide sum (correlator 1 + correlator 2) and difference (correlator 1 - correlator 2) outputs. These outputs are to serve as inputs to the appropriate servo actuators. The schematics are shown in the hashed box on Appendix B8.
4. The redesigned transducer module was mounted on the vertical shaft of a small dc servo moter with 500:1 gear reduction ratio. This motor, built many years ago by Ether Ltd., is capable of being driven by a 741 op-amp. The position of this shaft controlled the azimuth of the transducer module.

5. The transducer/servo assembly was mounted on a small trolley which was in turn connected via steel control cables to an ac-powered servo motor. The position of this motor shaft controlled the transducer trolly position, and hence, the transducer range to the target.
6. Controlling circuitry was constrcted to allow the range servo motor to be properly driven from an op-amp output. The controller is shown in Appendix B9.

The set-up for the prototype tracking system is shown in figure 8.2. In this experimental set-up, the system is preset to expect targets at the desired distance, the targets are placed within the system's range gate (approximately plus/minus 1.65 cm for the experimental system). The tracking system then attempts to maintain a constant range and azimuth with respect to the target.

The tracking system was tested by placing targets of various sizes at the preselected distance (32.5 cm) and noting the system's ability to maintain this distance along with a zero azimuth angle when the target was moved. The system proved to be successful in tracking targets varying in size from rods 1 cm in diameter to small wires 0.05 cm in diameter. It was able to acquire and track such difficult targets as that formed by the edges of a butt joint made by placing two 2 mm thick sheets of aluminium together. The tracking was unaffected by external transient noise having peak values over five times greater than the received signal. Clutter, formed by placing larger and smaller targets in the area around the principal target, did not affect tracking. Of course, the clutter was kept outside the approximately 3 cm range gate which was a characteristic of the experimental system.

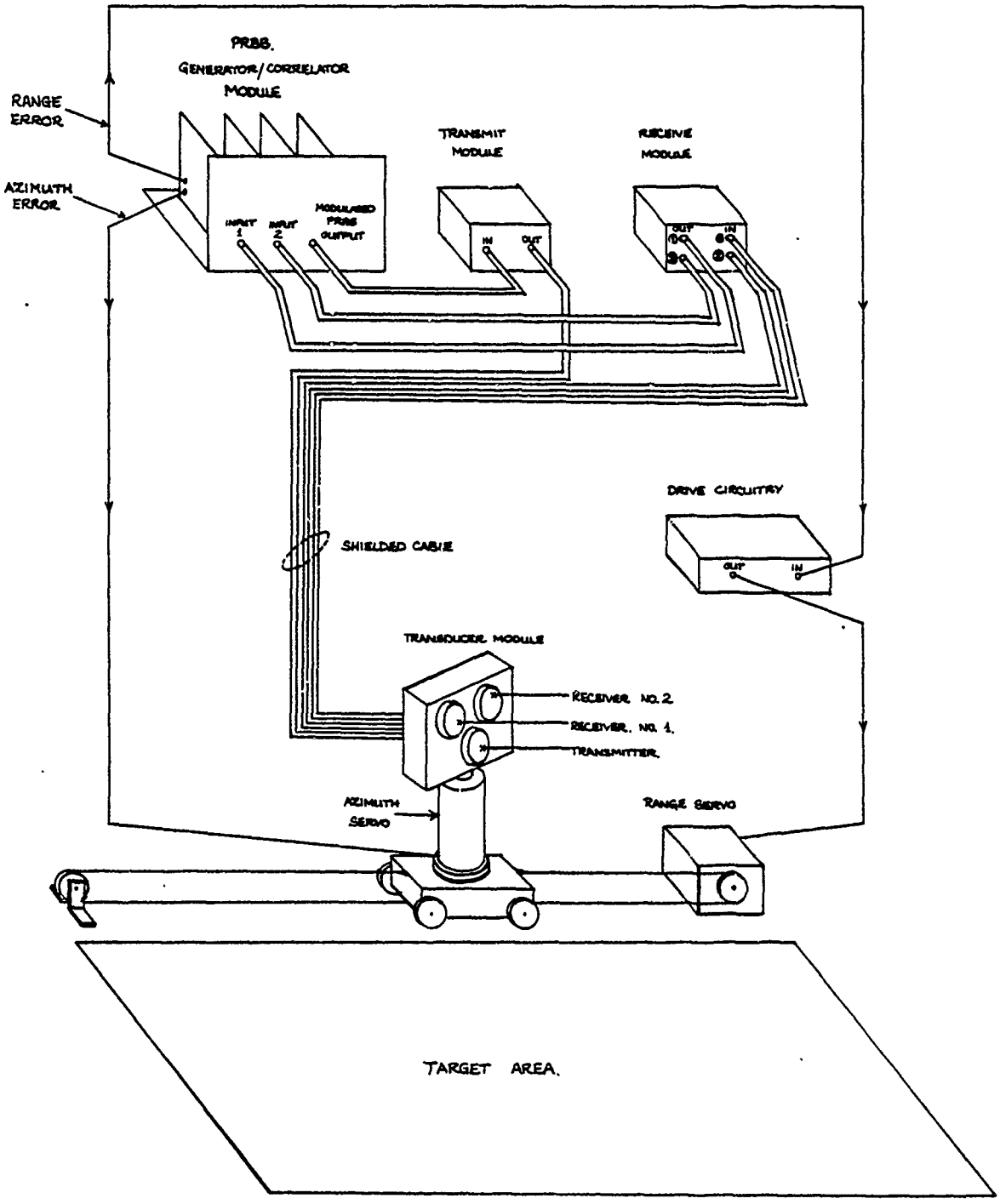

FIGURE 8.2. TYPE II TRACKING SYSTEM SET UP

8.4 TRACKING SYSTEM PROBLEMS

SIGNAL STRENGTH

One problem noted with the tracking tests was that the tracking gain was a direct function of the strength of the signal received from the target. This can be easily seen by reference to equation 6.6. The cross-correlation system ignores signals from all ranges outside the 'range gate' provided by the correlation function; however, the amplitude of the correlation function for a target at a range within this range gate will be a direct function of the target reflectivity. Because of this, system gains which provided good tracking of small targets were far too high to track large targets, with the result that the system became unstable and oscillated while trying to maintain the desired range and azimuth. Reducing the system gain eliminated this problem. However, it means that a tracking system will have to take expected target size (and reflected signal strength) into account if optimum servo-gain values are to be used. It may be possible to use automatic gain control on the sinusoid function which provides the final correlation function. However, the system bandwidth at the point of this sinusoid is considerably greater than the final system bandwidth; hence, the effects of noise might prove to be too great.

LAGS IN TRACKING

Preliminary tracking tests showed that there were definite limits to the speed with which the targets could be moved and still be tracked. This was due to the delays introduced by the reflected signal, correlator filters, and servo-systems. A successful controlling system will have to

take these factors into account. The factors affecting system reaction time will be discussed further in Chapter Nine. However, one effect of system tracking lag surfaced in a quite unexpected manner. It was noted that if the target was moved with a velocity for which the tracking system could not compensate, the transducer azimuth tracking seemed to transition from negative feedback to positive feedback. That is, the transducer azimuth angle seemed to diverge from zero azimuth and to attempt to increase the angle of divergence. Upon closer examination of the cross-correlation function, the reason becomes apparent.

Consider the hypothetical cross-correlation function shown in figure 8.3a. The cross-correlation function is idealized to a sinusoid of period P. Assume that a target is located at a position where the azimuth and range error signals are zero; that is, the target is located in the center of the range gate. If the target is moved at a velocity such that the azimuth and range correction servos cannot react fast enough, the change in range will soon be such that the cross-correlation function will diverge due to the range changes due to the azimuth error. This is illustrated in figures 8.3b. Should the range error continue to increase, the situation depicted in figure 8.3c will occur. As can be seen, the azimuth output reverses sign, and the correction voltages to the azimuth servo will be in error.

The most obvious solution to this problem is to adjust the servo gain such that the target is not allowed to have range errors exceeding, say, plus/minus 40% of the correlation range gate, where the width of the correlation range gate is half the distance that sound would travel in air during a time interval equal to the time width of the cross-correlation function.

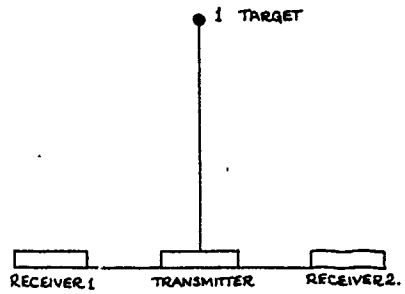

a) TARGET CENTERED OVER TRANSMIT TRANSDUCER AT POINT 1.

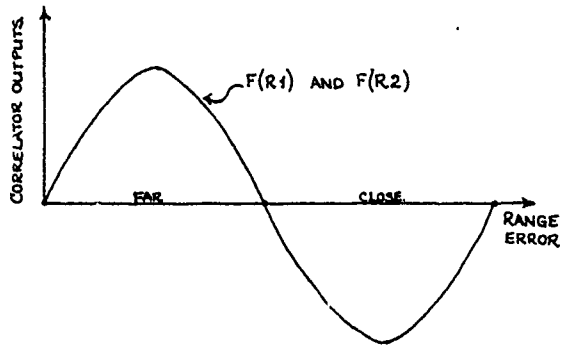

BOTH CORRELATION FUNCTIONS EQUAL.

$F(R1) + F(R2) = 0$ CORRECT RANGE

$F(R1) - F(R2) = 0$ CORRECT AZIMUTH.

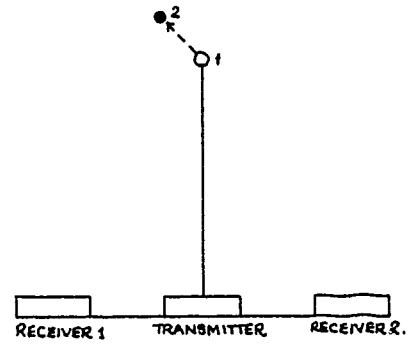

b) TARGET MOVES FROM 1 TO 2, AZIMUTH AND RANGE SERVOS NOT CORRECTING.

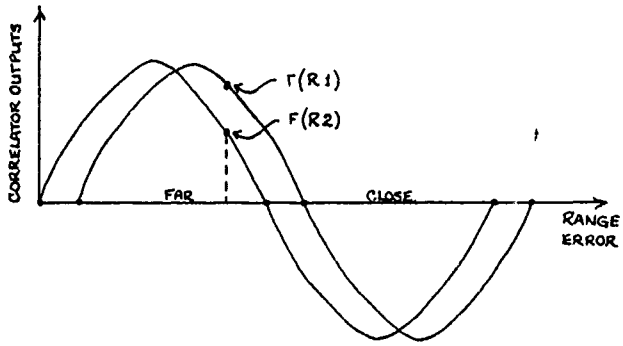

CORRELATION FUNCTIONS UNEQUAL,

$F(R1) + F(R2) > 0$ CORRECT RANGE ERROR FUNCTION.

$F(R1) - F(R2) > 0$ CORRECT AZIMUTH ERROR FUNCTION.

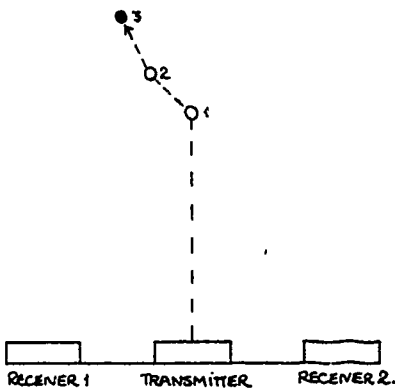

c) TARGET MOVES FROM 2 TO 3, AZIMUTH AND RANGE SERVOS NOT CORRECTING

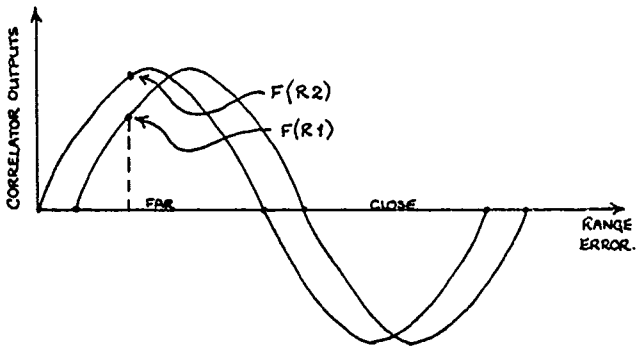

$F(R1) + F(R2) > 0$ CORRECT RANGE ERROR

$F(R1) - F(R2) < 0$ INCORRECT AZIMUTH ERROR FUNCTION

8.5 A PROPOSED ALTERNATIVE TYPE II TRACKING SYSTEM

In the Type II tracking system described thus far, the expected target range delay value is preset, and the tracking system provides range and azimuth errors for a target located within certain limits of the preset range delay value. While this type of arrangement is ideal for robotic situations in which the transducers can be mounted on the robot and error signals can drive the robot (and the transducers) to a correct position, it would be unusable in situations where the target range is able to change, but the transducers are fixed. In order tc provide usable range information, the tracking system would have to vary its delay time to match the target delay time.

One method of accomplishing this is to modify the Type II system in the manner shown in figure 8.4. The modifications to the existing system are shown in the hashed lines. In the experimental Type II system, both PRBS generators are set to zero upon command of the reset (RST) signal. When the RST signal is removed, PRBS generator one feeds binary sequences to the modulator and thence to the transmitter. PRBS generator two is held in the zero state for an additional amount of time determined by the timing counter shown in the diagram. The time difference between the two PRBS generators, γ_d , remains fixed unless the system is reset and another preset count is selected. The modifications allow the initial delay γ_d to be preset as before. However, once both PRBS generators are operating, the second PRBS generator is clocked by a voltage-controlled-oscillator (VCO) whose frequency is adjusted to be approximately equal that of the reference oscillator when fed a control voltage of zero volts. Targets deviating from the preset range will cause a change in the correlator output voltage from its original zero

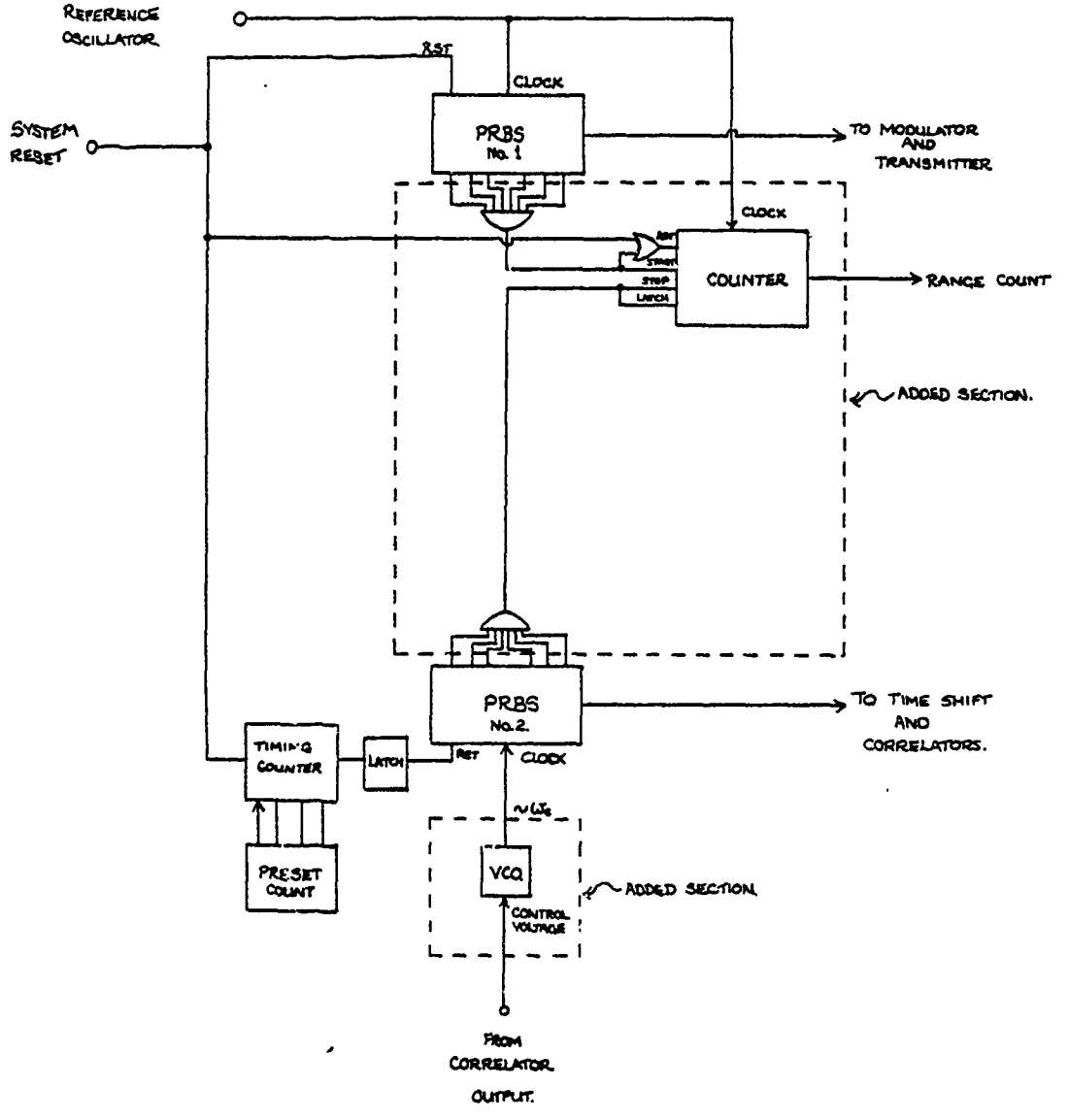

FIGURE; 8.4 TRACKING SYSTEM MODIFICATIONS, TYPE II SYSTEM WITH STATIONARY TRANSDUCERS.

point. These changes will in turn drive the VCO to a higher or lower frequency relative to the reference oscillator. The relative delay, γ_d, will then vary according to the amount of time that the VCO has been at a different frequency than the reference oscillator.

The time difference between the two PRBS generators can be determined by marking the times that identical states of each PRBS shift register are reached. These states can be determined by appropriate logic circuitry connected to each shift output (the all zero state provides an ideal reference point). If two receiver/correlators are available, the system will provide two independent range signals. These signals can be added and subtracted as before to provide both range and azimuth outputs.

This system is only a proposed system, and has not been built. Therefore, there are most probably additional factors to consider. However, the overall concept seems to merit further consideration.

8.6 SUMMARY

The Type II system was modified to incorporate an additional receiver/correlator. The output of this additional correlator was combined with the output of the original correlator in such as manner as to provide information on both target range and azimuth. This was done by using the sum of both correlator outputs for the range error signal, and the difference of the correlator outputs for the azimuth error signal. The range and azimuth signals were in turn used to drive servo-mechanisms which physically positioned the transducer module to maintain minimum range and azimuth errors. The modified Type II correlation system is capable of tracking a wide range of targets

including long wires of 0.05 cm diameter. The tracking system gain is a function of target reflectivity, and thus requires adjustment to allow for different target reflectivity functions. In a robotic system, these adjustments could be accomplished through the use of previous knowledge about the expected target, along with self-tuning controller mechanisms.

A further modification to the present experimental was proposed which would allow a stationary set of transducers to provide tracking information. This modification required that the PRBS generator used as a correlator reference be driven from its own oscillator, the frequency of which would be controlled by the correlator output. In such a system, target range could be determined by measuring the time difference between like states of the two PRBS generators. The circuitry required to determine this time difference was discussed. If two correlator boards, each fed by an independent receiver, are used, this system is also able to provide azimuth information by determining the time difference between the target range values provided by each correlator system. This proposed modification has not been constructed and tested.

CHAPTER NINE

FACTORS AFFECTING SYSTEM ACCURACY

Chapters Four through Eight have detailed the theory and development of an experimental pseudo-random signal cross-correlator which is capable of providing target range and azimuth information in less than ideal conditions. The thrust of the research detailed in this thesis has been directed towards the theory and development of an advanced noise and clutter immune tracking system. Accuracy, as such, has not been critically assessed, save for establishing that the system indeed was able to identify and track targets located at appropriate ranges. The system, when given information about target location, was indeed able to locate the desired targets, even when these targets were buried in noise and clutter. The tracking system was able to maintain transducer to target distances which were stable to within 2mm. Further accuracy tests were not made due to the fact that the ranging set-up would have had to be modified in order to provide repeatable measurements to sub-millimeter accuracies.

This chapter deals with factors which concern system accuracy and lists methods which may enable the effects to be reduced. In addition, it also comments on factors which will affect the control algorithms used to track the selected targets.

A recent study on the attainable accuracy of air-based sound ranging systems by Fox [17] utilized both a pulse echo system and also a phase sensitive system, both operating in a relatively noise-free environment. Fox has been able to attain absolute accuracies of less than plus/minus 0.04 cm, and an rms range error of 0.02 cm with the pulse echo system and range errors of less than 0.001cm with the phase measurement system. The phase measuring system attains its accuracy by making many separate measurements over periods of tens of seconds and averaging the results. Since a tracking system will have to make continuous measurements in order to provide timely tracking information, the accuracies attained by the pulse-echo system seem to be the most realistic criteria for use as a maximum accuracy criteria for the cross-correlating system. Therefore, in the subsequent analysis, factors which cause less than 0.04 cm variation will be considered to be not worth compensation.

The following sections will deal with accuracy factors which affect the ranging performance of the experimental Type II system discussed in Chapters Six and Seven. In this system, a PRBS reference signal is modulated by a carrier of 62.5 kHz and transmitted. The reflected signals are demodulated by a carrier of 62.515 kHz and then cross-correlated with two modified versions of the original PRBS. The cross-correlator outputs are then multiplied to produce the resulting correlator output which has the form of the ideal control signal shown in figure 4.6. Azimuth information is obtained by duplicating the receiver/correlator systems and using the difference in time-of-flight from the target to each receiver to provide the required correction signals.

In assessing the potential accuracy of the Type II system, a distinction must be made between two types of measurement which are involved: time and distance. A correlation system measures time, and this time measurement is used to obtain a measure of distance by utilizing knowledge of the speed of sound in air. As will be seen, the factors affecting time accuracy are easily controlled; factors affecting the assessment of the speed of sound are more variable. As a result, any final system calibration must used an absolute distance measure of some sort.

9.1 ACCURACY FACTORS AFFECTING THE TYPE II SYSTEM (INTERNAL TO SYSTEM)

OSCILLATOR STABILITY

The Type II system gains its estimates of target range by comparing signal time-of-flight against an internal time standard. The time standard used is a crystal-controlled 1 MHz oscillator which has a specified accuracy of 200 ppm over a temperature range of -20 C to +70 C. For target ranges of one meter or less, this frequency variation can be converted to an approximate range variation of 0.2mm. This is at the limit of range accuracy specified at the beginning paragraphs of this chapter. Further, the temperature variations encountered by any system operating in a production environment would not be expected to undergo such extreme temperature variations as those listed for the crystal tolerance. Therefore, it seems reasonable to conclude that master oscillator frequency variations are not considered to be great enough to require compensation. Should this be considered a factor, one method of lessening the errors is to use a crystal with tighter tolerances, and control the crystal temperature.

OFFSET VOLTAGES

The post-correlation stages of the Type II system are the only portions of the experimental set up which handle dc voltages. As such, any dc voltage present at these stages which is not caused by the cross-correlation function will introduce error into the final range measurements. Offset voltages are on the order of 5 mv for the 351 series of op-amps used in the Type II system. This offset voltage cannot be directly related to range deviations. This is because the amplitude of the cross-correlation function for a given range deviation is a function of the received signal amplitude. The received signal amplitude is, in turn, a function of target reflectivity. For instance, a given target at a range R may produce a correlator output of amplitude A if this range is in error by, say, 1cm. However, a different target at this same range and which has twice the reflectivity might produce a correlator output of 2A for the same range error. The constant offset voltage of x millivolts would exist in both situations, but in each would be a different percentage of the correlator output. Therefore, dc offsets will introduce constant range error, but a range error which is not easily calculated. The dc offset errors can be reduced by careful attention to dc offsets in the post-correlator stages. The system can still be calibrated to reduce the effects of dc offset errors by measuring the range of a selected calibration standard and adjusting offset adjustments so as to produce the required zero volt correlator output.

9.2 ACCURACY FACTORS AFFECTING THE TYPE II SYSTEM, EXTERNAL TO SYSTEM

External factors may be subdivided into influences of the wave conducting medium (air) on the velocity of sound, any motion of the air itself, and the effects of target motion on the system.

The velocity of sound in air is given in standard texts (Howatson [28]) as:

$$C = \sqrt{\gamma R \hat{T}} \qquad (9.1)$$

where γ is the ratio of specific heats, R is the gas constant, and $\hat{T}$ is the ambient temperature in degrees Kelvin. Using values of γ =1.4, R=287.1 $m^2/s\ ^\circ K$, and 293 for $\hat{T}$ at 20°C, the velocity of sound is calculated to be 343.17 metres/sec. The change in the sound velocity with respect to temperature at 20°C is approximately 0.59 metre/sec °C. Since sound velocity is a function of temperature, an accurate ranging system must take into account changes in ambient temperature if accuracy is to be maintained. Assuming a target at a maximum range of 1 meter, as before, a change in ambient temperature of 1°C (from 20°C) would produce a change in time-of-flight of approximately 0.01 millisecond, for a range error of approximately 1.7 mm. One method of compensating for this problem would be to use temperature sensing to adjust the frequency of the 1 MHz master oscillator. An increasing temperature would mean that sound takes slightly less time to traverse a given distance. Thus, the time-base of the system could be slightly decreased so as to compensate for this reduced time.

9.3 EFFECTS OF AIR CURRENTS

Any air movement between the transducers and targets will affect the range value. For a target located at range r, air currents parallel to the line between transducers and target will alternately increase and decrease the apparent sound velocity, as is shown in eq. 9.2.

$$T_{t+r} = \frac{2rc}{c^2 - v_y^2} \triangleq \frac{2r}{c}\left(1 + \frac{v_y^2}{c^2}\right) \qquad (9.2)$$

where T_{t+r} is the signal return time and Vy is the air velocity parallel to the direction of wave travel. For air currents at right angles to the line between transducers and targets, the apparent sound velocity changes as is shown in eq. 9.3.

$$T_{t+r} = \frac{2r}{c}\sqrt{1 - \frac{v_x^2}{c^2}} \triangleq \frac{2r}{c}\left\{1 + \frac{v_x^2}{2c^2}\right\} \qquad (9.3)$$

where Vx is the air velocity perpendicular to the direction of wave travel. The change in travel time as a function of each current is:

$$\Delta T_{\epsilon y} = \frac{2r}{c}\left(\frac{v_y^2}{c^2}\right) \qquad (9.4)$$

and

$$\Delta T_{\epsilon x} = \frac{r}{c}\left(\frac{v_x^2}{c^2}\right) \qquad (9.5)$$

for air motion in the y and x directions, respectively. For targets at a range of one metre, using a sound velocity of 343 metre/sec (at 20°C), the changes in travel time for currents of 1 metre/sec are, respectively:

$$\Delta T_{\epsilon y} \triangleq 50 \text{ n sec} \qquad (9.6)$$

and

$$\Delta T_{\varepsilon x} \simeq 25 \text{ n sec.} \qquad (9.7)$$

These time changes can be equated to apparant range changes of approximately 0.15 mm and 0.008 mm, respectively. These values are lower than the accuracy limits set at the beginning of this chapter. Therefore, air currents of velocities of 1 metre/sec or lower will cause deviations in apparent range which are less than the minimum deviation discernible, and can be safely ignored.

9.4 EFFECTS OF TARGET MOTION (DOPPLER EFFECTS)

If a target is moving with respect to the transducers, the time of travel of a signal from transducers to target and return is unchanged, but the frequency of the returned signal will be changed by a factor which is proportional to the speed of the target with respect to the transducers. The expression for the change in frequency is [64]:

$$f_2 = \frac{f_1(1 + V_y/c)}{(1 - V_y/c} \qquad (9.8)$$

where f_1 is the original frequency and f_2 is the Doppler shifted frequency. If Vy<<C, eq 9.8 can be simplified to:

$$f_d \simeq f_1 \frac{(2V_y)}{C} \qquad (9.9)$$

where f_d is difference in frequency between transmitted and received signals. In order to understand the effects of Dopper shift on the PRBS system a quick reiteration of the basic operation of the Type II system is in order. The system, as described in Chapter Seven, uses a reference

PRBS signal to modulate a carrier at 62.5 kHz. Following transmission and reflection from the target(s), the received signals are demodulated by an asynchronous carrier (62.515 kHz). The demodulated signals are then fed to two cross-correlation systems, each one being fed by a changed and delayed version of the reference PRBS. The cross-correlation functions emerging from these two correlators are sinusoids having a frequency of 15 Hz (the difference frequency of the transmitting carrier and demodulating carrier). The amplitude of each sinusoid is a function of the deviation of target delay time from the expected delay time. These two sinusoids are combined in order to yield a dc cross-correlation function resembling the ideal function shown in figure 4.6.

If the above system parameters are used eq 9.9 indicates that a 1 Hz difference frequency will be produced by a target motion of approximately 2.74 mm/sec. Since the post-correlator bandpass filters have a cutoff frequency of approximately 30 Hz, this means that a total frequency deviation of plus/minus 15 Hz from the expected 15 Hz can be tolerated. This yields a maximum allowed target velocity (Vy) of approximately 4.11 cm/sec. If higher velocities are expected, the 15 Hz difference frequency can be raised along with the low-pass filter cutoff frequency. Note that with the system as designed, the actual frequency of the post-correlation sinusoid does not affect the final correlator output. That is, the correlation output will still show a null when the target passes through the expected distance. However, the target velocity could be calculated separately by using any number of frequency measuring techniques. This independence of range and range rate signals is a useful feature of this type of ranging system. The Doppler shift of the cross-correlation sinusoids can be used directly to provide information concerning small target velocities. If a frequency analysis system (as described in Chapter Three, section 3.5) is added to the correlator

board, the output of the frequency comparator would be a dc signal proportional to target velocity. Of course, the accuracy of this system would be degraded for large velocities since the output function would be linear only for velocities close to zero. However, it could provide valuable information to the tracking controller, and have the effect of making less probable the tracking azimuth errors which can be introduced by targets moving towards the limits of the correlation range gate (see Chapter Eight).

A much more rigorous analysis of the effects of target motion on random signal correlating systems is given by Gassner [22]; however, he also concludes that the range and range rate functions of a cross-correlating system are independent.

9.5 FACTORS AFFECTING TARGET TRACKING

The Type II cross-correlation system, as designed, will produce two final output signals. One signal is an error signal relating the deviation in expected distance of target to the relative distance obtained through correlation. The other signal is the target deviation in azimuth obtained through comparison of two separate relative range signals. As mentioned in Chapter Eight dealing with a primitive tracking system, no efforts have been made optimize the control system, as this was not the goal of this thesis. However, there are delay factors introduced by the Type II system which must be attended to if an optimum control system is to be devised. These delay factors are: range delay, filter delays, and servo delays. Since servo delays are considered to be in the realm of the controller, they will not be discussed. In addition, servo delay problems would be avoided in the proposed alternative tracking system.

RANGE DELAY

If the system is assumed to be successfully tracking a stationary target at range r, any knowledge of change in target range will be delayed by a factor of:

$$\Delta \gamma_{\varepsilon} = \frac{r}{C} \qquad (9.10)$$

where this delay is due to the amount of time required for a signal to travel from the target to the receiving transducers. Further, this delay time is obviously variable. This must be taken into account by the hardware (or software) which determines the speed of response to any change in target range or azimuth.

FILTER DELAY

Following reception of a signal indicating altered target range, the received signal passes through many filter stages. Each stage will introduce a time lag which is normally taken to be the inverse of its bandwidth. Since the final low-pass filter has, by a large margin, the lowest bandwidth, this filter lag determines the overall correlator system lag. If the system response proves to be too slow, the intuitive solution is to increase the bandpass of these final filters. However, the bandwidth of these filters also determines the maximum signal-to-noise ratio enhancement attainable by the correlating system (Chapter Four). There is a thus a trade-off between the filter's ability to respond to a rapid target range change, and its ability to reject external noise.

9.6 SUMMARY

Even though previous chapters have described an experimental correlation system capable of tracking targets located in noise and clutter, only a small amount of attention has been paid factors affecting system accuracy. These factors include internal considerations as oscillator stability and voltage offsets. Oscillator stability should, in theory, be sufficient to allow measurements to the limit established for ranging systems acting in real time: 0.4 mm [22]. Voltage offsets will introduce variable errors which are not directly known due to target/correlator output interraction. However, calibration of the system using known distances will provide a means of reducing voltage offset errors.

External factors affecting the time-of-flight of target information include air temperature and currents. Temperature compensation is easily included into the system. Air currents of any reasonable amount should not affect the limiting accuracy.

The correlation system is capable of separately resolving distance and range velocity information. As such, the experimental correlation system is, in theory, capable of providing both range and range rate information to the controller. A relatively simple addition of a frequency comparison system as used in Chapter Four will allow the Type II correlation system to provide target velocity (range rate) information as well as range and azimuth error information.

CHAPTER 10

CONCLUSIONS AND RECOMMENDATIONS

The problem stated in Chapter One of this thesis was to develop and test an ultrasonic ranging system capable of tracking targets located in noise and clutter. During the course of research, three systems were developed and tested: A Frequency Modulated, Continuous Wave (FMCW) tracking system, a basic correlation system using pseudo-random binary sequences (PRBS) as the reference signal (the Type I system), and a carrier correlation system using asynchronous demodulation and cross-correlation with time-shift modulated versions of the reference signal (the Type II system). The overall results can be summarized as follows:

10.1 FMCW TRACKING SYSTEM

The FMCW tracking system covered in Chapters Two and Three offers great potential for signal-to-noise ratio (SNR) enhancement. Further, it is easily modified to provide single target tracking. It has been shown that, while this system is inherently limited in its ultimate ability to enhance SNR, the improvements afforded by the tracking system allowed an experimental system to provide tracking information where an unmodified FMCW system could not. The system tracked targets with receiver SNR values of approximately -26dB, although the range signal was still

measurably degraded by noise.

10.2 TYPE I CORRELATION SYSTEM

The first PRBS correlation system to be constructed, the Type I system, used techniques which are presently widely used in Non-Destructive Testing (NDT) systems: Cross-correlation of a PRBS signal with either itself or a phase-modulated version of itself. Unlike NDT systems, both phase-modulation and time-shift modulation were utilized in an effort to provide a modified correlation function capable of being used by a controller as well as shifting the PRBS spectrum to an area more efficiently usable by the transducers. This system did provide correlation information, but it was not the theoretical control function which was desired. However, the results were virtually identical to those obtained by other users of this type of system. The cause was the link between signal bandwidth and transducer center frequency. The higher the frequency, the higher the bandwidth. In all non-carrier systems surveyed, and in the experimental Type I system tested, the resulting signal bandwidth was beyond the transducer capability. The addition of equalization systems designed to increase transducer bandwidth showed that this method did produce workable cross-correlation functions in some cases; however, the results were dependent on transducer frequency response, which varied from unit to unit and changed in any one unit over time. Thus, this method of correlation was judged to be not worthy of further development.

10.3 TYPE II CORRELATION SYSTEM

The Type II correlation system uses modulation techniques to raise the PRBS spectrum to an area more efficiently usable by the transducers. The received signal is cross-correlated with two time-shift modulated versions of the delayed PRBS. The first prototype of the Type II system provided cross-correlation functions which were almost exactly as that described by theory.

The Type II correlation system described in Chapters Six and Seven proved to be successful in operating in extremely noisy environments, attaining and tracking targets in the presence of clutter, and providing real-time target range and azimuth information. The final system utilizes the following features:

1. PRBS used for the reference signal to be modulated and transmitted

2. Double sideband modulation and asynchronous demodulation used for the transmitter and receiver.

3. The received signal is cross-correlated with two modified versions of the reference PRBS, and the final cross-correlation output is a function of these two cross-correlated signals.

4. PRBS modification is accomplished through time-shift modulation. Time-shift modulation is capable of providing altered correlation functions which are extremely useful in systems which use the correlator output for control purposes.

5. Dual receiver/correlator systems, coupled with sum/difference circuitry and associated servos provided the system with target range and azimuth tracking capability. The feedback system used the correlator outputs as control inputs, with no further signal processing needed.

10.4 RECOMMENDATIONS

Given that the Type II correlation system is one which deserves further development, the following are suggestions for future research:

1. Construction and testing of the alternative tracking system described in the last portion of Chapter Eight. This alternative system used the correlation output to vary the frequency of the second, or delayed PRBS clock, thereby varying the relative delay between it and the reference PRBS. This system would allow target tracking using stationary transducers. The revised system will in all probably require digital control in order to fully realize its potential.

2. Implementation of a Doppler shift measuring system. As mentioned in Chapter Nine, the component of target motion normal to the transducer plane will produce frequency shifts in the correlation sinusoid. It is possible to construct a frequency comparison network similar to that described in Chapter Three which would provide a dc signal which would be proportional to the target velocity (for small velocities). This would add another degree of information for the target tracking

controller. This modification will probably require that the difference frequency between transmitting and receiving carriers will have to be increased. This will require only minor modifications on the Type II system divider/frequency synthesis board (board 2).The Doppler shift output will, of necessity, be more succeptible to noise effects due to the fact that it is operating in a portion of the correlating system which has a higher bandwidth than the final filters. It may be possible to overcome this problem through judicious design.

3. Changing the system carrier frequency to make use of the newer transducers which are capable of operating in air at very high frequencies. Fox [17] describes a 1MHz air-based transducer capable of operating in the pulse-echo mode over distances of 40 cm. The PRBS correlator system should, in theory, be able to operate over even greater ranges due to its enhanced SNR. A 1 MHz system should be able to resolve extremely small targets (the one described by Fox has a bandwidth of 80 kHz). This revised system might be capable of providing the extremely fine positional information required in some robotics applications, and do it as a much lower cost than vision systems. However, it must be remembered that higher operating frequencies will produce larger Doppler shifts, which will in turn require higher bandwidths in order to handle the Doppler frequencies.

10.5 CONCLUSION

FMCW and PRBS systems are indeed capable of providing increased SNR enhancement over basic pulse-echo systems due to their higher duty cycle and ability to apply advanced filtering techniques. Both systems are capable of being modified to provide ranging systems capable of active tracking of targets which are buried in noise and clutter.

The PRBS system offers the most potential for noise-immune tracking due to the fact that the final system has broken the link between system bandwidth and operating frequency. As such, the builder has control over these critical variables. The Type II PRBS system as described in this thesis is extremely versatile and capable of extensive development. It has the capability to provide relatively inexpensive, accurate ranging information in the high-noise and clutter working environments often found in robotics applications.

REFERENCES

1. Acton, W.I., "The Effects of Industrial Airborne Ultrasound on Humans," Ultrasonics, May 1974.

2. Arata, Y., Inoue, K., Futamata, M., Toh, T., "Investigation on Welding Arc Sound," Transactions of the Japaneese Welding Research Institute, Vol 8, No. 1, 1979.

3. Banks, D.S., "Continuous Wave Radar," IEEE EASCON, 1973.

4. Battye, J.S., "An Industrial Correlation Flowmeter," PhD Thesis, School of Control Engineering, University of Bradford, 1976.

5. Beck, M.S., "Powder and Fluid Flow Measurement Using Correlation Techniques," PhD Thesis, School of Control Engineering, University of Bradford, 1969.

6. Biltugay, N.M., Furgason, E.M., Newhouse, V.L., "Evaluation of a Random Signal Correlation System for Ultrasonic Flaw Detection," IEEE Transactions on Sonics and Ultrasonics, Vol. SU-23, No. 5, Sept 1976.

7. Bloch, A., Buecks, K.E., Herton, A.G., "Improved Radio Altimeter," Wireless World, Vol. 60. Mar 1954.

8. Boys, J.T., Strelow, E.R., Clark, G.R.S., "A Prosthetic Aid for a Developing Blind Child," Ultrasonics, Jan 1979.

9. Boys, J.T., Mason, J.L., Hodgson, R.M., "Improved Continuous Wave Frequency Modulated Sonars with Aural Displays," Ultrasonics, May 1978.

10. Briot. M., Talou, J.C., Bauzil, G., "The Multi-Sensors Which Help a Mobile Robot Find Its Place, " Sensor Review, Jan 1981.

11. Chapelon, J.Y., Cathignol, D., Fourcade, C., " Improved Ultrasonic Sensitivity Using Pseudo-Random Binary Code Phase Modulated Signals," Ultrasonic Imaging I, Academic Press, 1979.

12. Clement, Johnson, "Electrical Engineering Science, " McGraw-Hill, London, 1960.

13. Coulthard, J., " Ultrasonic Cross Correlation Flowmeters, " Ultrasonics, Mar 1973.

14. Erikson, K.R., Fry, F.J., Jones, J.D., "Ultrasound in Medicine - A Review," IEEE Transactions on Sonics and Ultrasonics, Vol. SU-21, No. 3, Jul 1974.

15. Elias, C.M., "A Pseudo Random Binary Noise NDE Ultrasonic Correlation System," IEEE Ultrasonics Symposium, 1978.

16. Elias, C.M., "An Ultrasonic Pseudorandom Signal Correlation System," IEEE Transactions on Sonics and Ultrasonics, Vol. SU-27, No. 1, Jan 1980.

17. Fox, J.D., Kuri-Yakub, B.T., Kino, G.S., "High-Frequency Acoustic Wave Measurements in Air," IEEE Ultrasonics Symposium, Atlanta, Oct 1983.

18. Furgason, E.S., Newhouse, V.L., Bilgutay, N.M., Cooper, G.R., "Application of Random Signal Correlation Techniques to Ultrasonic Flaw Detection," Ultrasonics, Jan 1975.

19. Furgason, E.S., "Optimal Operation of Ultrasonic Correlation Systems," IEEE 1982 Ultrasonics Symposium.

20. Ganes, M., "Tornato Interceptor Unveiled," Flight International, 24 Mar 1984.

21. Gabel, R.A., Roberts, R.A., "Signals and Linear Systems," J. Wiley and Sons, New York, 1980.

22. Gassner, R.L.M., "Analysis of a Wideband Random Signal Radar System," PhD Thesis, Purdue University, 1966.

23. Gatzke, R.D., Fearnside, J.T., Karp, S.M., "Electronic Scanner for a Phased Array Ultrasound Transducer," Hewlett-Packard Journal, Dec 1983.

24. Gough, P.T., deRoos, A., Cusdin, M.J., "Continuous Transmission FM Sonar with One Octave Bandwidth and no Blind Time," IEE Proceedings, Vol 131, Part F, No 3, June 1984.

25. Gregorian, R., Martin, K.W., Termes, G.C., "Switched Capacitor Circuit Design," Proceedings of the IEEE, Vol. 71, No. 8, Aug 1983.

26. Ho, B.,Fang,C.G., " Ultrasound Imaging Techniques," Proceedings, Twentieth Annual Rocky Mountain Bioengineering Symposium, Apr 1983.

27. Horowitz, Paul, "The Art of Electronics," Winfield-Hill, Cambridge University Press, 1980.

28. Howatson, T.F., Lund, P.G., Todd, J.D., "Engineering Tables & Data," Chapman and Hall, 1977.

29. Hueter, T.F., Bolt, R.H., "Sonics," John Wiley and Sons, Inc, Chapman and Hall Ltd, London, 1955.

30. Karoda, S.-I., Jitsumori, A., Inari, T., "Ultrasonic Imaging System for Robot Using Electronic Scanning Method," Proceedings 1983 International Conference on Advanced Robots, Tokyo, Sep 1983.

31. Kay, L., "A Comparison Between Pulse and Frequency Modulation Echo Ranging Systems," Journal of the British IRE, Vol. 19, 1959.

32. Kay, L., "An Experimental Comparison Between a Pulse and a Frequency Modulation Echo Ranging System, " Journal of the British IRE, Vol. 20, 1960.

33. Kay, L., "A Sonar Aid to Enhance Spatial Perception of the Blind, Engineering Design and Evaluation," The Radio and Electronic Engineer, Vol. 44, No. 11, Nov 1974.

34. Kay, L., "A New or Improved Apparatus for Furnishing Information as to the Position of Objects, " Patent Specification 978741, Dec 1964.

35. Keating, P.N., Sawatari, T., Zilinskas,G., "Signal Processing in Acoustic Imaging," Proceedings of the IEEE, Vol. 67, No. 4, 1979.

36. Kennedy, J. C., Woodmansee, W.E., "Signal Processing in Non-Destructive Testing, " Boeing Publication SAOPI--FOI, RB2, Apr 1973.

37. Kinsler, Frey, Coppens, Sanders, "Fundamentals of Acoustics," John Wiley and Sons, 1982.

38. Lam, F.K., Hui, M.S., "An Ultrasonic Pulse Compression System for Non-Destructive Testing using Maximal Length Sequences," Ultrasonics, May 1982.

39. Lancaster, D., "Active Filter Cookbook, " Howard W. Sams & Co., 1975.

40. Larcombe, M.H.E., "Mobile Robots for Industrial Use," Robots '79, British Robot Association, Nottingham, Mar 1979.

41. Larcombe, M.H.E., "The Free Runing Automated Industrial Truck Project," Proceedings SERC Robotics Initiative Grantees Conference, Birmingham, 1982.

42. Lee, B.B., Furgason, E.S., "Golay Codes for Simultaneous Multi-Mode Operation in Phased Arrays," IEEE Ultrasonics Symposium, 1982.

43. Lozano-Perez, T., "Robot Programming," Proceedings of the IEEE, Vol. 71, No. 7, Jul 1983.

44. Manes, G., "A Novel Device: The Sequentially Accessed Tapped Delay Line," IEEE Ultrasonics Symposium, 1978.

45. Mason, W.P., "Sonics and Ultrasonics: Early History and Applications," IEEE Transactions on Sonics and Ultrasonics, Vol. SU-23, No. 4, Jul 1976.

46. McLachlan, N.W., "Loudspeakers - Theory, Performance, Testing, and Design," Clarendon Press, Oxford, 1934.

47. Mims, F.M III, "Use of Ultrasonic Sound," Computers and Electronics, June 1983.

48. Moravec, H.P., "The Standford Cart and the CMU Rover," Proceedings of the IEEE, Vol. 71, No. 7, Jul 1983.

49. Morgan, C.G., Bromley, J.S.E., Clocksin, W.F., Davey, P.G., Vidler, A.R., "Visual Guidance for Robot Arc Welding," Proceedings of the 12th International Symposium on Industrial Robots. Paris, Jun 1982.

50. Newhouse, V.L., Furgason, E.S., Bilgutay, N.M., Cooper, G.R., "Random Signal Flaw Detection," IEEE Ultrasonics Symposium, 1974.

51. Newhouse, V.L., Furgason, E.S., "Ultrasonic Correlation Techniques," Research Techniques in Nondestructive Testing, Vol. III, R.S. Sharpe, Ed., Academic Press , New York, 1977.

52. Nitzan, D., "Assessment of Robotic Sensors," Proceedings, Robotic Vision and Sensory Controls," Stratford Upon Avon, 1981.

53. Nitzan, D., Barrouis, C., Cheeseman, P., Smith, R., "Use of Sensors in Robot Systems," Proceedings of the 1983 International Conference on Advanced Robotics, Tokyo, 1983.

54. Olinger, M., Cooper, D., Siegel, M., "Implementation of a High Resolution Bloodflow Imaging System using Large Time-Bandwidth Pseudo-Noise Sequences," Proceedings,1978 IEEE Ultrasonics Symposium.

55. Payne, P.A., "Ultrasonics for Dermatology," Department of Instrumentation and Anyletical Science, UMIST, Manchester.

56. Proceedings of the 2nd International Conference on Robot Vision and Sensory Controls," Stuttgart, Nov 1982.

57. Ramp, HlO., Wingrove, E.R., "Principles of Pulse Compression, " Radars Vol. III, David K. Barton, Ratheon Company, Bedford Mass., 1978.

58. Saja, N., Gen. P.H.-S., "Disproportionate Tonoptic Representation for Processing CF-FM Sonar Signals in the Mustache Bat Auditory Cortex," Science, Vol. 194.

59. Seydell, J.A., "Improved Discontinuity Detection in Ceramic Material Using Computer Aided Ultrasonic Non-Destructive Techniques," Proceedings of the Symposium of 2nd Army Materials Techniques Conference, USA, Nov 1973.

60. Schoenwald, J.S., Martin, J.F., Ahlberg, L.A., "Acoustic Scanning for Robotic Range Sensing and Object Pattern Recognition," 1982 IEEE Ultrasonics Symposium.

61. Schwartz, M., "Information Transmission, Modulation, and Noise," McGraw-Hill, London, 1959.

62. Shioazki, A., Senda, S., Kitabatake, A., Inoue, M., Matsou, H., "A New Modulation Method with Range Resolution for Ultrasonic Doppler Flow Sensing," Ultrasonics, Nov 1979.

63. Skolnik, M., "Radar Handbook," McGraw-Hill, New York, 1970.

64. Skolnik, M., "Introduction to Radar Systems," McGraw-Hill, New York, 1980.

65. Thurstone, F.L., "Acoustical Imaging of Biological Tissue," IEEE Transactions on Sonics and Ultrasonics, Vol. SU-17, No. 3, Jul 1970.

66. Tornberg, Jounis, Karras, Matti, Harkonon, E.M., Hirsimaki, O., "Analysis of Ultrasonic Correlation Flowmeters for Pulp Suspension," IEEE Transactions on Sonics and Ultrasonics, Vol. SU-30, No. 4, Jul 1983.

67. Trivedi, A.S., "A Non-Contacting Ultrasonic Cross-Correlation Flowmeter for Liquids," PhD Thesis, Postgraduate School of Control Engineering, University of Bradford, 1977.

68. Wimbert, F.T., Lane, J.F. Jr., "The AN/APN-22 Radio Altimeter," IRE Transactions-Aeronautical and Navigational Electronics, Jun 1954.

69. Yaen, C.K., Fraser, D., "Digital Spectral Analysis," Pitman Publishing LTD, London, 1979.

70. Ziemer, R.E., Tranter, W.H., "Systems, Modulation, and Noise," Houghton Mifflin Company, Boston, 1976.

APPENDIX A

FMCW TRACKING SYSTEM

This appendix contains the schematic diagrams and photos for the FMCW tracking system described in Chapter Three. The FMCW system is constructed on two separate chassis; one contains the VCO, transmitter, receiver, and demodulating circuitry, the other contains the frequency comparason, control, and range counting circuitry. The transducers are in a separate module. Page A2 contains the schematics for the voltage controlled oscillator (VCO), transmitter, receiver, 200 volt bias supply, frequency changer (mixer), and low-pass filter. A3 contains the schematics for the frequency comparison and automatic volume control section. A4 contains schematics for the proportional plus integral control, and ramp generator. A5 contains schematics for the digital interface and counting circuitry. Pages A6 and A7 contain photographs of the transmitter/receiver/demodulator chassis, control chassis, and transducer module. A block diagram for the complete FMCW tracking system is contained in Chapter Three.

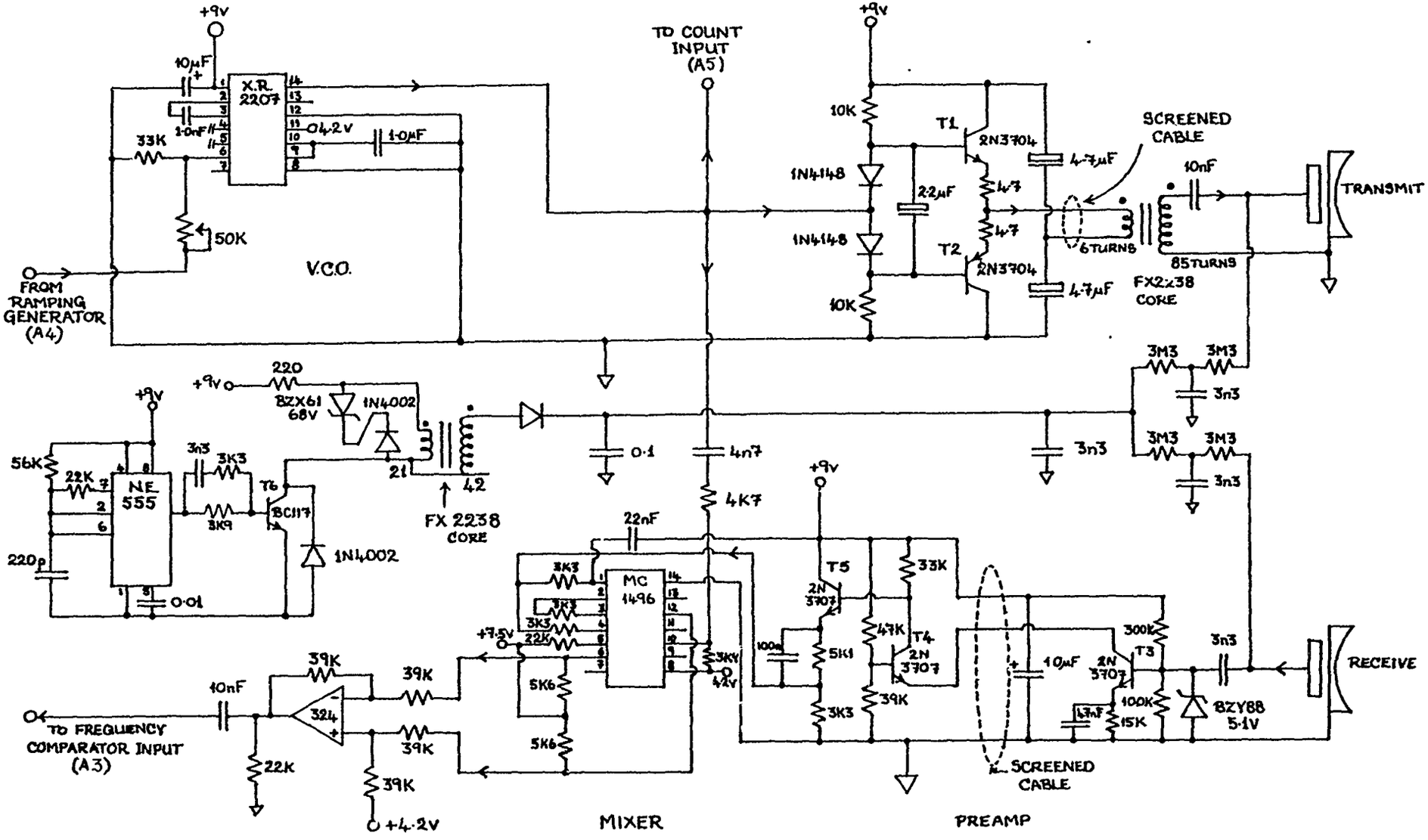
+9v
10µF
X.R. 2207
1·0nF
33K
50K
V.C.O.
FROM RAMPING GENERATOR (A4)
+4·2v
1·0µF
TO COUNT INPUT (A5)
10K
T1
2N3704
1N4148
2·2µF
T2
4·7µF
4·7
SCREENED CABLE
10nF
TRANSMIT
6 TURNS
85 TURNS
FX2238 CORE
220
BZX61 68V
1N4002
56K
22K
NE 555
3n3
3K3
3K9
T6
BC117
220p
0·01
21
42
FX 2238 CORE
0·1
4n7
4K7
3M3
22nF
MC 1496
5K6
+7·5v
3K9
4·2v
T5
2N 3703
33K
47K
T4
2N 3707
100n
5K1
39K
3K3
10µF
T3
300K
100K
15K
BZY88 5·1V
RECEIVE
10nF
324
TO FREQUENCY COMPARATOR INPUT (A3)
22K
MIXER
PREAMP

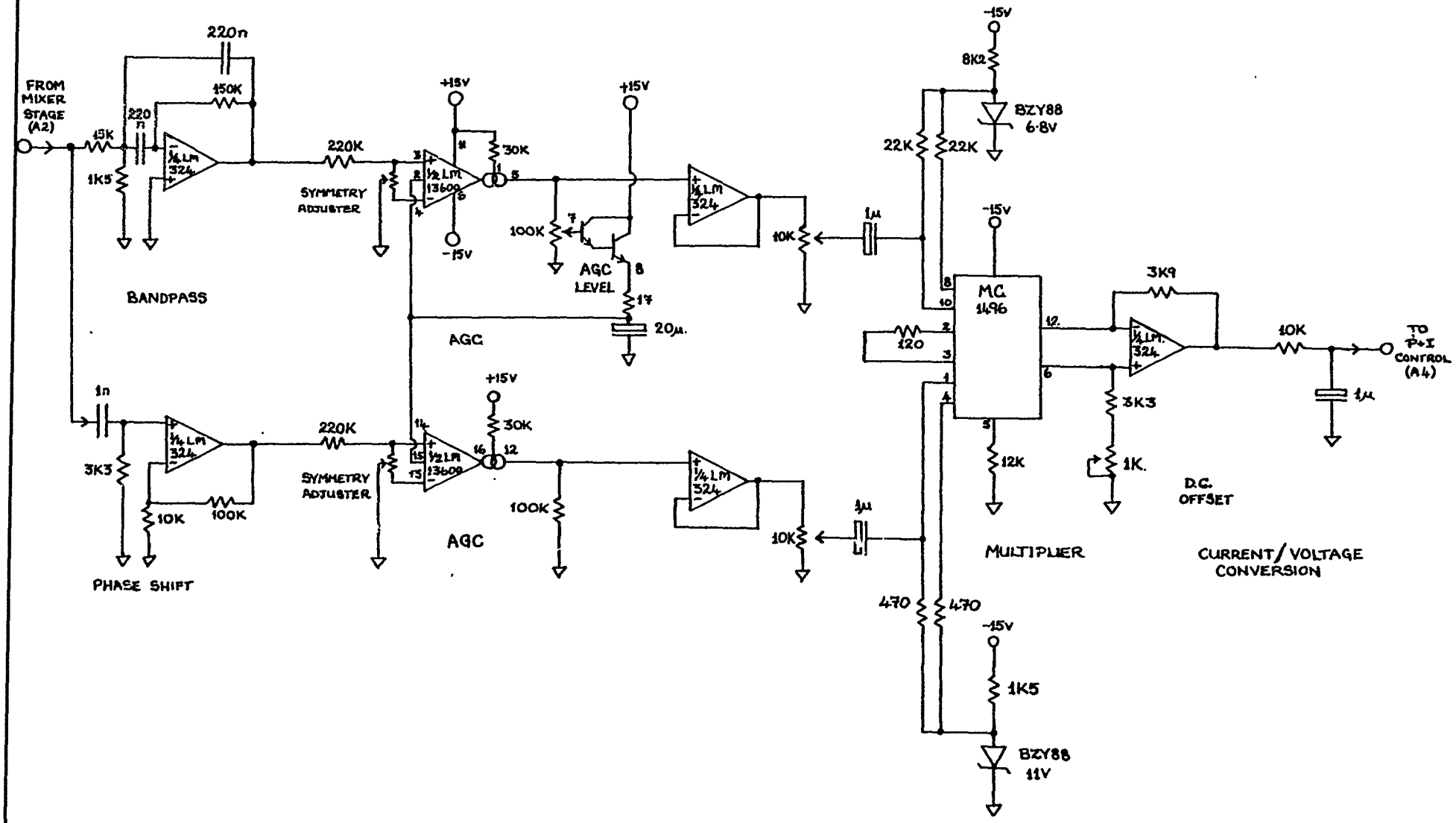
FROM MIXER STAGE (A2)
220n
150K
220 Fl
15K
1K5
220K
SYMMETRY ADJUSTER
+15V
30K
-15V
100K
AGC LEVEL
20µ.
BANDPASS
AGC
1n
3K3
10K
100K
PHASE SHIFT
1µ
8K2
BZY88 6·8V
22K
MC 1496
120
12K
3K9
3K3
1K.
D.C. OFFSET
TO P+I CONTROL (A4)
MULTIPLIER
CURRENT/VOLTAGE CONVERSION
470
1K5
BZY88 11V

A3

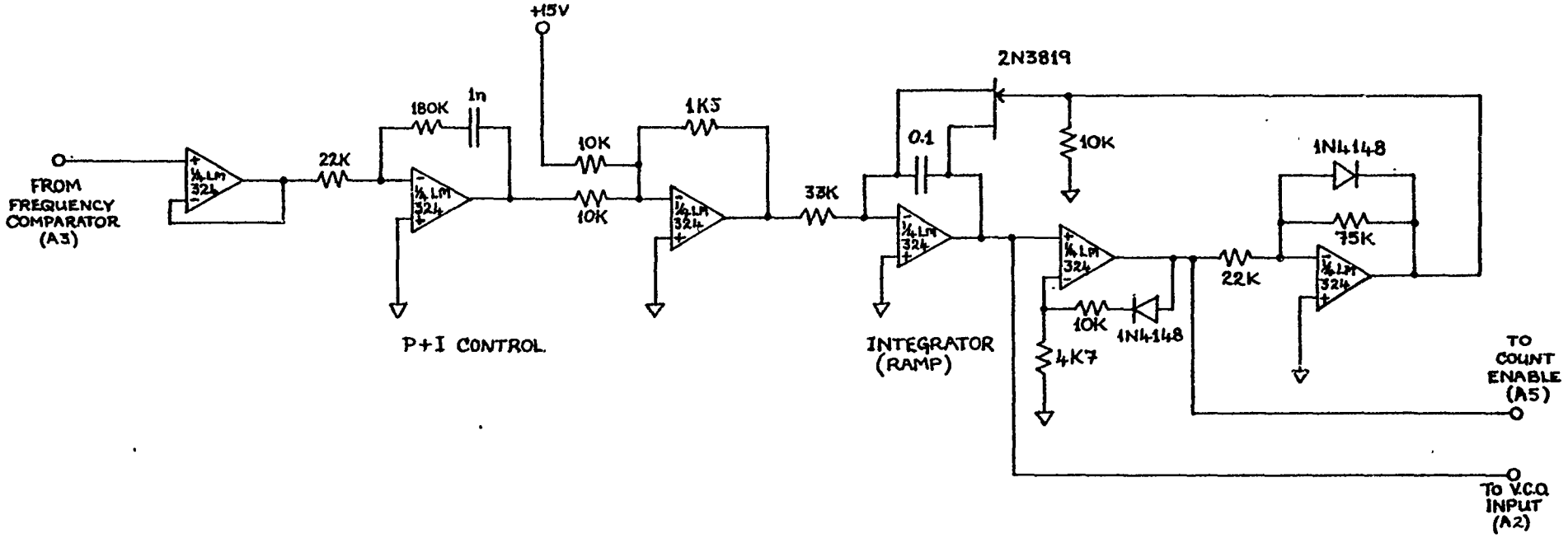
+15V
2N3819
180K
1n
1K5
0.1
10K
1N4148
FROM FREQUENCY COMPARATOR (A3)
22K
10K
10K
33K
75K
22K
10K
1N4148
4K7
P+I CONTROL
INTEGRATOR (RAMP)
TO COUNT ENABLE (A5)
To V.C.O. INPUT (A2)

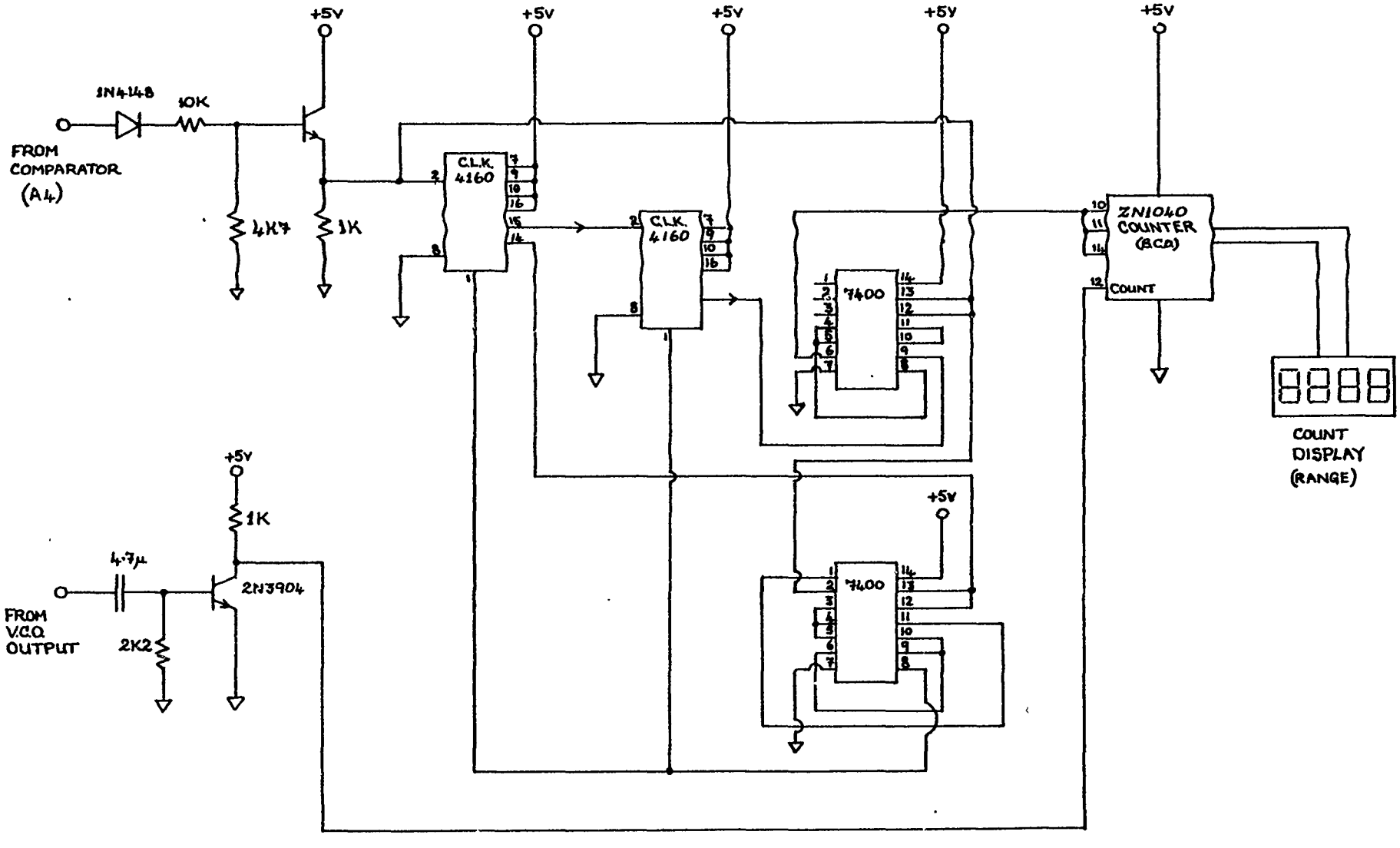
+5V
1N4148
10K
FROM
COMPARATOR
(A4)
4K7
1K
C.L.K.
4160
C.L.K.
4160
7400
7400
ZN1040
COUNTER
(BCD)
COUNT
COUNT
DISPLAY
(RANGE)
1K
4.7µ
2N3904
FROM
V.C.O.
OUTPUT
2K2

FMCW TRACKING SYSTEM - MAIN CHASSIS UNITS (FRONT VIEW)
CONTROL/COUNTER CHASSIS (LEFT)
TRANSMITTER/RECEIVER/DEMODULATOR CHASSIS (RIGHT)

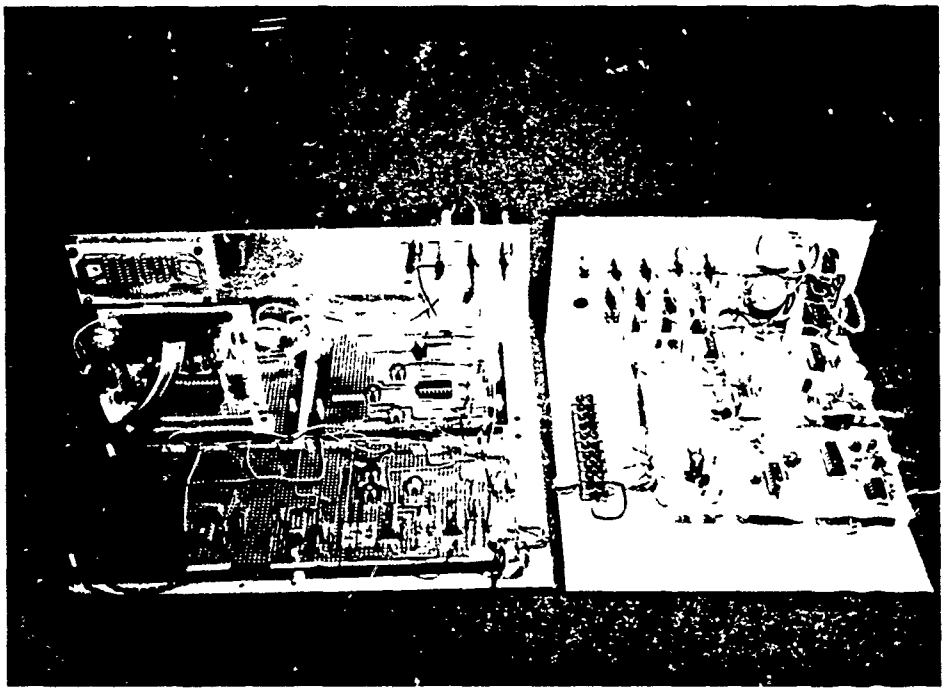

FMCW TRACKING SYSTEM - MAIN CHASSIS UNITS (REAR VIEW)
CONTROL/COUNTER CHASSIS (LEFT)
TRANSMITTER/RECEIVER/DEMODULATOR CHASSIS (RIGHT)

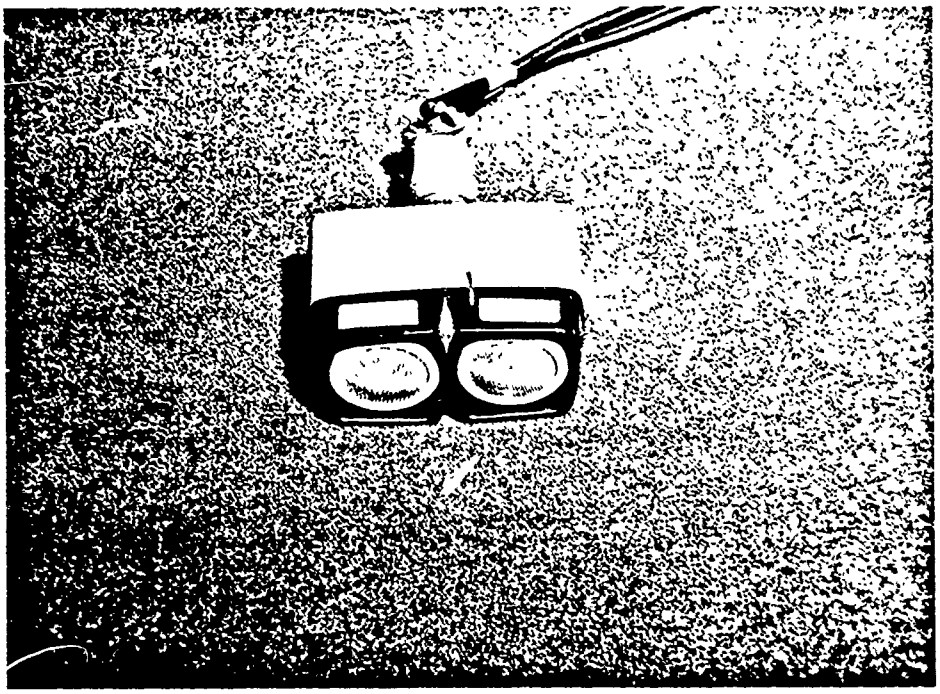

PMCW TRACKING SYSTEM - TRANSDUCER MODULE

APPENDIX B

PRBS CORRELATION SYSTEM

This appendix contains schematics of the experimental pseudo-random binary sequence (PRBS) Correlation systems described in Chapter Five (Type I system) and Chapter Seven (Type II system). These systems are constructed in modules. The circuit board module consists of two plug in circuit boards for the Type I system, and four plug-in circuit boards for the Type II system. The circuit boards contain PRBS generation, modulation, transmitting, receiving, demodulating and cross-correlating circuitry. In addition to the plug-in circuit boards, the transmitter/200 volt bias, and receiver circuits are contained in separate modular chassis. As in the FMCW system, the transducer modules are also separate. The Type I correlation system uses the same transducer modules as did the FMCW system. The Type II system uses the Type I transducer modules for the cross-correlation tests, and different transducer modules for the tracking tests. The modified transducer modules were required due to the necessity of adding another receiving transducer. All circuitry is identical, except for the addition of another receiving transducer and its associated circuitry. Also included in this appendix are the schematics for the interface circuitry needed to drive the ac servo which controls transducer range.

Page B3 contains the schematics for the master oscillator/ PRBS generator/phase and time-shift modulation systems. This board is used on both the Type I and Type II systems. Page B4 contains the delayed PRBS/Correlator board for the Type I system. Page B5 contains the divider/frequency synthesis, time-shift modulation circuitry for the Type II system. Pages B6 and B7 contain the demodulator/correlator/ranging circuitry for the Type II system. As noted previously, only one of the two boards built from the schematics shown contains the range and azimuth error circuitry. Page B8 has schematics for the transmit, receive, transducer, and 200 volt bias modules. Page B9 contains the schematic for the range servo driver.

Pages B10, B11, and B12 contain photographs of the completed system as used in the correlation tests.

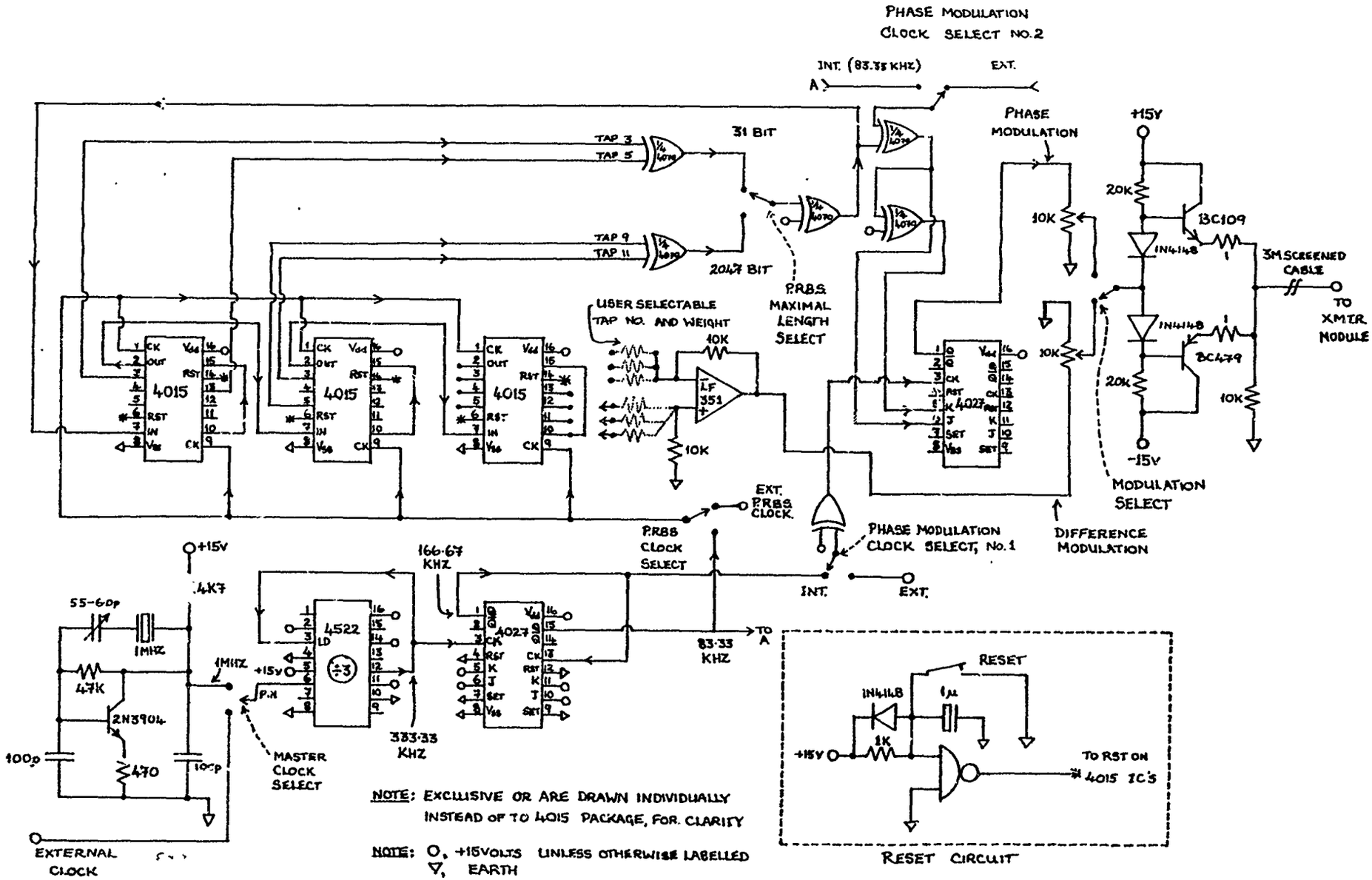

NOTE: EXCLUSIVE OR ARE DRAWN INDIVIDUALLY INSTEAD OF TO 4015 PACKAGE, FOR CLARITY

NOTE: O, +15VOLTS UNLESS OTHERWISE LABELLED
▽, EARTH

P.R.B.S. OSCILLATOR/DIVIDER/P.R.B.S. GENERATOR/MODULATOR BOARD

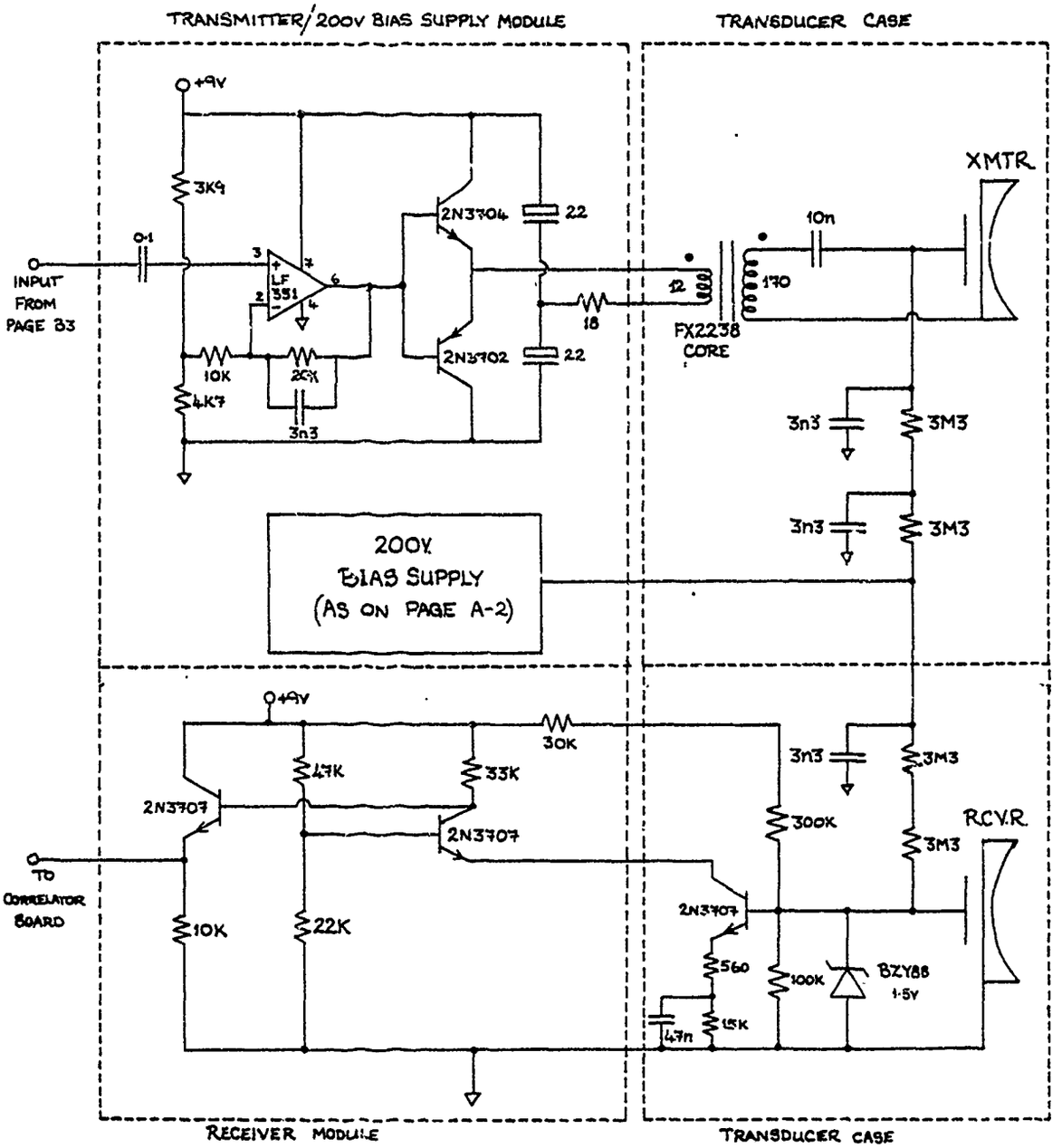
TRANSMITTER/200V BIAS SUPPLY MODULE
TRANSDUCER CASE
+9V
3K9
0·1
INPUT FROM PAGE 33
LF 351
2N3704
2N3702
22
22
18
10K
4K7
20K
3n3
12
FX2238 CORE
170
10n
XMTR
3n3
3M3
3n3
3M3
200V BIAS SUPPLY (AS ON PAGE A-2)
+9V
30K
47K
33K
2N3707
2N3707
TO CORRELATOR BOARD
10K
22K
3n3
3M3
300K
3M3
RCVR
2N3707
560
100K
BZY88 1·5V
47n
15K
RECEIVER MODULE
TRANSDUCER CASE

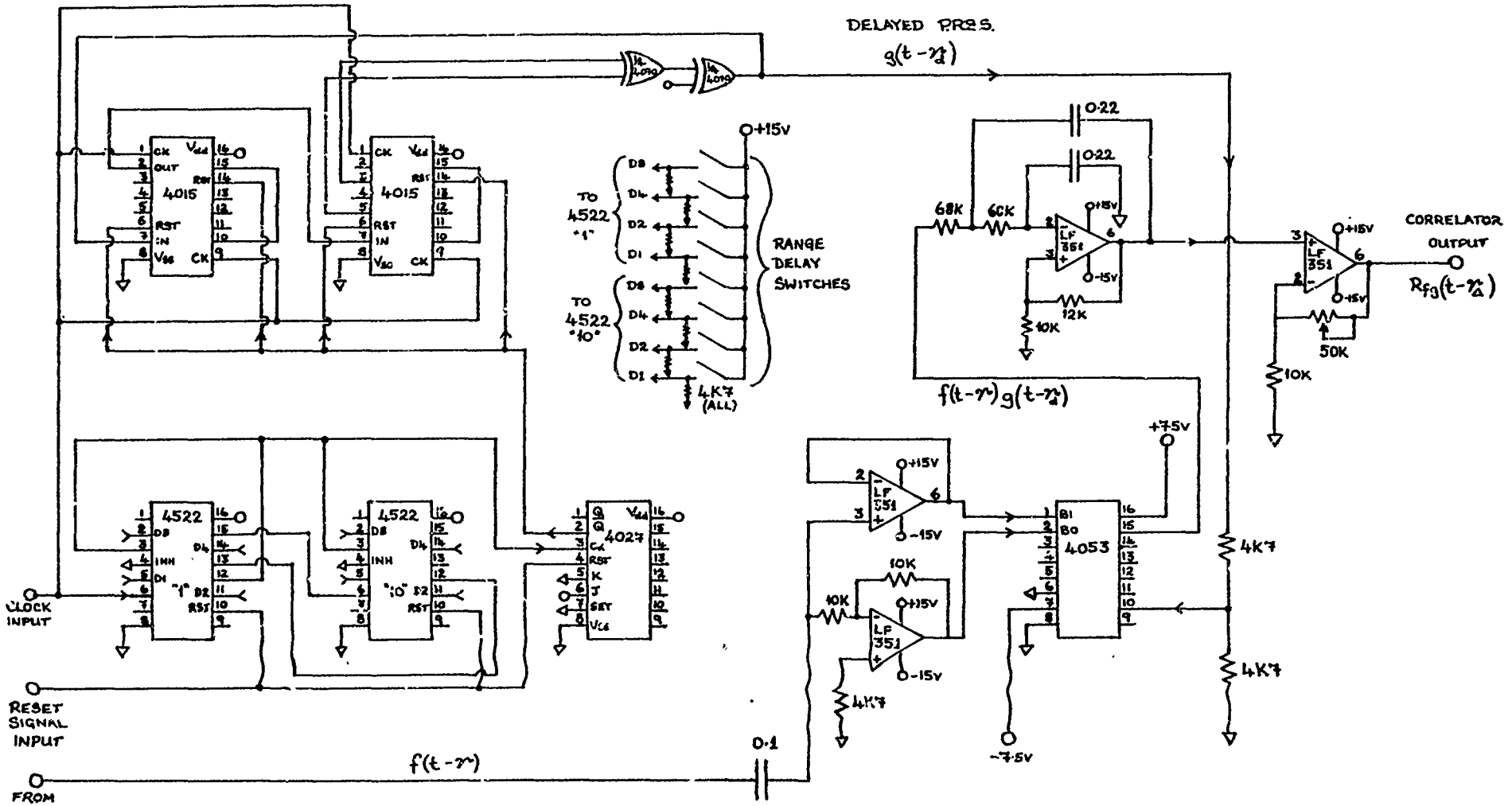

NOTE: O = +15 VOLTS UNLESS OTHERWISE LABELLED
▽ = EARTH

DELAYED PRBS/CROSS CORRELATOR MODULE

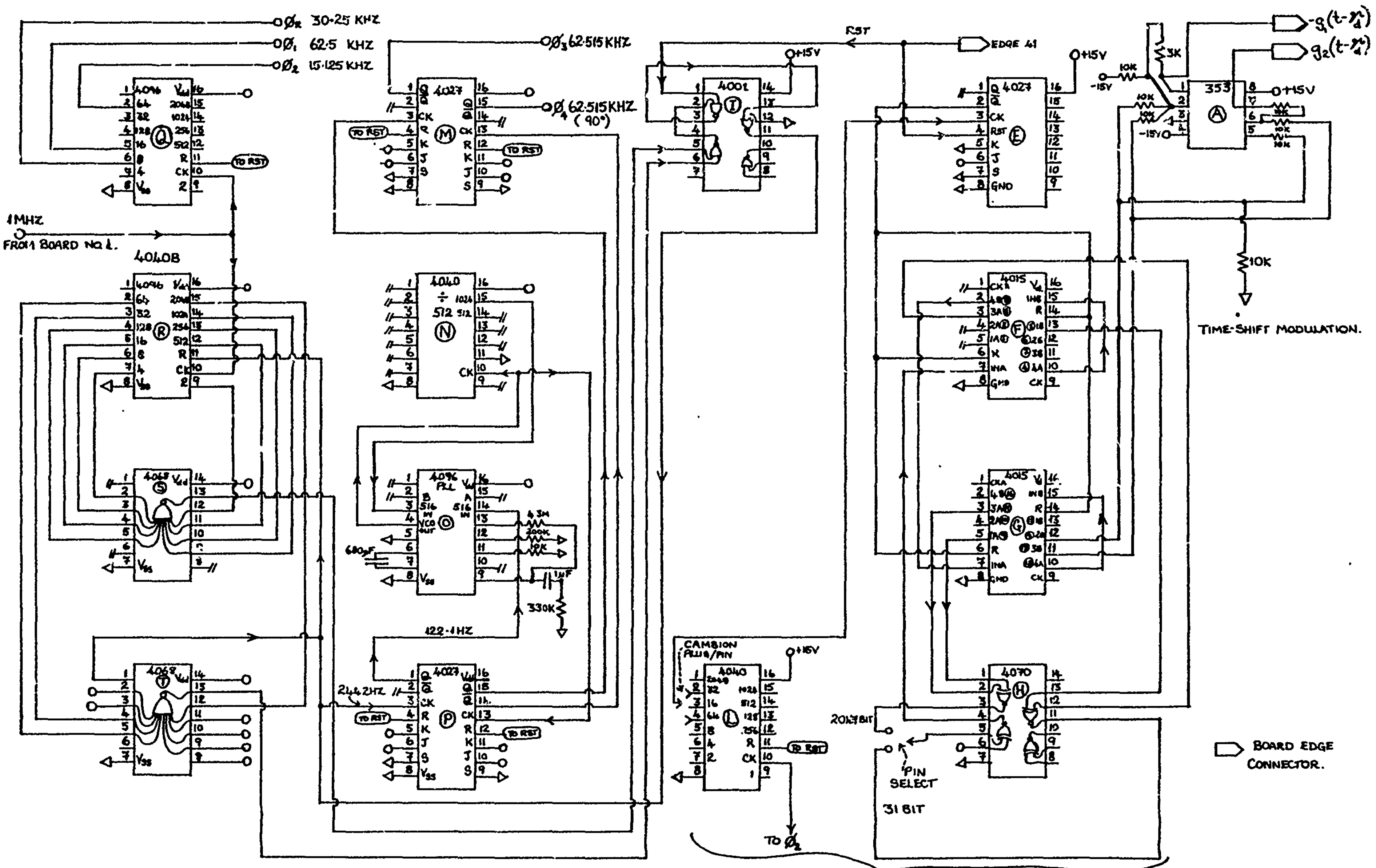

DIVIDERS/FREQUENCY SYNTHESIS/ PHASE SHIFT.

g(t-τ) PRBS + DELAY NETWORK.

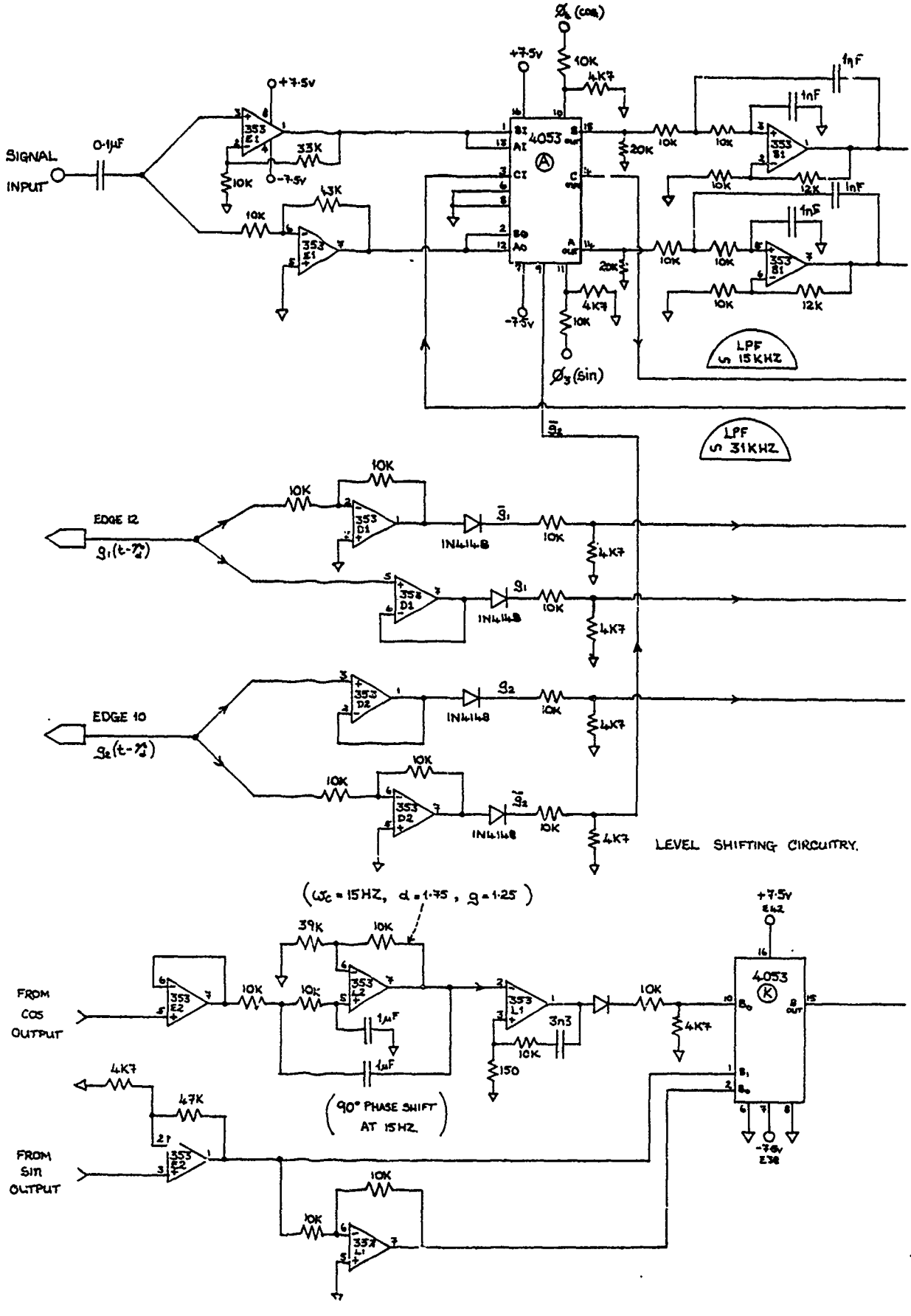

V⁺ PIN 8 353
PIN 7 351, 741
V⁻ PIN 4 ALL

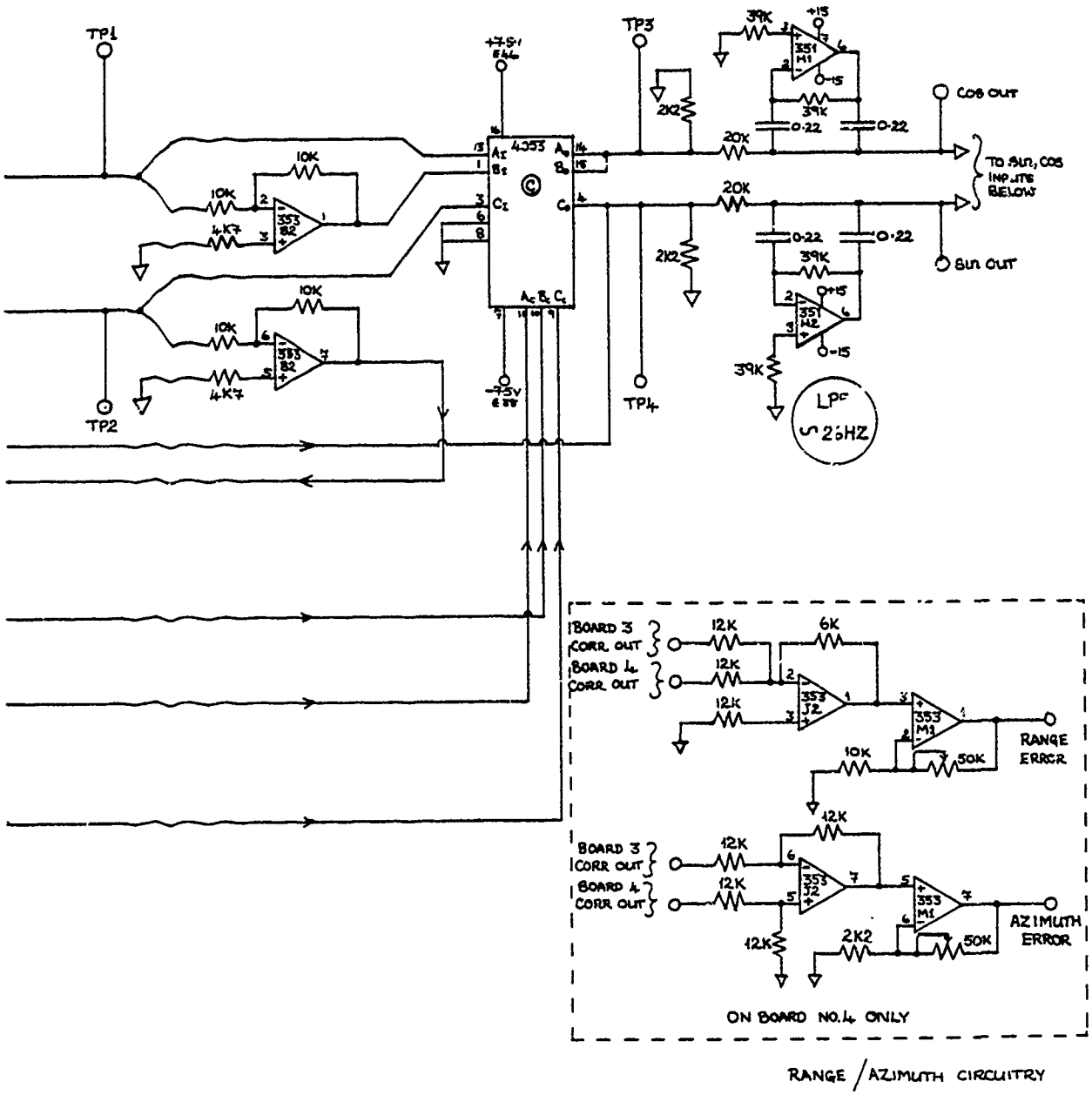

RANGE / AZIMUTH CIRCUITRY

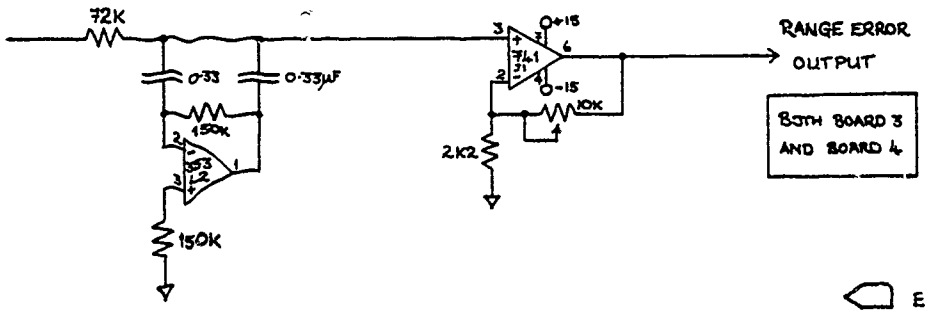

EDGE-CONNECT

TEST CONNECTOR PIN.

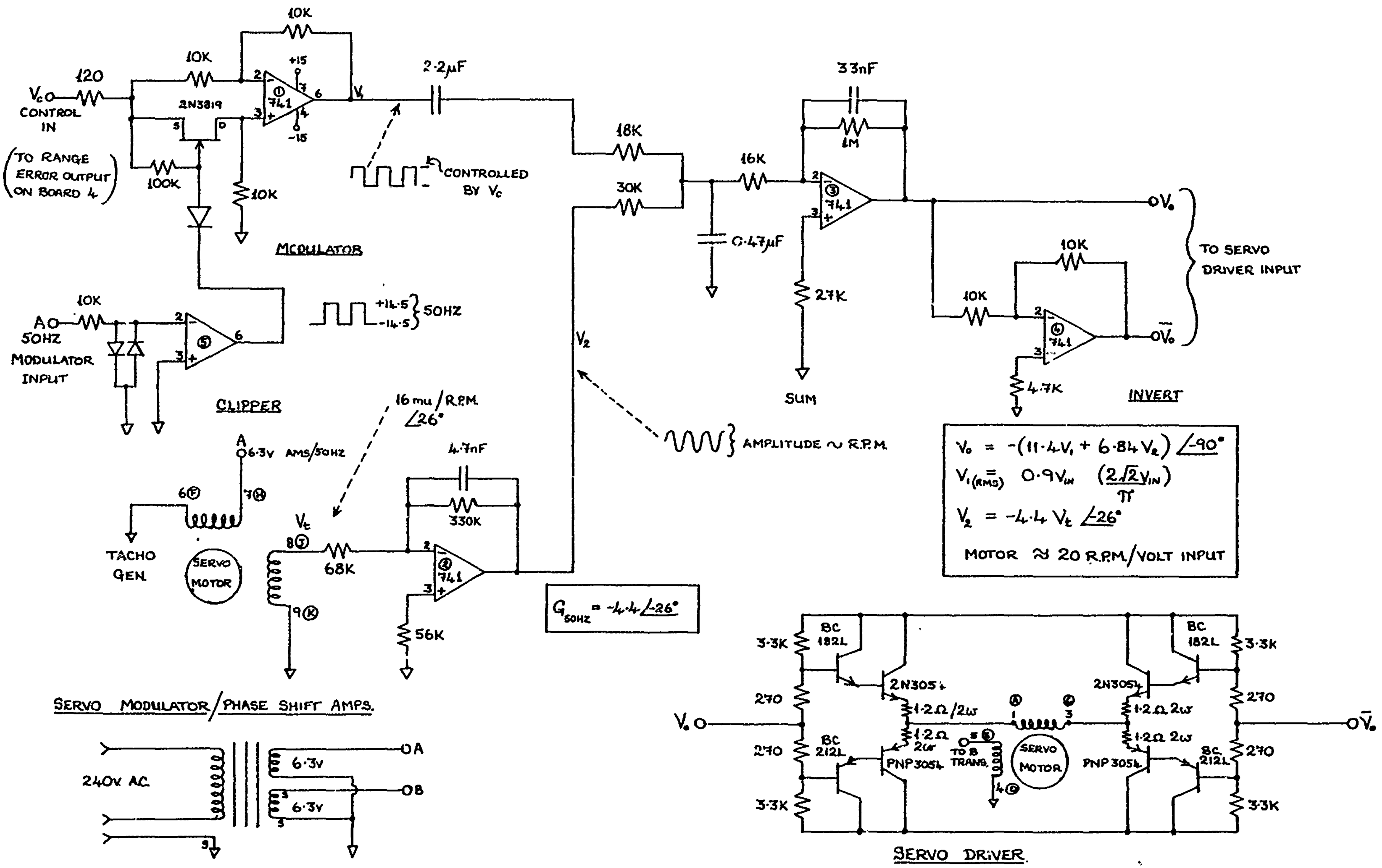

MODULATOR
CLIPPER
SUM
INVERT
TO SERVO DRIVER INPUT
CONTROLLED BY Vc
AMPLITUDE ∼ R.P.M.
16 mv/R.P.M. ∠26°
$G_{50Hz} = -4.4 \angle -26°$
$V_o = -(11.4V_1 + 6.84V_2) \angle -90°$
$V_{1(RMS)} = 0.9V_{IN} \; (2\sqrt{2}V_{IN}/\pi)$
$V_2 = -4.4 V_t \angle 26°$
MOTOR ≈ 20 R.P.M./VOLT INPUT
(TO RANGE ERROR OUTPUT ON BOARD 4)
Vc CONTROL IN
A 50HZ MODULATOR INPUT
TACHO GEN.
SERVO MOTOR
6.3V RMS/50HZ
SERVO MODULATOR/PHASE SHIFT AMPS.
240V AC.
SERVO DRIVER.
TO B TRANS.

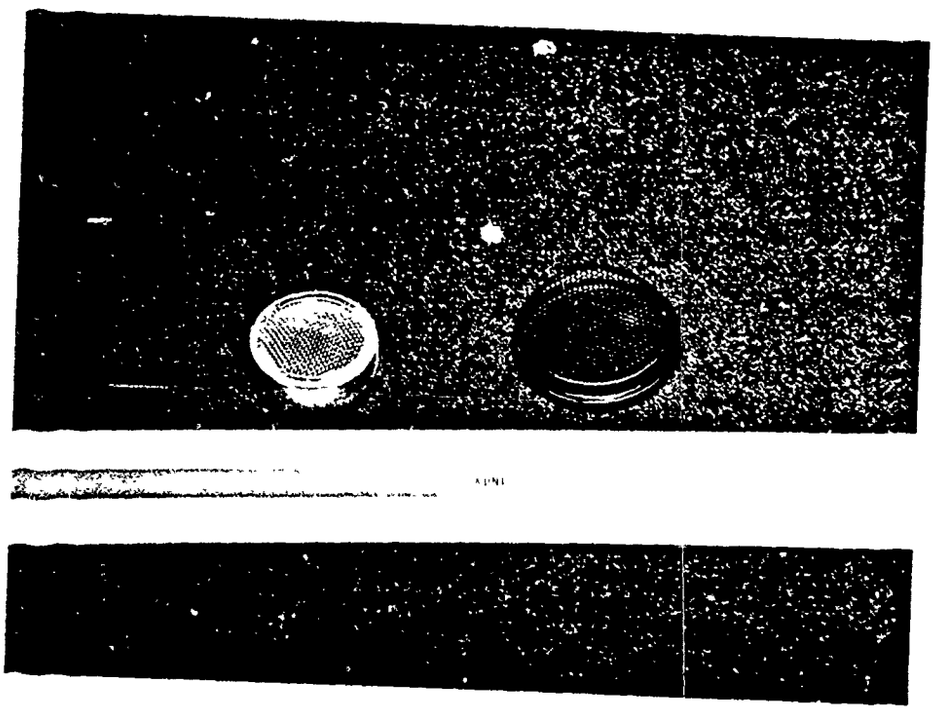

OXFORD AND POLAROID TRANSDUCERS
(Type I and Type II systems)

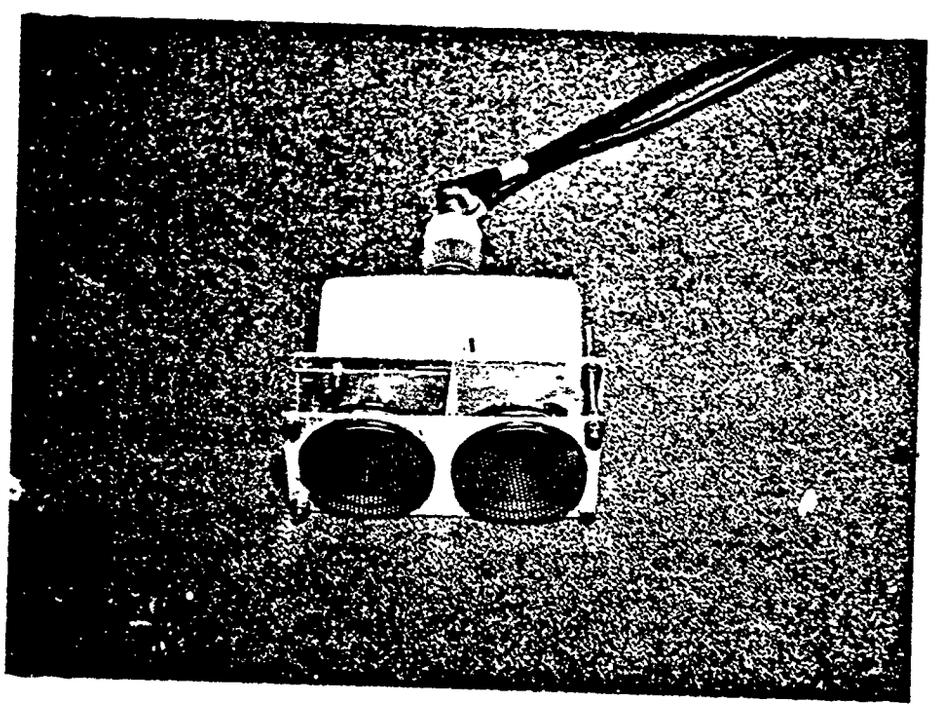

TRANSDUCER MODULE WITH POLAROID TRANSDUCERS
(Type I and Type II systems)

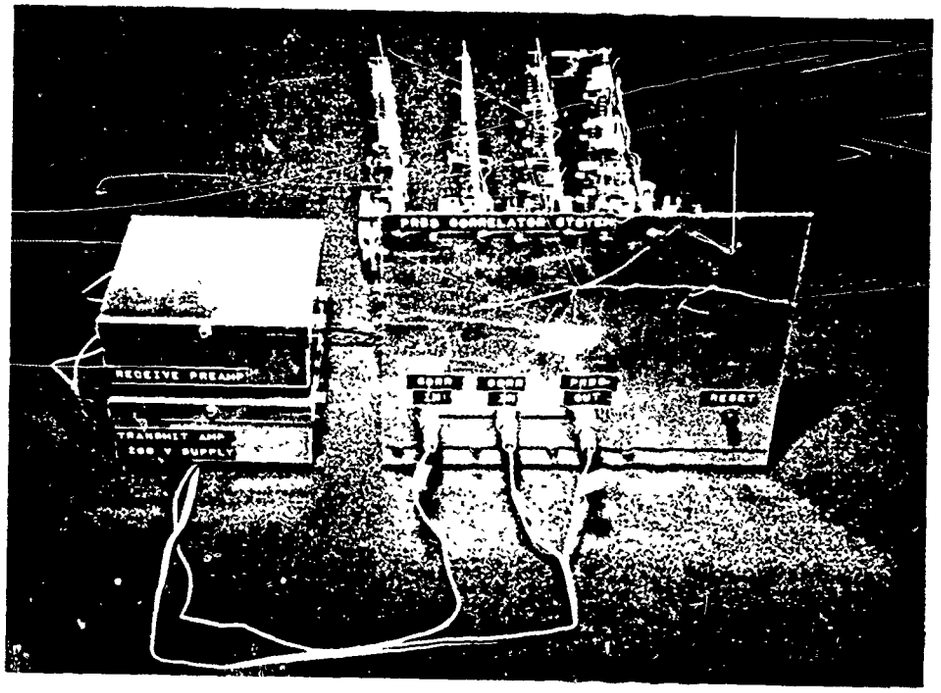

MAIN CIRCUIT BOARD CHASSIS
TRANSMITTER/200 VOLT SUPPLY, RECEIVER MODULE
(Type I and Type II systems)

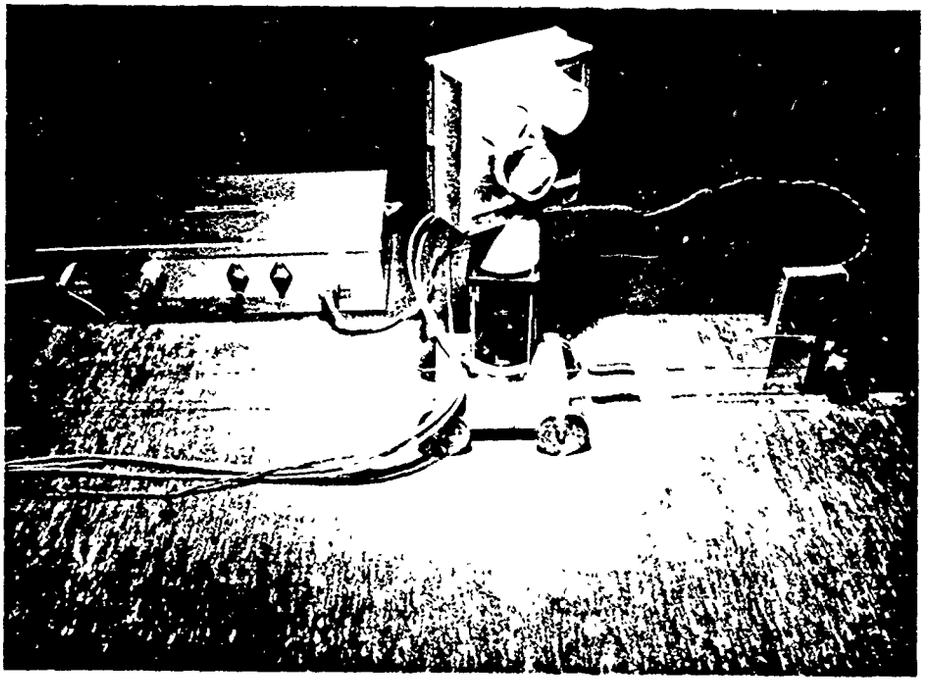

AC SERVO DRIVE CHASSIS, TRACKING MODULE ON AZIMUTH SERVO
RANGE SERVO (ac) (Type I system)

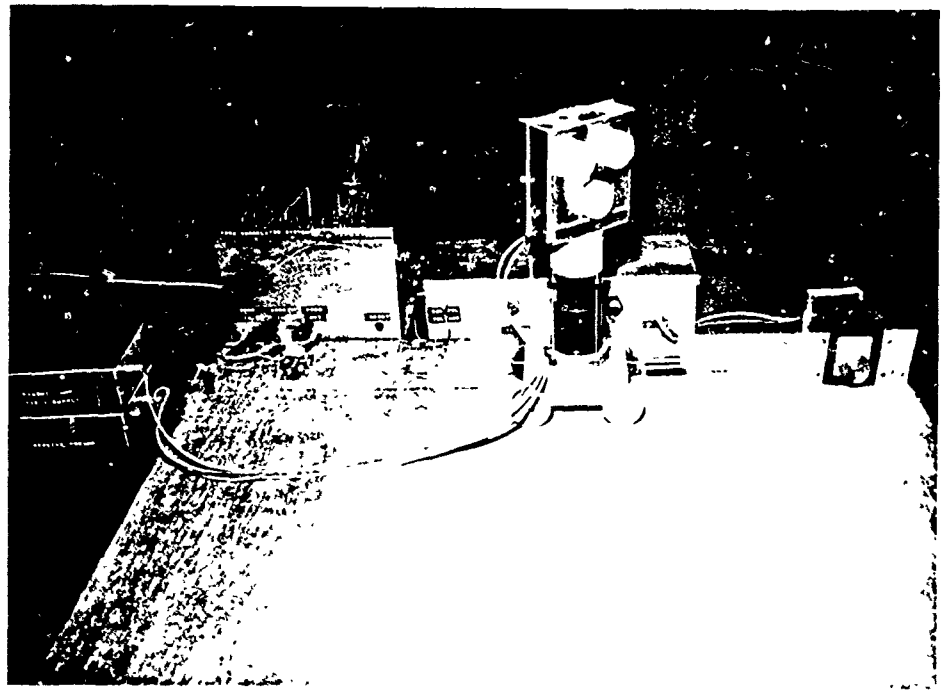

COMPLETE TYPE II TRACKING SYSTEM

APPENDIX C

CROSS-CORRELATION FUNCTIONS

TYPE I SYSTEM

This appendix contains the cross-correlation functions obtained from the Type I system as described in Chapter Five. Each page contains the functions obtained from one set of transducers. The cross-correlation functions for two types of modulation are shown: phase-shift and time-shift modulation, with the phase shift modulation function occuring first in each trace. The first graph shows the basic cross-correlation function. The succeeding three graphs show how the function is modified by the addition of successive stages of 20 dB/octave equalization starting at roughly 20 kHz. The phase-shift range delay was set to approximately 26 cm, and the time-shift range delay was set to approximately 31 cm. As the target moved past the phase-shift correlation points, the modulation selector was moved to the time-shift position. Thus, both cross-correlation functions were obtained on one chart recorder run. The chart recorder was then reset, and the x-axis offset was changed so as to provide a different plot. The receiving equalizer was changed, and the next cross-correlation run was accomplished. Six sets of cross-correlation results are shown. Each set is obtained from one pair of transducers (either Oxford or Polaroid). Oxford transducers are manufactured in the Department of Engineering

Science at Oxford University (see text in Chapter Three). The Polaroid transducers were purchased from a London supplier and are used only in the PRBS system tests.

Appendix E contains further information on the transducer frequency responses, along with a list of the pairs of transducers which comprises each group.

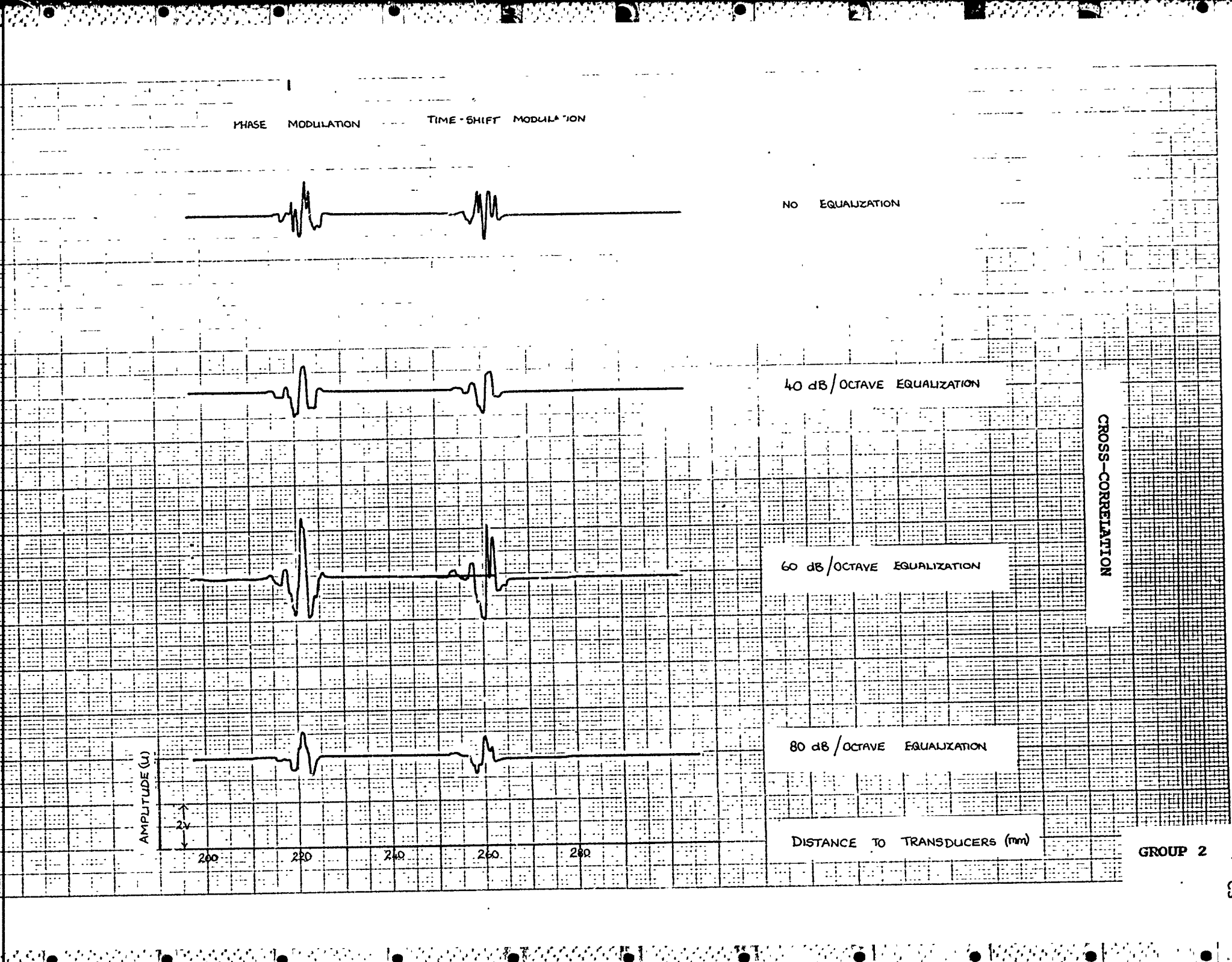
PHASE MODULATION
TIME-SHIFT MODULATION
NO EQUALIZATION
40 dB/OCTAVE EQUALIZATION
60 dB/OCTAVE EQUALIZATION
80 dB/OCTAVE EQUALIZATION
CROSS-CORRELATION
AMPLITUDE (u)
2V
200
220
240
260
280
DISTANCE TO TRANSDUCERS (mm)
GROUP 2

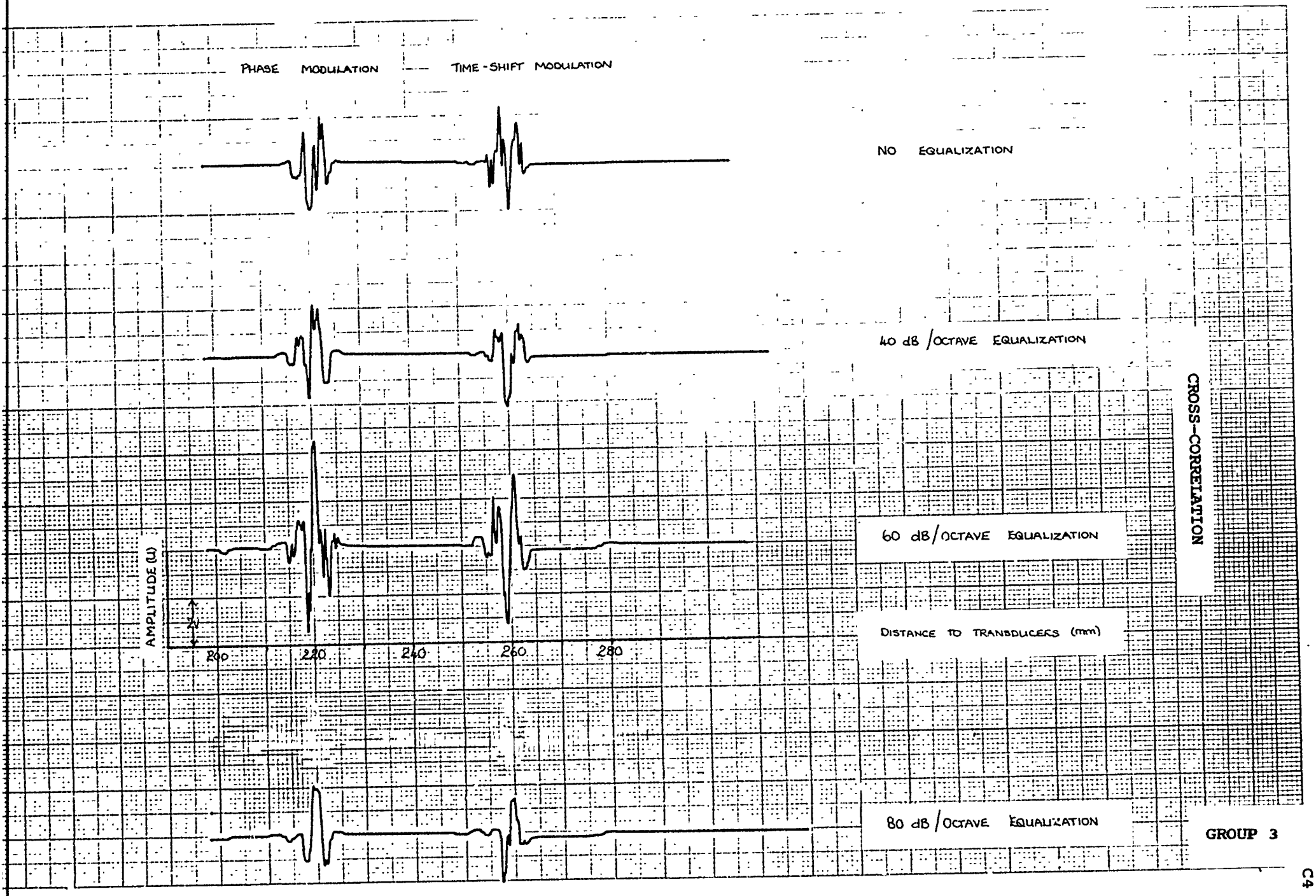
PHASE MODULATION
TIME-SHIFT MODULATION
NO EQUALIZATION
40 dB/OCTAVE EQUALIZATION
60 dB/OCTAVE EQUALIZATION
80 dB/OCTAVE EQUALIZATION
CROSS-CORRELATION
AMPLITUDE (V)
2V
200
220
240
260
280
DISTANCE TO TRANSDUCERS (mm)

GROUP 3

PHASE MODULATION ---- TIME-SHIFT MODULATION

Ⓐ

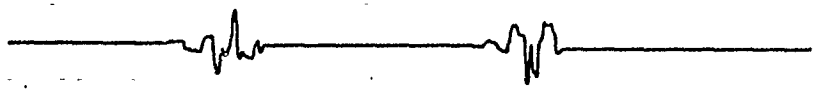

NO EQUALIZATION

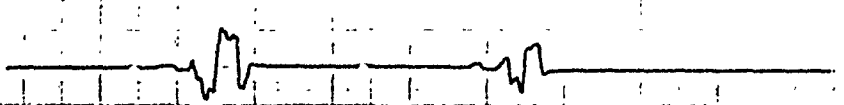

40 dB/OCTAVE EQUALIZATION

60 dB/OCTAVE EQUALIZATION

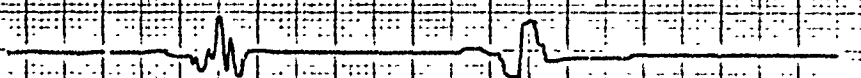

80 dB/OCTAVE EQUALIZATION.

DISTANCE TO TRANSDUCERS (mm)

CROSS-CORRELATION

GROUP 4

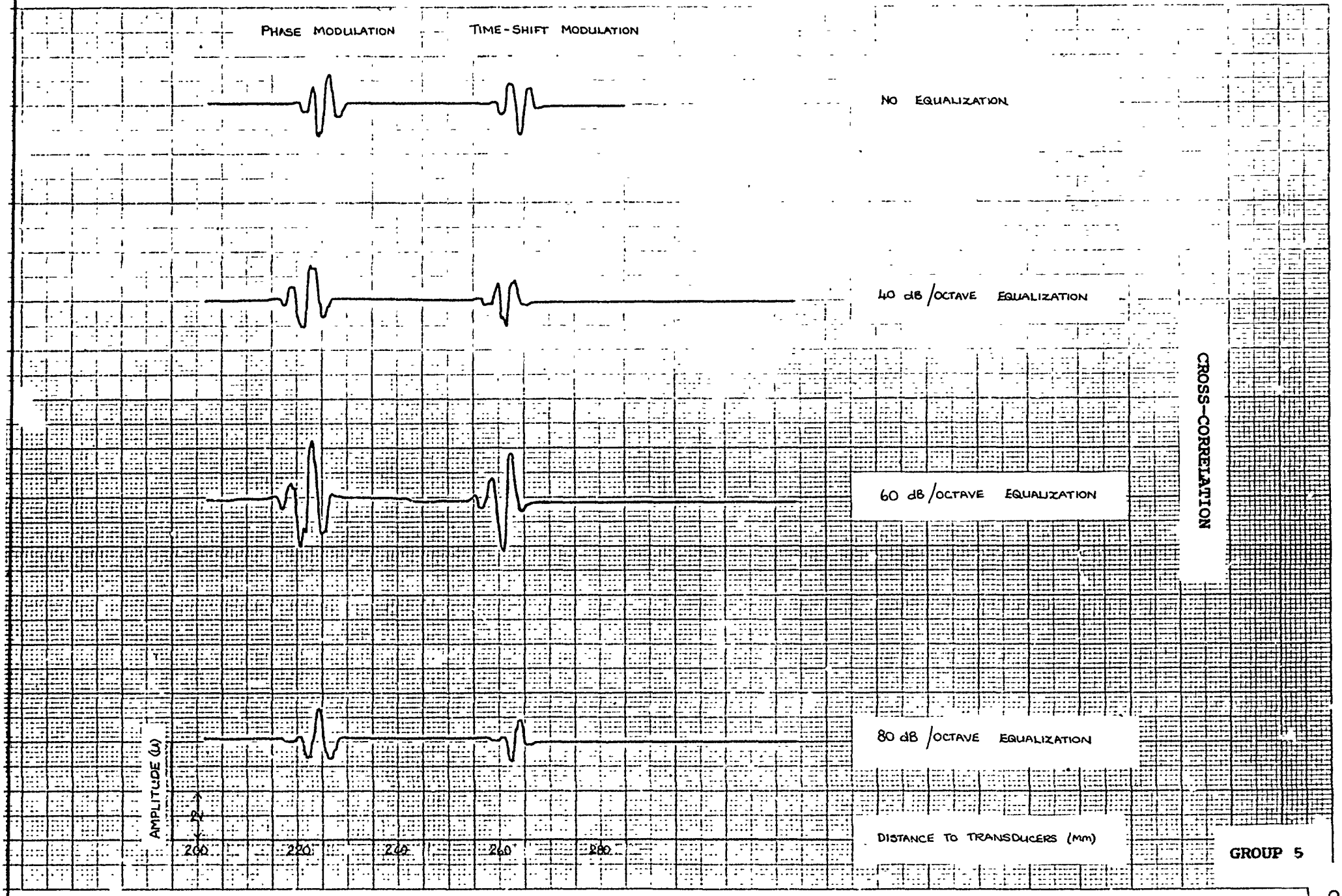
PHASE MODULATION
TIME-SHIFT MODULATION
NO EQUALIZATION
40 dB/OCTAVE EQUALIZATION
60 dB/OCTAVE EQUALIZATION
80 dB/OCTAVE EQUALIZATION
CROSS-CORRELATION
AMPLITUDE (A)
200
220
240
260
280
DISTANCE TO TRANSDUCERS (mm)
GROUP 5

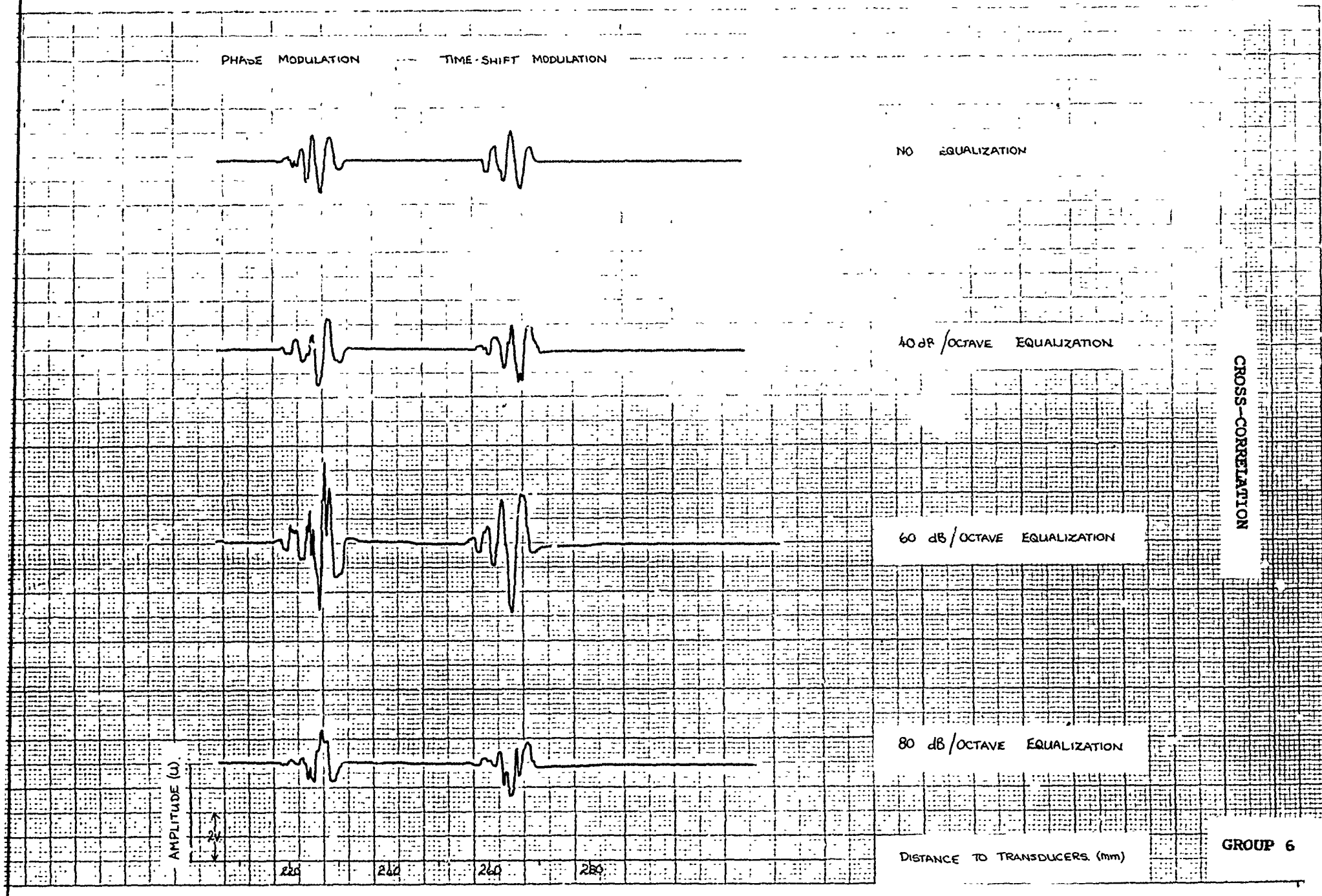
PHASE MODULATION
TIME-SHIFT MODULATION
NO EQUALIZATION
40 dB/OCTAVE EQUALIZATION
60 dB/OCTAVE EQUALIZATION
80 dB/OCTAVE EQUALIZATION
CROSS-CORRELATION
AMPLITUDE (U)
2V
220
240
260
280
DISTANCE TO TRANSDUCERS (mm)
GROUP 6

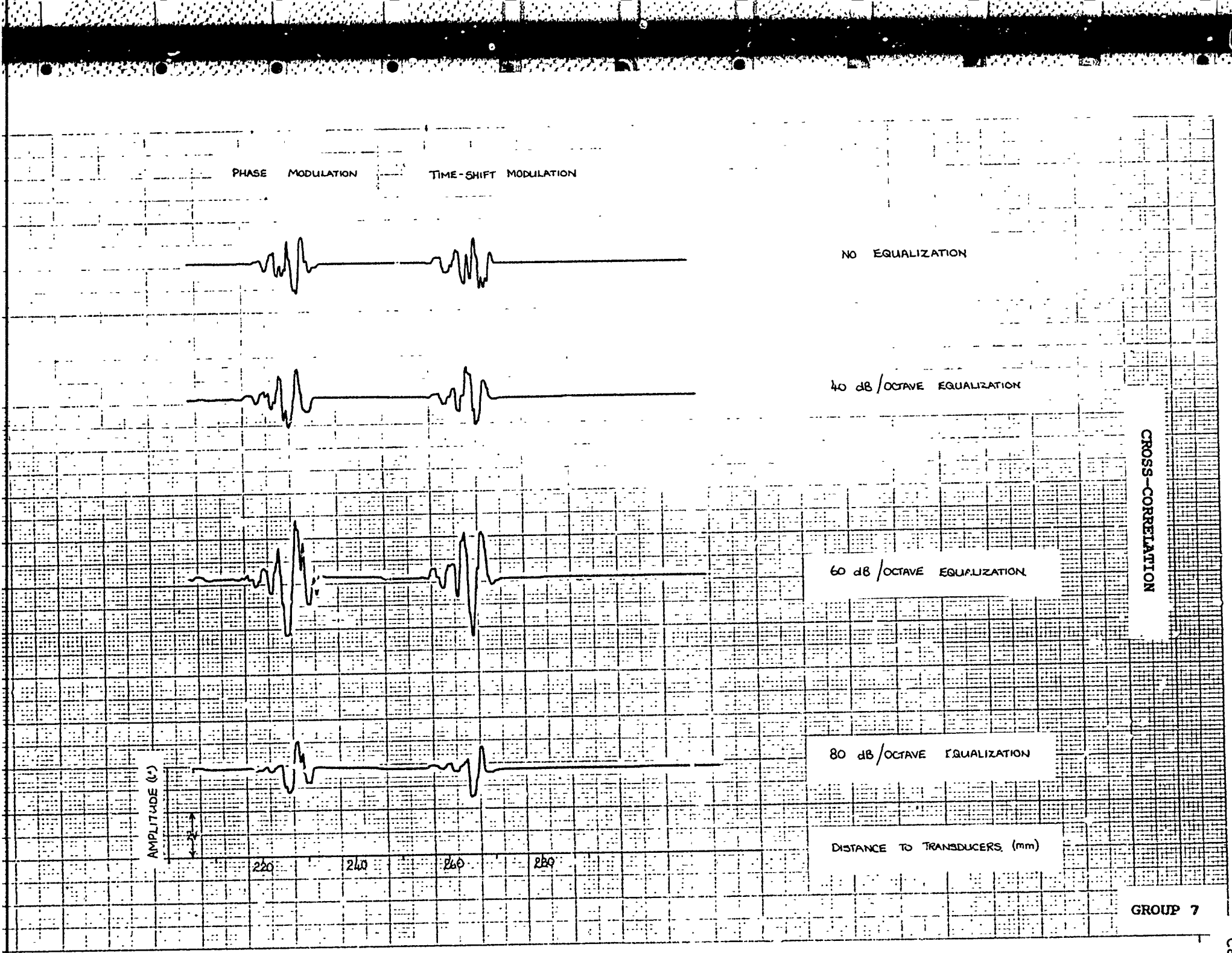
PHASE MODULATION
TIME-SHIFT MODULATION
NO EQUALIZATION
40 dB/OCTAVE EQUALIZATION
60 dB/OCTAVE EQUALIZATION
80 dB/OCTAVE EQUALIZATION
CROSS-CORRELATION
AMPLITUDE (L)
220
240
260
280
DISTANCE TO TRANSDUCERS (mm)
GROUP 7

APPENDIX D

CARRIER CORRELATION SYSTEM

CROSS-CORRELATION FUNCTIONS

The cross-correlation functions shown on the following pages of this appendix are obtained from the carrier correlation system described in Chapter Seven. This system is termed a Type II system. The system was set up as done for the Type I system correlation tests. Cross-correlation range was preset to approximately 32 cm for these runs. Page D2 contains the cross-correlation functions for four sets of transducers, and page D3 contains the cross-correlation functions for the remaining three sets of transducers. Correlation runs two through seven are for the same sets of transducers used in Appendix C. Correlation run number one is for a set of modified Oxford transducers which were not used in the Appendix C tests. The modification was a revised backing plate having different ridge spacings. This was an unsuccessful attempt to produce a wider bandwidth transducer.

Appendix E contains further information on transducer frequency response and the transducer pairs used in each group.

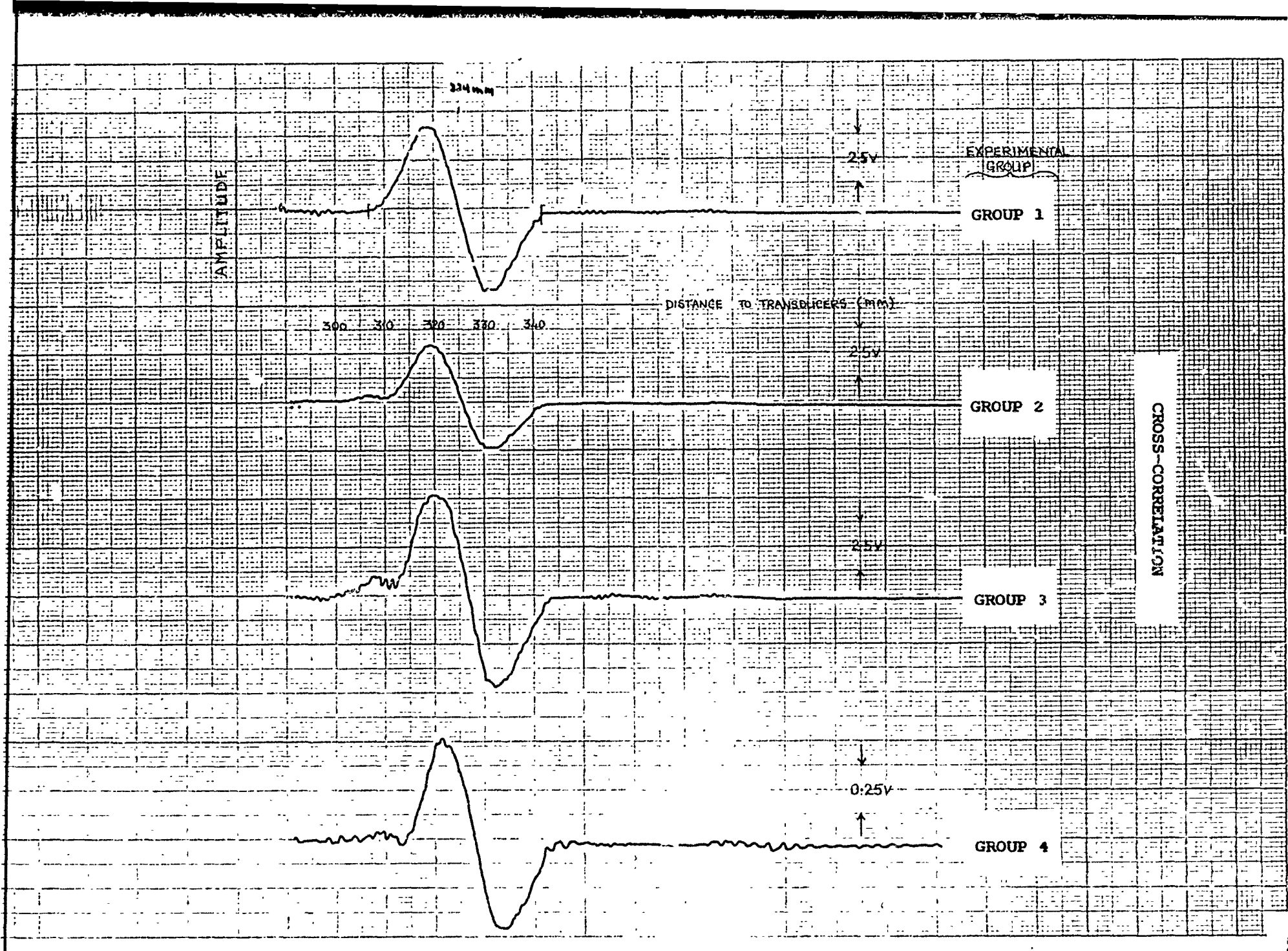
334 mm
AMPLITUDE
2·5V
EXPERIMENTAL GROUP
GROUP 1
DISTANCE TO TRANSDUCERS (mm)
300
310
320
330
340
2·5V
GROUP 2
CROSS-CORRELATION
2·5V
GROUP 3
0·25V
GROUP 4

D2

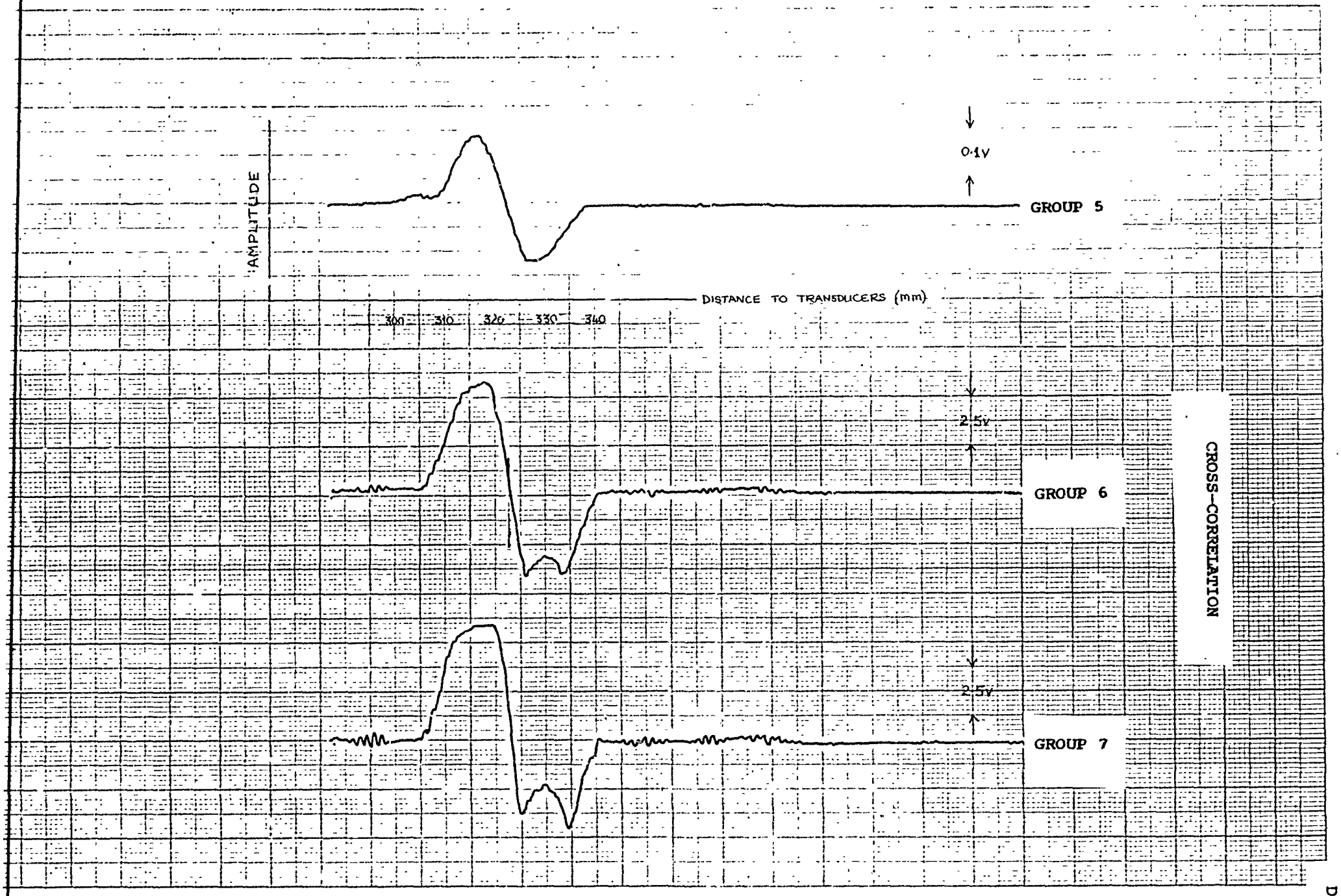
AMPLITUDE
0·1V
GROUP 5
DISTANCE TO TRANSDUCERS (mm)
300
310
320
330
340
2·5V
GROUP 6
CROSS-CORRELATION
2·5V
GROUP 7

APPENDIX E

TRANSDUCER FREQUENCY RESPONSE TESTS

This appendix contains the results of the frequency response runs which were taken for sets of transmitting/receiving transducers. The basic test set-up is shown in figure E1.

The frequency response tests were done as follows. A voltage controlled oscillator was adjusted to oscillate between approximately 100 Hz and 100 kHz. The VCO frequency was controlled by a ramping generator. The ramping generator output was also fed to the x-axis of the chart recorder. A higher ramp voltage causes a higher frequency VCO output and also causes the chart recorder x position to increase. The VCO output was fed to the transmittor stages of the Type II system. A 19.5 mm disc was used as a stationary target located at 26 cm from the transducer module. The echo signal was passed through the Type II system receiver, and then sent to a precision rectifier circuit whose schematic is shown in figure E2. The output of this rectifier was then fed to the y-axis of the chart recorder. The frequency response plots shown on pages E5 through E11. The experimental group noted on each response chart is the same as for the groups listed in Appendices C and D.

These frequency response plots represent the Type I and Type II System transmit/receive frequency responses. Tests on the associated transmitting and receiving circuitry show that the circuit response is essentially flat from approximately 20 kHz to well over 100 kHz.

Occasionally, the frequency response plots contain two separate amplitude functions. This was done if the transducer output was judged to be unusually low. The additional response plot was done with the chart recorder sensitivity at a higher setting.

The frequency response were done for seven sets of transducers: five pairs of Oxford Transducers and two pairs of Polariod transducers. The first response test on Oxford transducers (experimental group 1) was run on a set of modified transducers. The modification consisted of altering the ridge spacing on the backing plate from the 0.51mm described in Chapter Three to three sets of spacings: 0.25, 0.5, and 0.75 mm, starting with the narrowest ridges at the outer edge of the backing plate. The frequency response was widened slightly, and the single response peak was change to two closely spaced peaks. However, the bandwidth improvement was not judged sufficient to justify the labour involved in further modifications, and the modifications were stopped. This modified set of transducers was used on the Type II cross-correlation tests, but was not used on the Type I tests.

The remaining Oxford transducers (experimental groups 2 through 5) were taken from two batches: one batch contained transducers which had easily passed the production test requirements, and one batch which had barely passed these requirements. The transducer number of those coming from first batch is preceeded by a +, and the transducer number of those coming from the second batch is preceeded by a -.

The Polariod transducers (experimental group 6 and 7) were obtained after completion of the FMCW tests. Two sets were obtained, and one set is approximately six months older than the other. The polariod transducers are labelled accordingly in Table E1.

TRANSDUCER PAIRS TESTED (transmit, receive)	EXPERIMENTAL GROUP
Oxford E1, Oxford E2	1
Oxford +1, Oxford +4	2
Oxford +2, Oxford +3	3
Oxford -1, Oxford -4	4
Oxford -2, Oxford -3	5
Polaroid 1 (old), Polaroid 2 (old)	6
Polaroid 3 (new), Polaroid 4 (new)	7

TABLE E1 ELECTROSTATIC TRANSDUCER PAIRS TESTED

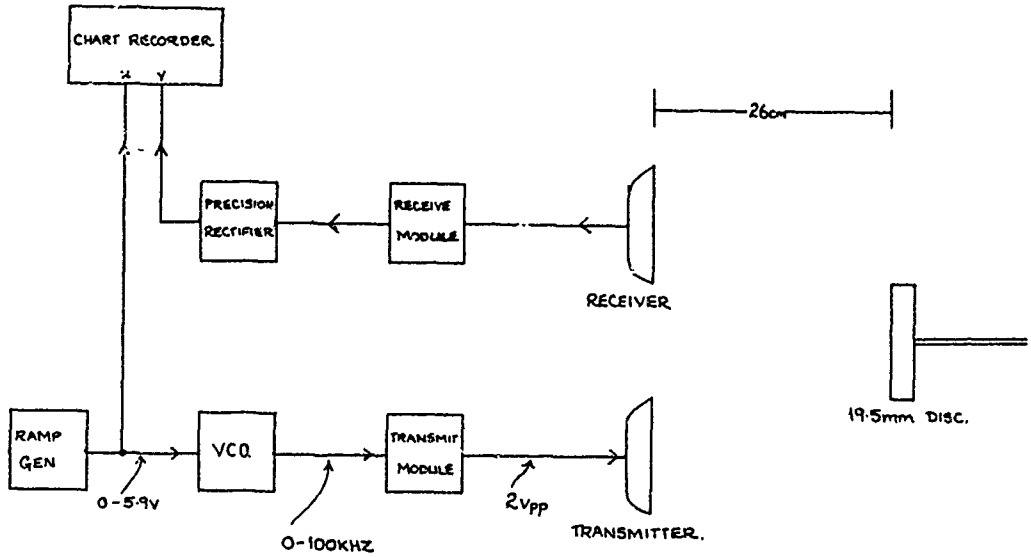

FIGURE E1 Transducer Frequency Response Test Set-Up

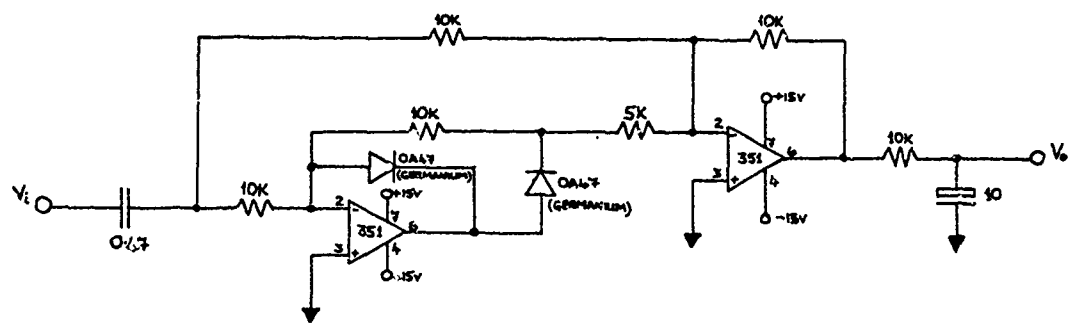

FIGURE E2 Precision Rectifier Circuit

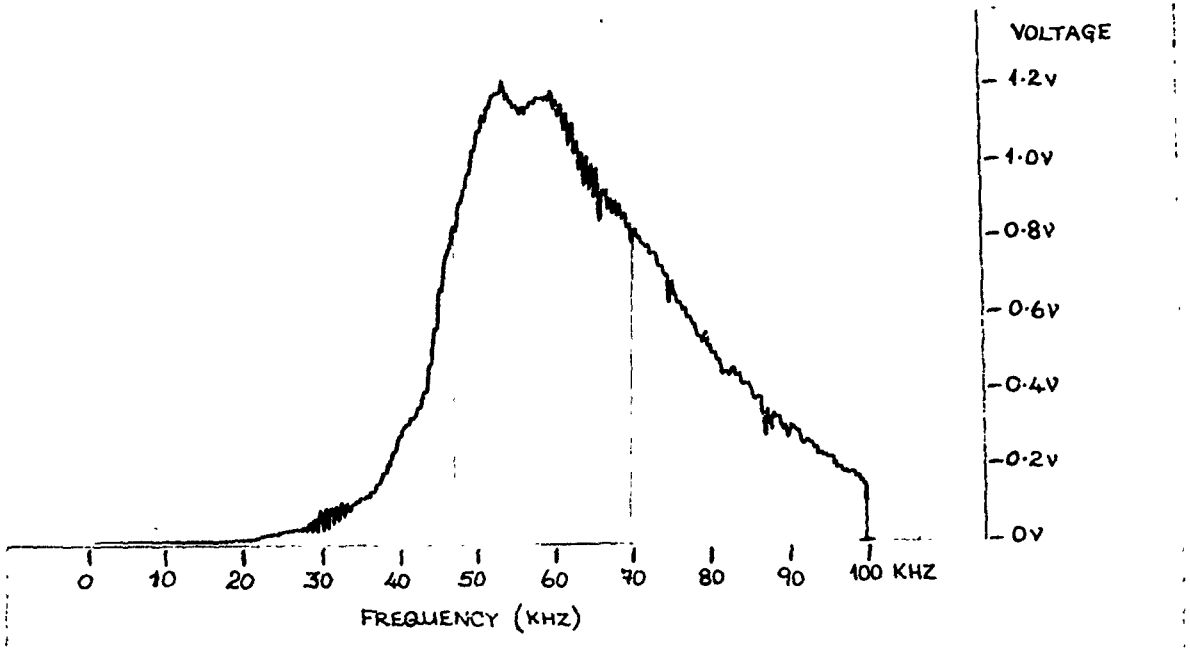

TRANSDUCER FREQUENCY RESPONSE

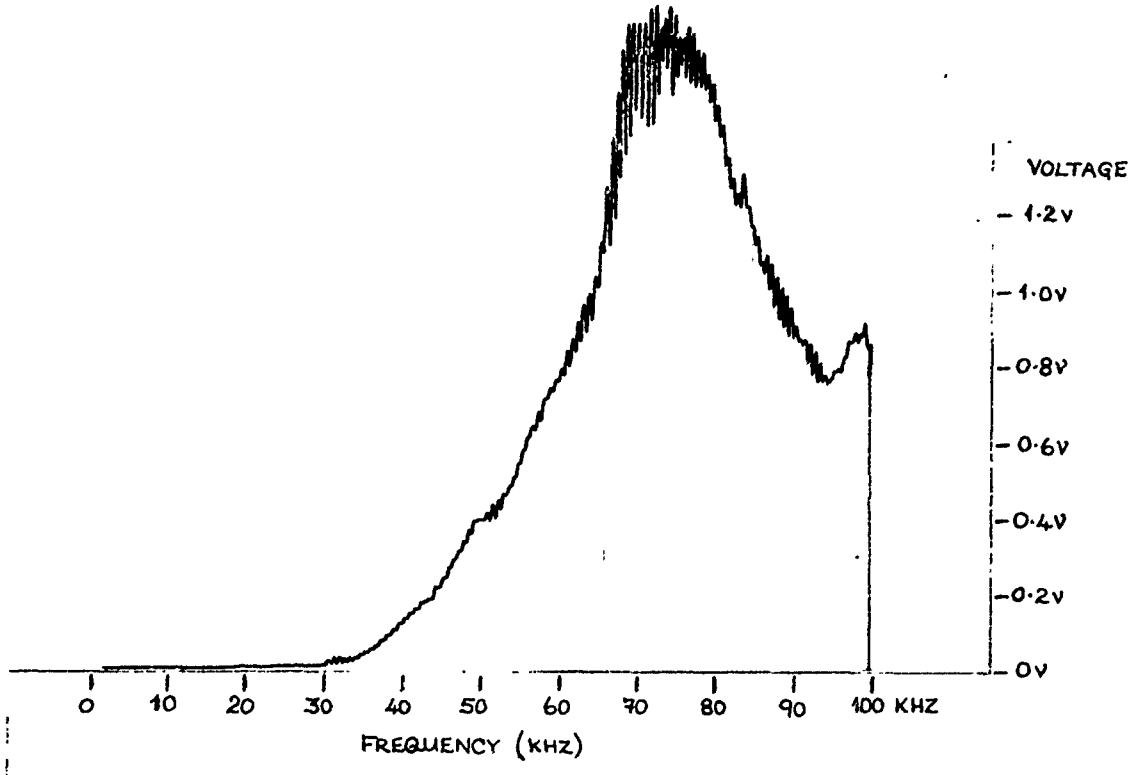

TRANSDUCER FREQUENCY RESPONSE

GROUP 3

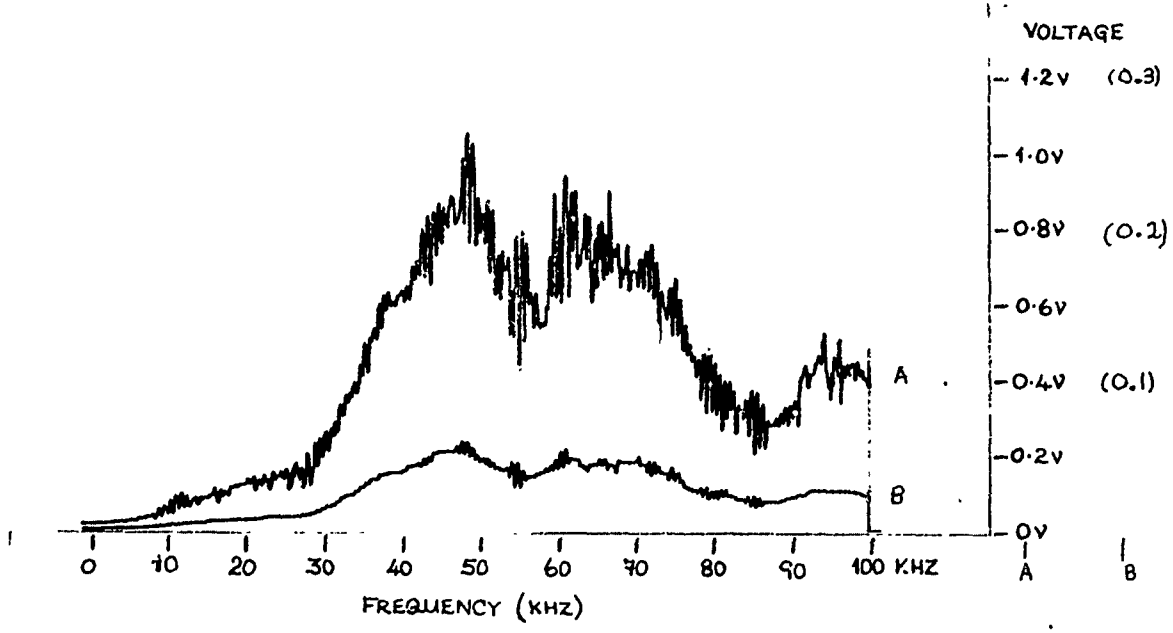

GROUP 4

TRANSDUCER FREQUENCY RESPONSE

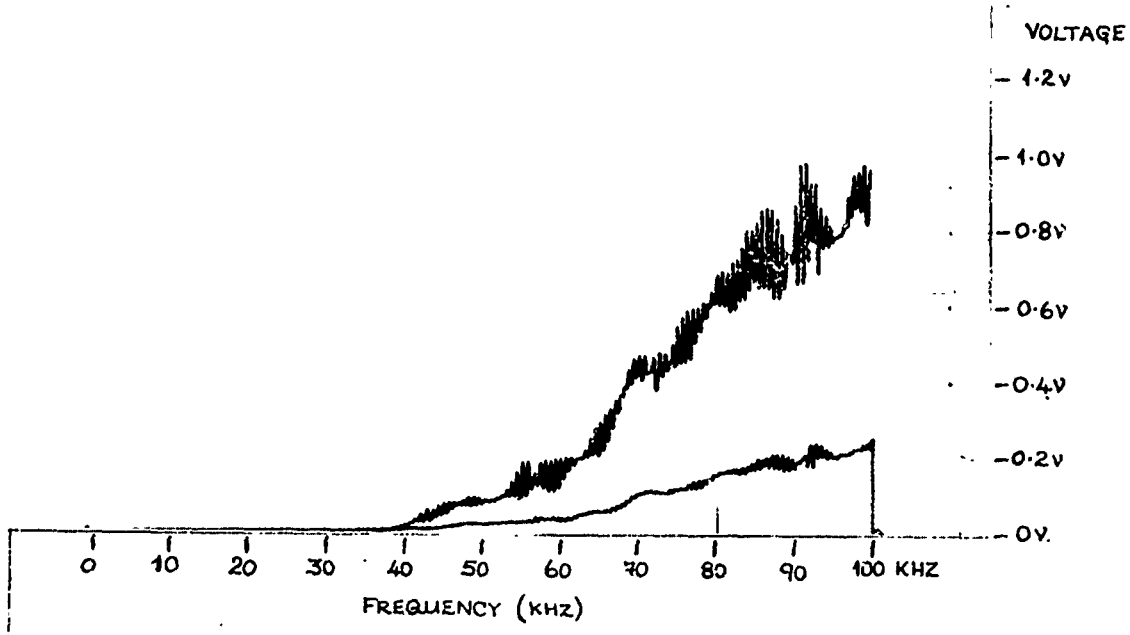

TRANSDUCER FREQUENCY RESPONSE

GROUP 5

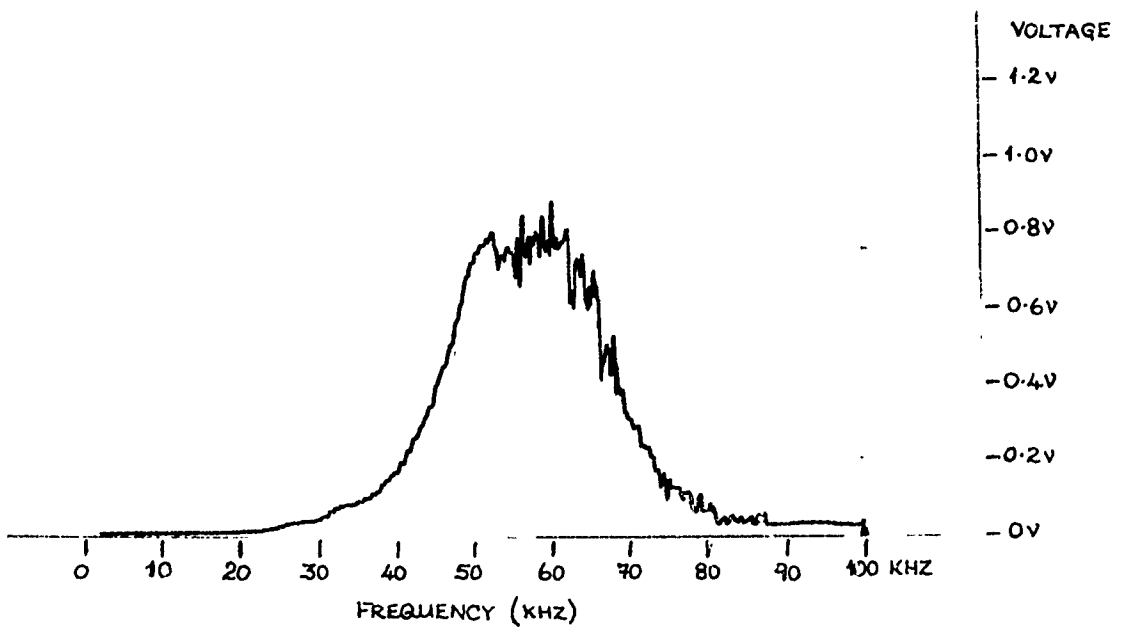

GROUP 6

TRANSDUCER FREQUENCY RESPONSE

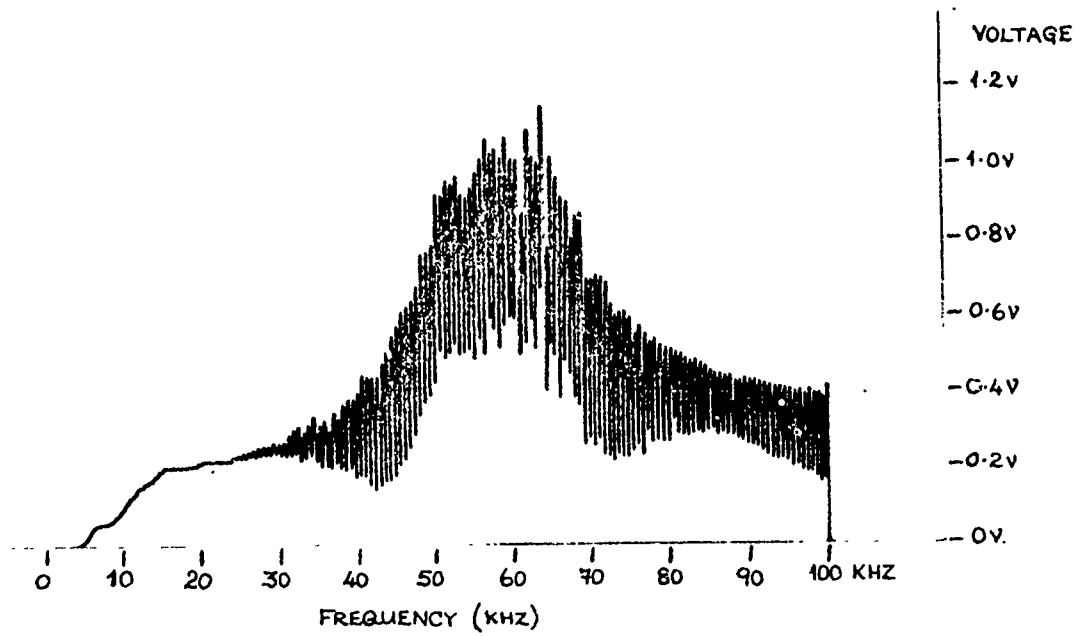

GROUP 7

TRANSDUCER FREQUENCY RESPONSE